THE UNIVERSITY OF MANITOBA

LIBRARY

AUTHOR ...BEWS, Jeff.....

TITLE ....MAGNETORESISTANCE OF DILUTE PtMn ALLOYS.....

.....

.....

THESIS ...M.Sc., 1983.....

I, the undersigned, agree to refrain from producing, or reproducing, the above-named work, or any part thereof, in any material form, without the written consent of the author:

.....

.....

.....

.....

.....

.....

.....

.....

.....

.....

.....

.....

.....

.....

.....

.....

.....

.....

CONTENTS

Chapter I

THEORETICAL

1.1 INTRODUCTION

When small quantities of transition metals or rare earths are dissolved in nonmetallic hosts, they often assume definite ionic valence states. In such instances, well-defined magnetic moments can be associated with these impurities. When metallic hosts are used, the presence of a broad conduction band tends to delocalize the impurity electrons and thereby destroy any atomic moment. Thus, d-shell or f-shell impurity electrons tend to possess a dual nature, being responsible for the observed magnetic moments (being localized) and participating to some degree in the conduction process of the sample. Describing a dilute alloy system therefore requires one to determine which characteristic is dominant. Is there local moment formation and if so, to what extent? A number of models have been formulated which attempt to describe such dilute impurity systems.

1.2 FRIEDEL MODEL

One model which attempts to explain the formation of magnetic moments in dilute alloys was put forward by Friedel.[1,2] This model considers a transition impurity possessing a single, orbitally nondegenerate, atomic d-state dissolved in a noble metal host; the unperturbed energy of this d-state is assumed to lie within the conduction band of the host. An s-d covalent admixture interaction, V, between the localized d-state and the conduction electron s-states is a direct consequence of this overlap. This interaction will induce transitions between the two. Because of this, the localized state of the impurity shifts in energy from its unperturbed value and acquires a finite energy width. A virtual bound state is said to have formed. Such an orbitally nondegenerate virtual d-state can accommodate a maximum of one electron per spin orientation (see figure 1 and 2).

If the intra-atomic interactions between the localized d-electrons are neglected, the virtual bound states for both spin orientations will have the same energy. However, because electrons in virtual levels can be almost as localized as those in an isolated atom, such forces play an important role and must not be overlooked. Thus, exchange and correlation effects, which are of importance in atomic d-levels, must also be of significance in virtual d-levels. These effects split the virtual bound state into two

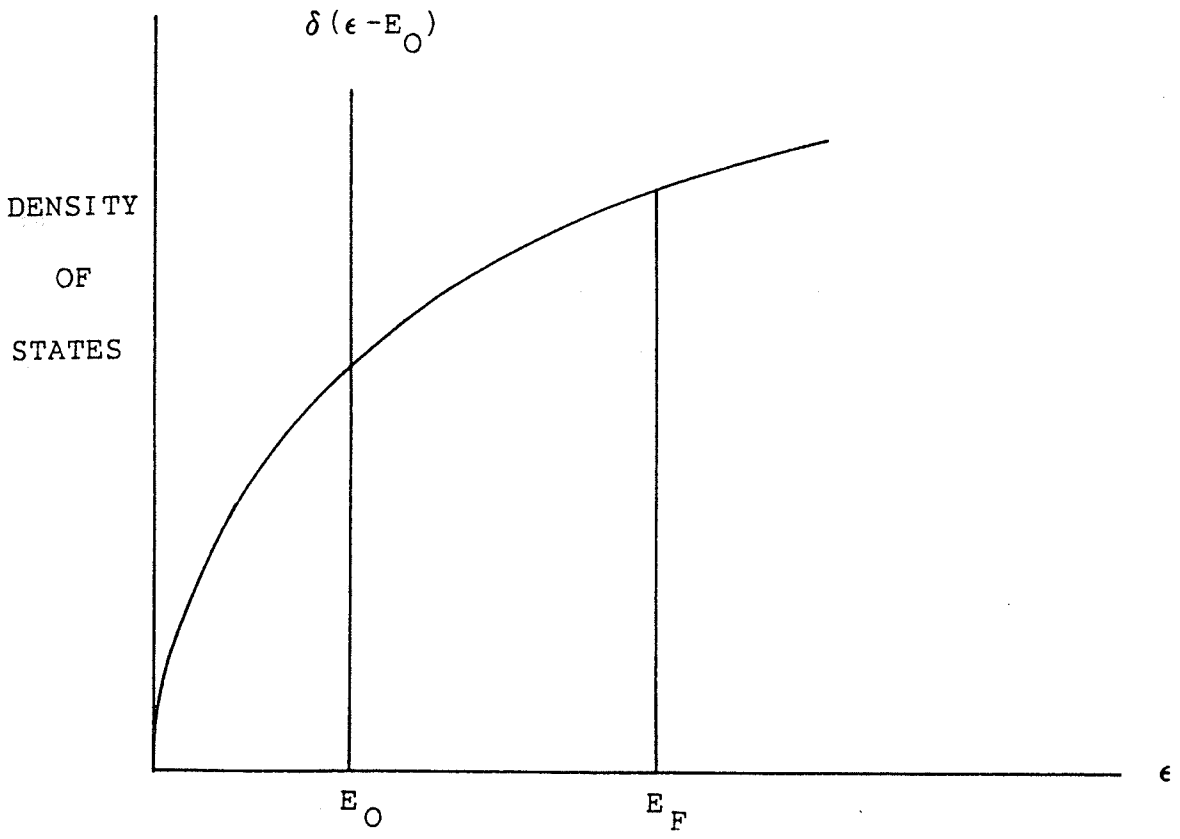

Figure 1: The unperturbed localized d-state of the impurity embedded in a free-electron conduction band.

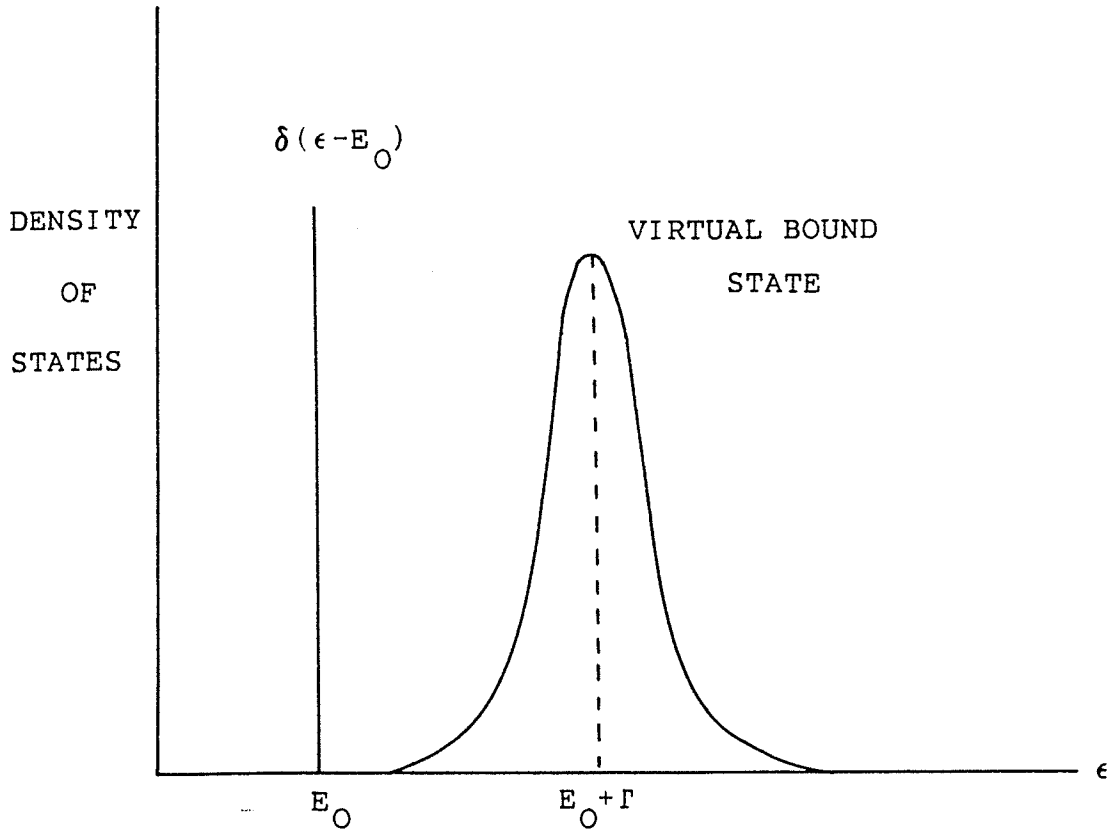

Figure 2: The formation of a virtual bound state due to the s-d mixing interaction. The unperturbed localized d-state of the impurity is shown for comparison purposes.

substates of differing energy, one for each spin. As a result, the spin up and spin down virtual states accommodate unequal numbers of electrons up to the Fermi level. In other words, a magnetic moment is formed (see figure 3).

1.3 ANDERSON MODEL

Another model used to describe dilute impurity systems is that developed by Anderson. The Anderson model[3] utilizes the ideas of Friedel, putting them on a more quantitative basis. The Hamiltonian for the system is given by

$$H = H_{COND} + H_{IMP} + H_{kd}$$

H_{COND} is the unperturbed conduction electron Hamiltonian.

$$H_{COND} = \sum_{k\sigma} \epsilon_k c^*_{k\sigma} c_{k\sigma}$$

where ϵ_k is the energy of the free-electron state with wavevector k and $c^*_{k\sigma}$, $c_{k\sigma}$ are the creation, annihilation operators for the state with wavevector k and spin σ. H_{IMP} describes the isolated impurity atom, assumed representable by a single nondegenerate d-shell orbital.

$$H_{IMP} = E_o(n_{d+} + n_{d-}) + U n_{d+} n_{d-}$$

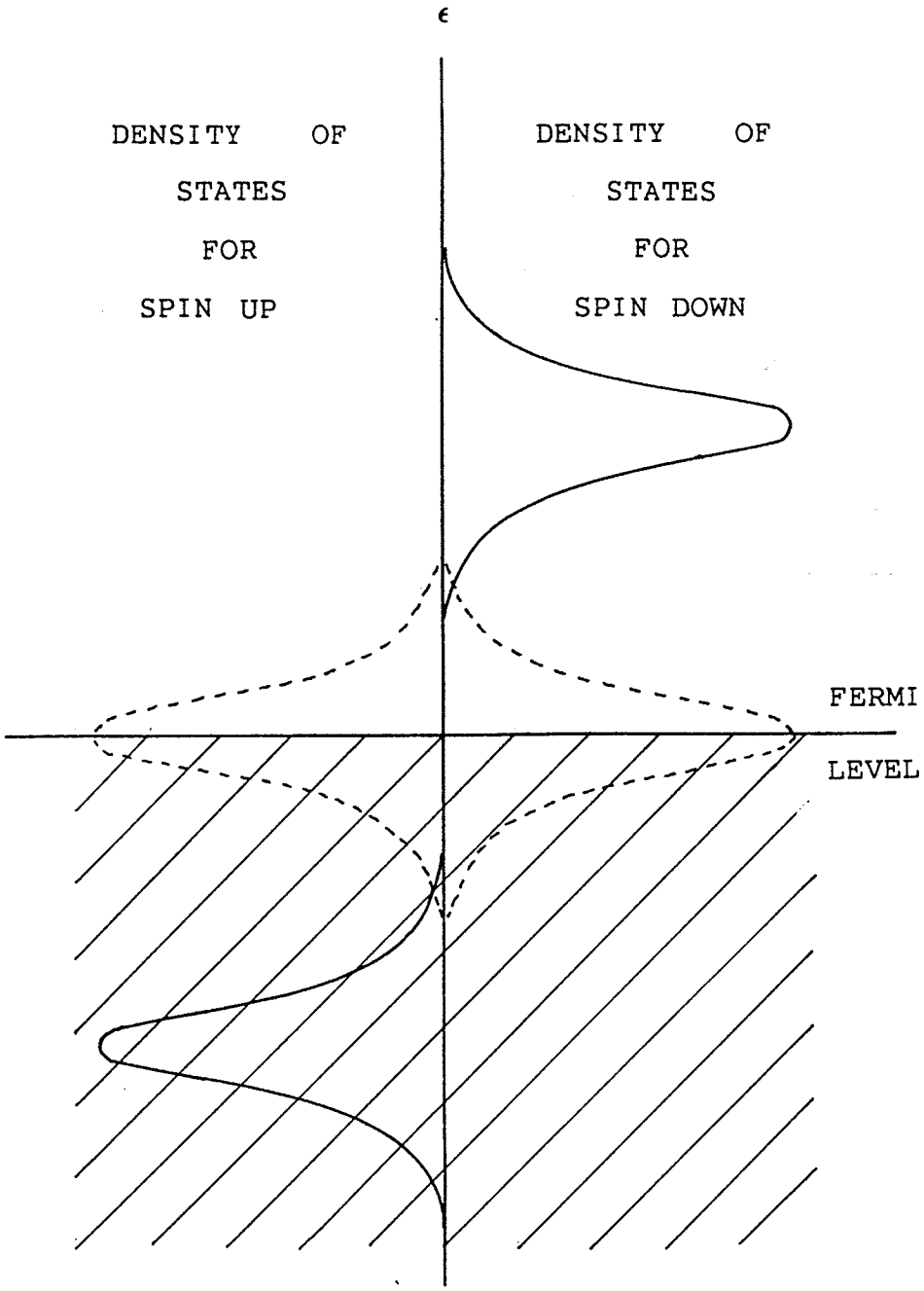

Figure 3: The splitting of a virtual bound state into two substates of differing energy due to exchange and correlation effects. The dotted lines indicate the position of the two substates in the nonmagnetic case.

E_O being the energy of the isolated d-orbital of the impurity atom, U being a Coulomb correlation integral and $n_{d\pm}$ the number of spin up(+) and spin down(-) localized d-electrons. The term $Un_{d+}n_{d-}$ represents the repulsion between d-impurity electrons of opposite spins; it describes the tendency towards the formation of a magnetic moment on the impurity site by reducing the probability of double occupancy of the orbital. A d-state containing two electrons (of opposite spin) will, because of this Coulomb repulsion, possess a higher energy (the difference being E_O+U) than if it were only singly occupied (see figure 4). The term H_{kd} in the Hamiltonian allows for the mixing of conduction and impurity electrons. It tends to delocalize the d-electrons and to destroy impurity magnetism, acting in a fashion opposite to H_{IMP}.

$$H_{kd} = \sum_{k\sigma} V_{kd}(c^*_{k\sigma} c_{d\sigma} + c^*_{d\sigma} c_{k\sigma})$$

where V_{kd} is the covalent admixture matrix element between the d-state and the conduction electron states and $c^*_{d\sigma}$, $c_{d\sigma}$ are the creation, annihilation operators for a d-state electron of spin σ. When the Hamiltonian is solved, it is found that the effect of this s-d mixing term is to shift and broaden the sharp spin up and spin down impurity energy levels into virtual bound states (see figure 5). The energies of the virtual states are given by

$$E_{d\sigma} = E_O + U < n_{d-\sigma} >$$

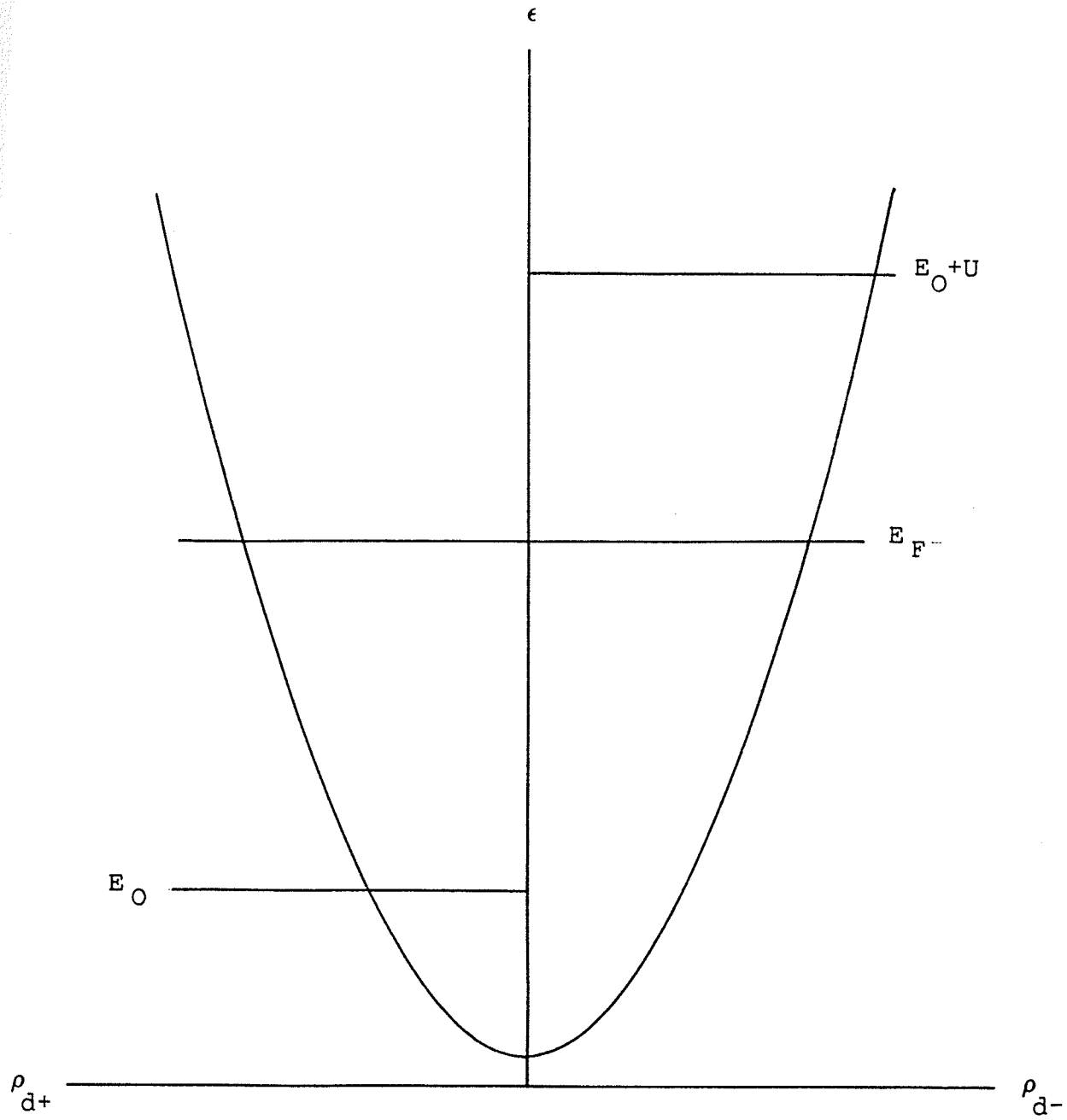

Figure 4: The energy levels of the unperturbed d-state of the impurity.

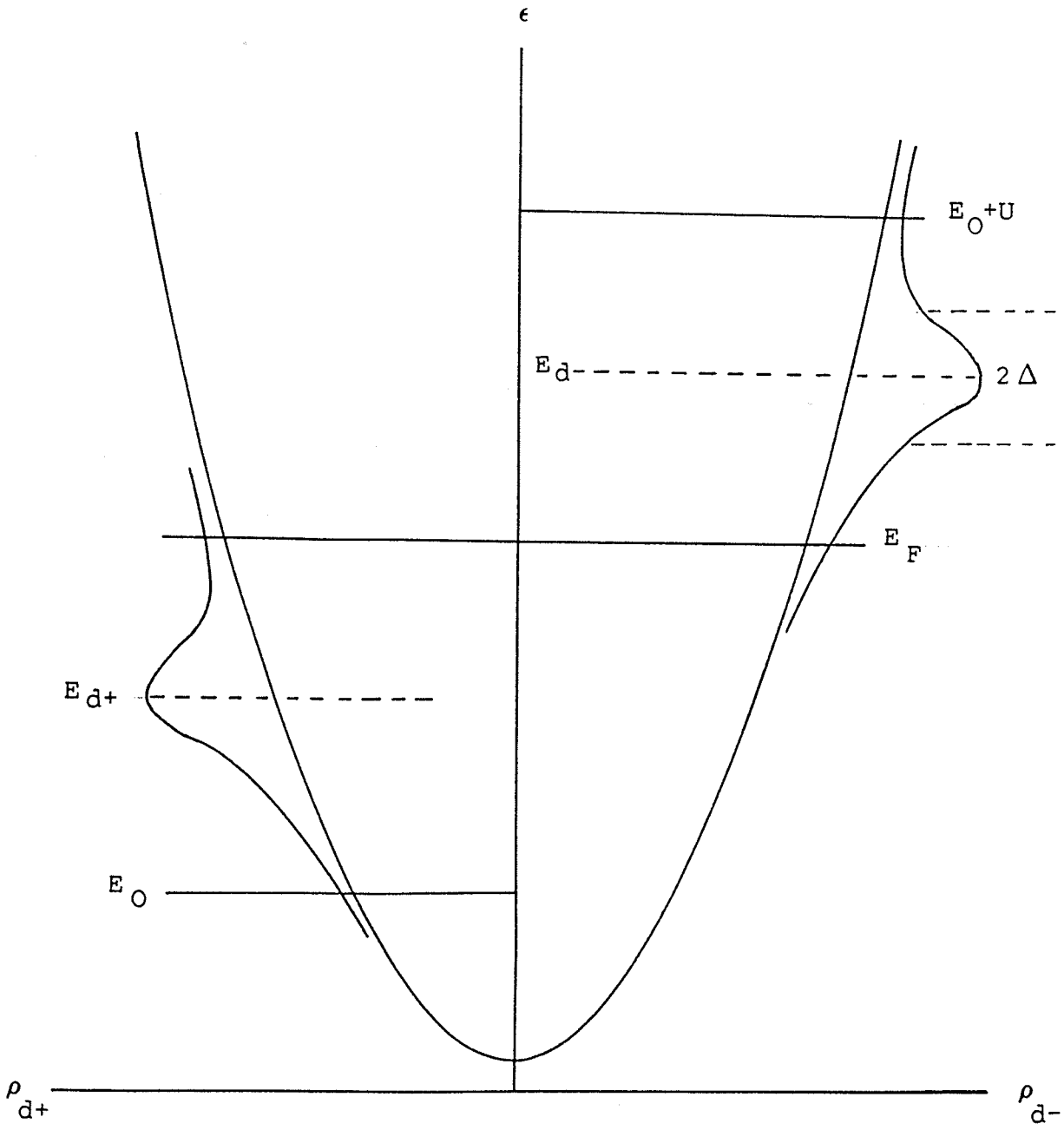

Figure 5: The effect of s-d mixing on the energy levels of the impurity d-state.

The width of these states is given by

$$\Delta = \pi \overline{|V_{kd}|^2} N(\epsilon)$$

where $N(\epsilon)$ is the density of states with energy ϵ in the conduction band of the host.

The occupation numbers of the spin up and spin down virtual bound states are found to be

$$< n_{d+} > = \pi^{-1} \cot^{-1}(E_O - E_F + U < n_{d-} > / \Delta)$$

$$< n_{d-} > = \pi^{-1} \cot^{-1}(E_O - E_F + U < n_{d+} > / \Delta)$$

where E_F is the Fermi level energy. This system of two coupled self-consistent equations may have one or two solutions, depending on the relative values of the parameters $E_O - E_F$, U and Δ. If the system has a single solution, $< n_{d+} > = < n_{d-} >$, the impurity will be nonmagnetic. When two symmetrical solutions exist, $< n_{d+} > \neq < n_{d-} >$, the impurity will be magnetic.

A "Magnetic Behavior" phase diagram can be obtained by plotting $< n_{d+} >$ against $< n_{d-} >$. The graph is shown in figure 6. For given values of the Coulomb integral, U, and the d-state energy relative to the Fermi energy, $E_O - E_F$, there is a critical value of level width Δ_C which separates the magnetic and nonmagnetic behavior of the system. If Δ is greater than Δ_C, the impurity will be nonmagnetic. On the other hand, a Δ less than Δ_C means the impurity will be magnetic. When Δ/U becomes very small, the spin up and spin

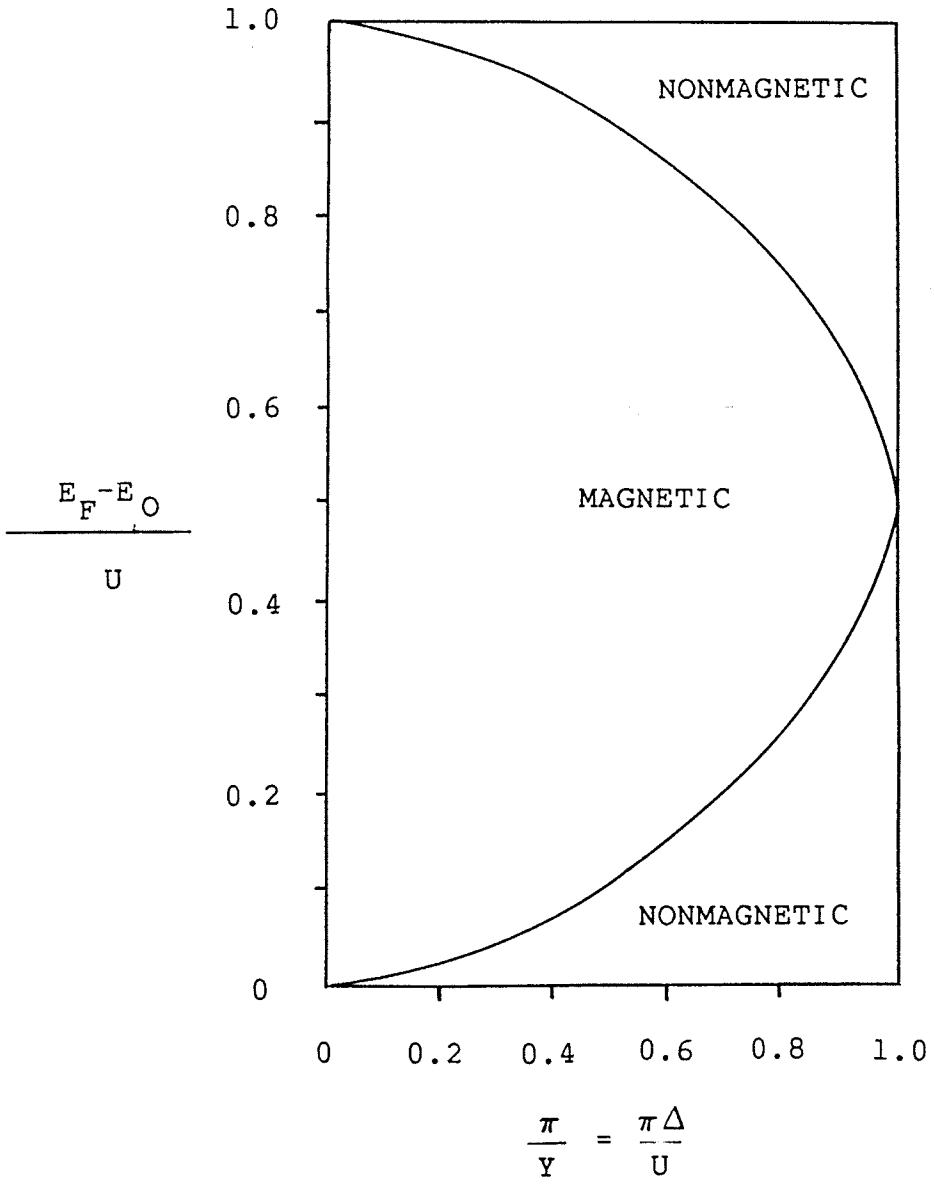

Figure 6: A "Magnetic Behavior" phase diagram.

down electrons become strongly correlated via the Coulomb interaction so as to avoid the simultaneous occupancy of the local level. This leads to the formation of a magnetic moment. This magnetic behavior is illustrated in the phase diagram.

1.4 HIRST MODEL

In the Friedel and Anderson models, the Coulomb interaction and other intra-ionic correlations between the local impurity electrons are treated as weak perturbations. They tend to overemphasize the itinerant aspects of local moment formation. An alternative model for dilute alloys, one which corrects for this shortcoming, is the configuration-based approach (sometimes referred to as the Hirst model).[4] In this description, the unperturbed 3d and 4f impurity states are assumed to be conventional ionic many-electron states corresponding to well defined configurations $3d^n$ and $4f^n$. These states will rarely ever be wiped out, in most instances being only perturbed, by interactions with conduction electrons. The central feature of this model is, therefore, the integral occupation of the impurity's 3d or 4f valence shell; such a characteristic is assumed to be the result of intra-ionic Hund's rule correlations.

In the Hirst model, the potentially magnetic impurity possesses a Hamiltonian given by

$$H = H_{ION} + H_{COND} + H_{MIX}$$

H_{ION} describes the localized intra-atomic interactions at the impurity site.

$$H_{ION} = -Vn + [Un(n-1)/2] + H_{INTRA}$$

where n is an operator for the total number of 3d or 4f electrons, V is the nuclear potential energy at the impurity site and U is the 3d-3d or 4f-4f Coulomb interaction. H_{INTRA} is the intraconfigurational splitting energies (they are responsible for the formation of l-s multiplets and spin-orbit levels etc.). H_{ION} describes a tendency towards the formation of ionic many-electron states belonging to definite configurations $3d^n$ and $4f^n$. H_{COND} represents the energy of the noninteracting conduction electrons of the host.

$$H_{COND} = \sum_{k\sigma} \epsilon_k a^*_{k\sigma} a_{k\sigma}$$

where ϵ_k is the energy of a conduction electron with wavevector k, spin σ and creation, annihilation operators $a^*_{k\sigma}$, $a_{k\sigma}$. H_{MIX} is a one-electron mixing interaction between localized impurity states and the conduction electron states. It tends to break up the many-electron states of definite configurations, mixing the impurity electrons into the conduction band.

$$H_{MIX} = V_{MIX} \sum_{k l \sigma} (a^*_{k l \sigma} c_{l\sigma} + c^*_{l\sigma} a_{k l \sigma})$$

$c^*_{l\sigma}$, $c_{l\sigma}$ being the creation, annihilation operators for the 3d or 4f electrons of angular momentum l and spin σ.

Describing the impurity system basically becomes a problem of determining which tendency, H_{ION} or H_{MIX}, is dominant. A measure of the mixing strength is given by the quantity

$$\Delta = \pi |V_{MIX}|^2 N(E_F)$$

where $N(E_F)$ is the density of conduction electron states at the Fermi level. An estimate of the strength of H_{ION} is given by the Coulomb energy U. When U is greater than Δ, the impurities are potentially magnetic.

Figure 7 shows the Hirst energy level diagram for the case where mixing interactions are ignored. The energies E(n) of the various configurations, n, fall on a parabola (when intraconfigurational splittings, shown schematically, are ignored). n_o is the stable configuration. n_{min} is given by the equation

$$n_{min} = (V/U) + (1/2)$$

If the impurity is initially in the state n_o, the minimum excitation energy needed to reach the n_o-1 configuration is obtained when a 3d electron is transferred to the conduction band at the Fermi energy. This is given by

$$E_{EXC} = [\, E(n_o - 1) + E_F \,] - E(n_o)$$

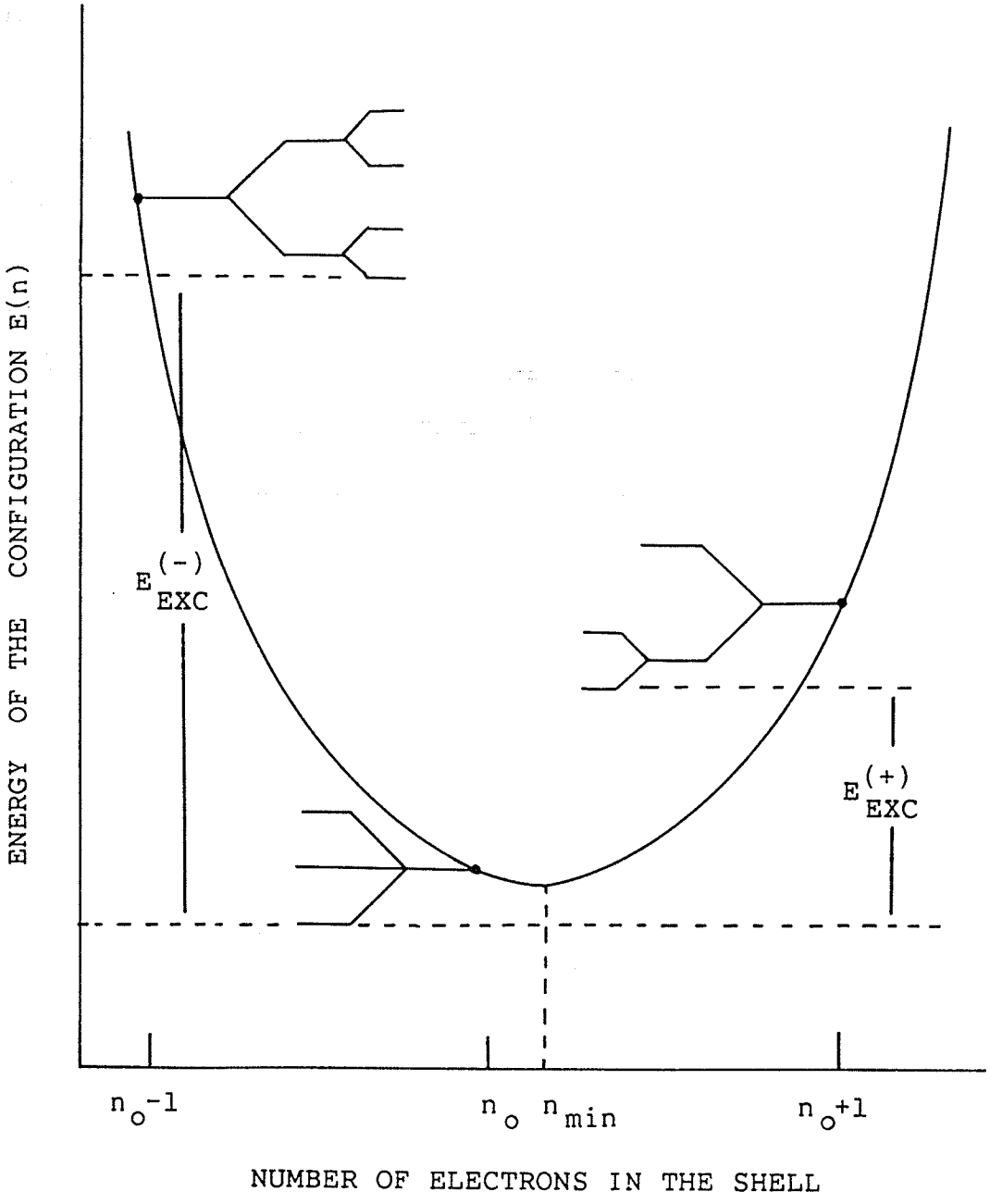

Figure 7: Hirst energy level diagram for the case where mixing interactions are ignored.

where $E(n_o)$ is the energy of the configuration n_o. The minimum energy needed to add a 3d electron is

$$E^{+}_{EXC} = E(n_o+1) - [\, E(n_o)+E_F \,]$$

If n_o is to be the stable configuration, both E^{+}_{EXC} and E^{-}_{EXC} must be positive. The configuration n_o with the lowest energy depends on n_{min} and hence V/U. Thus, if the binding potential V is decreased, n_{min} shifts to the left and n_o-1 becomes the stable configuration.

The effect of the interaction between the localized impurity electrons and the conduction electrons is to transfer the former from the impurity 3d-shell to the conduction band and back. If the impurity is initially in the stable configuration, n_o, then (to first order) mixing can only occur if the ion is excited from the ground state $E(n_o)$ to the next higher state, either $E(n_o+1)$ or $E(n_o-1)$. Such a transition can take place only if the mixing strength is larger than the excitation energy E^{-}_{EXC} or E^{+}_{EXC}. If this condition does not hold, the impurity remains in the stable configuration n_o. On the other hand, if the impurity is initially in an unstable configuration n_o -1, it will spontaneously absorb a conduction electron via the mixing interaction; in doing so, the system returns to its stable configuration n_o. Thus, in the presence of a finite mixing strength Δ, the condition that the interconfiguration excitation energies E^{-}_{EXC} and E^{+}_{EXC} be positive is not

sufficient to ensure a particular configuration n_o be stable. E^-_{EXC} and E^+_{EXC} must also be larger than Δ. When this holds, mixing transitions are suppressed by energy conservation requirements. When a more detailed calculation is carried out, the condition for configurational stability in the presence of a finite mixing becomes

$$E_{EXC} > \Delta, \quad \text{with } E_{EXC} = \{ [E^+_{EXC}]^{-1} + [E^-_{EXC}]^{-1} \}^{-1}$$

Figure 8 is a plot of this equation in the plane of the binding potential V and the mixing strength Δ. The solid curve represents $\Delta = E_{EXC}$. Above the curve, $\Delta > E_{EXC}$ while below $\Delta < E_{EXC}$.

A Δ value of zero represents the case of an isolated impurity; in such an instance, each configuration n is stable over a region of V given by $n-1 \leq V/U \leq n$. For a finite Δ, the configuration stability condition ($E_{EXC} > \Delta$) is most easily satisfied for a value of V lying at the middle of the stability range of the isolated impurity (ie. for a configuration n, when $V/U=n-0.5$). When the ratio of V/U approaches an interger value, the maximum allowed Δ goes to zero. In the interior parts of the stable-configuration phase (denoted by sc) the behavior of the impurity approaches that of an isolated ion. Thus, the stabilization of a single configuration is the necessary condition for local-moment formation at an impurity site. Outside the sc region, nonmagnetic behavior results.

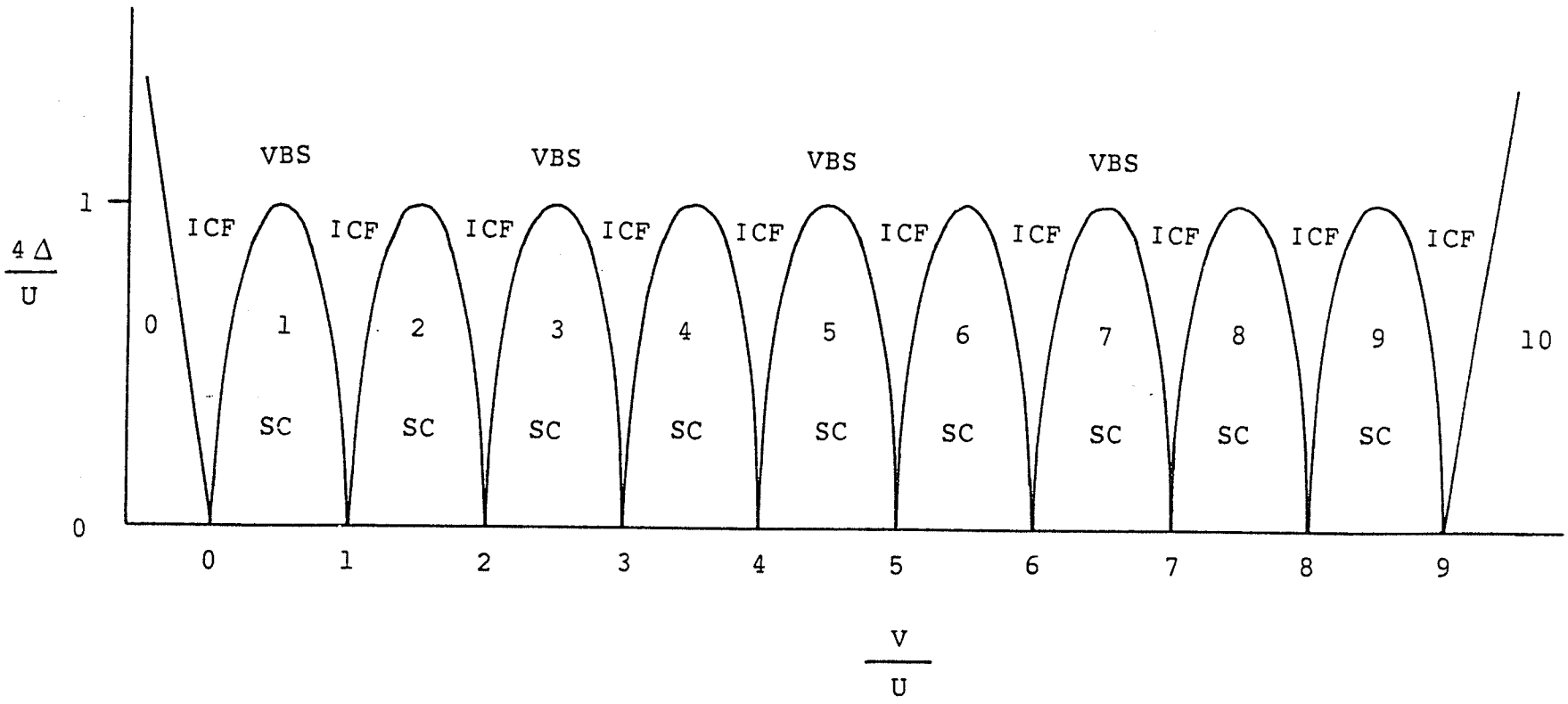

Figure 8: Configurational stability phase diagram for an impurity atom. Regions labelled with SC represent areas of stable configurations. ICF and VBS denote regions of interconfiguration fluctuations and virtual bound state spin fluctuations, respectively.

1.5 THE S-D MODEL

When dilute alloys reside in the strongly magnetic region of the Anderson model, $U/\Delta >> 1$, or in the interior of a stable-configuration phase of the Hirst model, their impurity atoms can be assumed to possess well defined magnetic moments. When such is the case, the s-d model[5] can be utilized in interpreting the experimental data obtained from measurements of their electric and magnetic properties. This model assigns the impurity a spin S which interacts with the conduction electron spins s through an exchange interaction given by

$$H_{sd} = -JS \cdot s$$

where J is the exchange coupling constant. Such an exchange coupling can be shown to evolve directly out of the Anderson model using the Schrieffer-Wolff transformation.

Besides shifting and broadening the impurity energy levels, this s-d mixing interaction also shifts the energies of the free electron states in the conduction band. For magnetic impurities, the virtual level for one spin orientation, say the spin up, is below the Fermi level and filled, while the spin down virtual level is above the Fermi level and empty. Because of this, the energy shift for spin up conduction electrons at the Fermi surface will be positive while that for spin down conduction electrons at

the Fermi surface will be negative. Hence, the effect of the interaction is to raise the Fermi level for spin up conduction electrons and lower the Fermi level for their spin down counterparts. Spin up conduction electrons will then flow into spin down states so as to equalize the Fermi levels. This results in a conduction electron spin polarization which is antiparallel to the impurity spin. The alloy behaves as though an antiferromagnetic exchange coupling existed between the impurity spin and the conduction electron spins. In this case, J will be negative. If one starts with the Anderson Hamiltonian and uses the Schrieffer-Wolff transformation to arrive at an effective exchange interaction, J will necessarily turn out to be negative. However, coupling constants greater than zero do exist in nature. For J positive, the conduction electron spin polarization will be parallel to the impurity spin. A ferromagnetic coupling is said to exist.

1.6 ANOMALOUS RESISTIVITY IN PT-MN

The anomalous behavior in the resistivity found in dilute Pt-Mn alloys can be explained in terms of an s-d exchange interaction between current carrying s-conduction electrons of the platinum host and d-electron induced spins localized

at the manganese impurity sites. This perturbing interaction must be treated in second order to be consistant with experimental results.

In Yosida's formulation[6] of this s-d interaction induced anomalous resistivity, the perturbing potential consisted of both a spin dependant and spin independant part. The former is a direct result of an exchange interaction while the latter origionates from an ordinary screened Coulomb potential around the manganese ions, assumed to be in an Mn^{++} state. Effects due to lattice vibrations are neglected.

The Hamiltonian describing the interaction between conduction electrons and impurity ions is given by

$$H = \sum_{in} V(r_i - R_n) - 2 \sum_{in} J(r_i - R_n)(s_i \cdot S_n)$$

where r_i and R_n represent the position vector of the conduction electron and the Mn ion respectively. $V(r_i - R_n)$ is the deviation from the spin-independant periodic potential due to the Mn impurity. $J(r_i - R_n)$ is the effective exchange integral between the conduction electron with spin operator s_i and the Mn ion with spin operator S_n.

In the second quantized form, this Hamiltonian becomes

$$\begin{aligned} H = {} & N^{-1} \sum_{kk'} V(k,k') \exp[i(k-k') \cdot R_n] (a^*_{k'+} a_{k+} + a^*_{k'-} a_{k-}) \\ & - N^{-1} \sum_{kk'} J(k,k') \exp[i(k-k') \cdot R_n] \\ & * [(a^*_{k'+} a_{k+} - a^*_{k'-} a_{k-}) S^f_n + a^*_{k'-} a_{k+} S^+_n + a^*_{k'+} a_{k-} S^-_n] \end{aligned}$$

where ω, η and ζ denote the coordinate axes, the latter being the quantization axis of spins. $S_n^{\pm}$ is defined as being equal to $S_n^{\omega} \pm iS_n^{\eta}$. The quantities $a^*_{k\pm}$ and $a_{k\pm}$ are the creation and annihilation operators for the conduction electrons with wavevector k and spin parallel or antiparallel to the ζ axis. N is the total number of lattice points while V(k,k') and J(k,k') are related to the matrix elements of $V(r_i - R_n)$ and $J(r_i - R_n)$ between the two states with wavevectors k and k' as follows

$$V(k,k') = N\exp[-i(k-k')\cdot R_n] \int \phi^*_{k'}(r) V(r-R_n) \phi_k(r) d\tau$$

$$J(k,k') = N\exp[-i(k-k')\cdot R_n] \int \phi^*_{k'}(r) J(r-R_n) \phi_k(r) d\tau$$

ϕ_k being the wavefunction of the conduction electron.

A number of assumptions are made in deriving an expression for the resistivity from this perturbing potential:

1. The conduction electron energy can be represented by $(\hbar k)^2/2M$ where M is an effective mass.
2. V(k,k') and J(k,k') depend on $|k-k'|$ only.
3. The distribution of Mn impurities is random with no interference of the scattered wave from different ions.

An applied electric field $\mathcal{E}$ in a direction X results in the deviation of the distribution functions $f^{\pm}(E_k)$ of the conduction electrons with + and - spins from their common zero field value $f_o(E_k)$. These functions can be expressed as a Taylor series

$$f^{\pm}(E_k) = f_o(E_k) - k_x \mathcal{E} \phi^{\pm}(E_k) \left[\partial f_o(E_k)/\partial E_k \right] \quad I$$

where k_x is the component of the electron wavevector in the X direction. The $\pm$ signs represent the spin direction of the conduction electrons while the quantities $\phi^{\pm}(E_k)$ are yet to be determined. The resulting shift in the Fermi sphere by the electric field gives rise to an electric current density

$$j^{\pm} = nqv = -(1/V) \sum_k (\hbar k_x/M)[f^{\pm}(E_k) - f_o(E_k)]e$$

where V is the total volume, n is the number of electrons per unit volume and v is their velocity. Upon substitution of $f^{\pm}(E_k)$, the current density expression becomes

$$j^{\pm} = -(e/6\pi^2)(1/\hbar)(2M/\hbar^2)^{3/2} E_F^{3/2} \phi^{\pm}(E_F) \mathcal{E}$$

where E_F is the Fermi energy. The total sample current density is given by the sum of the current density due to up spin electrons and that due to down spin electrons. From Ohm's Law, the expression for resistivity becomes

$$\rho = \mathcal{E}/j^{+} + j^{-} = -(6\pi^2/e)(\hbar/E_F^{3/2})(\hbar^2/2M)^{3/2} \{ \phi^{+}(E_F) + \phi^{-}(E_F) \}^{-1}$$

The functions $\phi^{\pm}(E_F)$ are determined using the Boltzman equation for the distribution functions $f^{\pm}(E_k)$.

1.7 THE BOLTZMAN EQUATION

If a relaxation-time approximation is utilized, one can construct an explicit representation of the nonequilibrium distribution functions $f^{\pm}(E_k)$ in terms of the solutions to the semiclassical equations of motion. Such an approximation assumes that the form of the nonequilibrium electronic distribution function has no effect on either the rate at which a given electron experiences collisions or on the distribution of electrons emerging from collisions. Unfortunately, when the situation is studied in detail, these simplifying assumptions prove to be incorrect. Because the Pauli exclusion principle allows an electron to be scattered only into empty electronic levels, the rate at which an electron collides depends on the distribution of the other electrons. The distribution of the electrons that emerge from collisions also depends on the electronic distribution functions; this is due to the fact that the net output from collisions depends on the form of the input, which is determined by the electron distribution functions.

When the relaxation-time approximation is abandoned, construction of an explicit representation of the nonequilibrium distribution function is no longer possible. One can, however, arrive at an expression for $f^{\pm}(E_k)$ from its value an infinitesimal time dt earlier.[7] The derivation begins by ignoring the possibility of collisions taking

place between t-dt and t, correcting for this omission later. Consider up spin electrons only. With no collisions occurring during this time span, the position r and wavevector k coordinates of every electron would evolve according to the semiclassical equations of motion

$$\dot{r} = v(k) \qquad \hbar\dot{k} = -e(\mathcal{E}+vxH/c) = F(r,k)$$

where H is the magnetic field and F(r,k) represents the total force acting on the electron. Because dt is infinitesimal, it is possible to find explicit solutions of these equations to linear order in dt; an electron at r,k at time t must have been at r-v(k)dt,k-Fdt/$\hbar$, at time t-dt. Without collisions, this is the only point electrons at r,k could have come from, every electron at this point being assured of reaching r,k in a time dt. Thus

$$f(r,k,t) = f(r-v(k),k-Fdt/\hbar,t-dt)$$

f(r,k,t) being the electron distribution function. When correcting for collisions, one must realize that the right hand side of this equation is inaccurate for two reasons. Firstly, it ignores the fact that some electrons from r-vdt,k-Fdt/$\hbar$ are deflected by collisions and don't reach r,k in the time dt. Secondly, it fails to take into account the possibility of electrons reaching r,k at a time t as a result of a collision between t-dt and t. Adding correction terms

$$f(r,k,t) = f(r-v(k)dt, k-Fdt/\hbar, t-dt) \quad \text{COLLISIONLESS EVOLUTION}$$

$$+[\partial f(r,k,t)/\partial t]_{OUT}dt \quad \text{CORRECTION: SOME FAIL TO GET THERE BECAUSE OF COLLISIONS}$$

II

$$+[\partial f(r,k,t)/\partial t]_{IN}dt \quad \text{CORRECTION: SOME GET THERE ONLY BECAUSE OF COLLISIONS}$$

$[\partial f(r,k,t)/\partial t]_{OUT}$ is a quantity defined such that the number of electrons per unit volume with wavevectors in the infinitesimal volume element dk about k that suffer a collision in the infinitesimal time interval dt is

$$- [\partial f(r,k,t)/\partial t]_{OUT}[dkdt/(2\pi)^3] \qquad \text{III}$$

Because of the infinitesimal nature of dk, any collisions by an electron in this volume element will remove it from the volume element. Thus, expression III can be defined as the number of electrons scattered out of the volume element dk about k in the time interval dt.

Let dt/T(k) be, by definition, the probability that any electron in the neighborhood of k be scattered in the time interval dt. Then, the total number of electrons per unit volume in dk about k that suffer a collision will be dt/T(k) times the number of electrons per unit volume in dk about k. In otherwords,

$$[dt/T(k)]\ f(r,k,t)dk/(2\pi)^3$$

Comparing this with III,

$$[\partial f(r,k,t)/\partial t]_{OUT} = - f(r,k,t)/T(k) \qquad \text{IV}$$

The scattering probability of an electron is written in terms of a quantity $W_{kk'}$, defined as follows: The probability in an infinitesimal time interval dt that an electron with wavevector k is scattered into anyone of the group levels (with the same spin) contained in the infinitesimal k-space volume element dk' about k' (assuming that these levels are all unoccupied) is

$$W_{kk'} dt dk'/(2\pi)^3$$

The actual rate of transition must be reduced by the fraction of these levels that actually are unoccupied (transitions to occupied levels are forbidden by the exclusion principle). This fraction is 1-f(r,k',t). Summing over all final wavevectors k', one arrives at the total probability per unit time for a collision

$$1/T(k) = \int [dk'/(2\pi)^3] W_{kk'} [1-f(r,k',t)]$$

Substituting this into IV

$$[\partial f(r,k,t)/\partial t]_{OUT} = - f(r,k,t) \int [dk'/(2\pi)^3] W_{kk'} [1-f(r,k',t)]$$

One arrives at an expression for $[\partial f(r,k,t)/ \partial t]_{IN}$ in a similar manner.

$$[\partial f(r,k,t)/\partial t]_{IN} = \int [dk'/(2\pi)^3] W_{kk'} f(r,k',t)[1-f(r,k,t)]$$

Expanding the left hand side of II to linear order in dt and then taking the limit as dt$\rightarrow$ 0, one arrives at the Boltzman equation

$$[\partial f(r,k,t)/\partial t] + v[\partial f(r,k,t)/\partial r] + (F/\hbar)[\partial f(r,k,t)/\partial k] = [\partial f(r,k,t)/\partial t]_{COLL}$$

Assuming $[\partial f(r,k,t)/\partial t]$ and $[\partial f(r,k,t)/\partial r]$ are zero in the steady state, the above Boltzman equation becomes

$$(F/\hbar)(\partial f/\partial k) - (\partial f/\partial t)_{COLL} = 0$$

Substituting $F = e\mathcal{E}$ and $k = (2ME_k/\hbar^2)^{1/2}$, as well as absorbing the negative sign,

$$(\partial f/\partial E_k)(\hbar k_x/M)e\mathcal{E} + (\partial f/\partial t)_{COLL} = 0$$

$\mathcal{E}$ is the sample voltage, in this case applied in the X direction. Because the first term does not involve the effect of collisions, f can be replaced by f_o, its value in the absence of collisions. The Boltzman equations, for spin up and spin down electrons, can be written as

$$[\partial f_o(E_k)/\partial E_k](\hbar k_x/M)e\mathcal{E} + [\partial f^{\pm}(E_k)/\partial t]_{COLL} = 0$$

1.8 DETERMINATION OF $\phi^{\pm}(E_k)$

$[\partial f^{\pm}(E_k)/\partial t]_{COLL}$ is the rate of change of the distribution functions $f^{\pm}(E_k)$ due to the collisions with Mn ions. This term contains both an elastic and inelastic part. The former origionates from the scattering process in which the electron spin is not reversed and is given by

$$[\partial f^{\pm}/\partial t]_{EL} = \sum_{k'} W(k'_{\pm} \rightarrow k_{\pm}) f^{\pm}(k')[1-f^{\pm}(k)] - W(k_{\pm} \rightarrow k'_{\pm}) f^{\pm}(k)[1-f^{\pm}(k')] \qquad V$$

where $W(k'_{\pm} \rightarrow k_{\pm})$ represents the transition probability from a $k'_{\pm}$ state to a $k_{\pm}$ state. From assumption 3, this probability is given by the sum of the transition probabilities due to each Mn ion.

$$W(k'_{\pm} \rightarrow k_{\pm}) = (2\pi/\hbar N^2) \sum_n |V(k'-k) \mp S_n^f J(k'-k)|^2 \delta(E_k - E_{k'})$$

Let N_A denote the number of Mn ions. Also, let the probability that S_n^f takes on a value of m be given by $W_m^{\pm}$, the + and - representing spin up and spin down electrons respectively. Then, the summation over n can be replaced by a summation over m.

$$W(k'_{\pm} \rightarrow k_{\pm}) = (2\pi/\hbar N^2) \sum_m^{\pm} W_m^{\pm} |V(k-k') \mp mJ(k-k')|^2 \delta(E_k - E_{k'})(N_A/2) \qquad VI$$

The above summation is taken over m from S to -S and over W_m^+ and W_m^-. The inverse probability is given by the same expression. Using I

$$\begin{aligned} & f^{\pm}(k')[1-f^{\pm}(k)] - f^{\pm}(k)[1-f^{\pm}(k')] \\ &= f^{\pm}(k') - f^{\pm}(k')f^{\pm}(k) - f^{\pm}(k) + f^{\pm}(k)f^{\pm}(k') \\ &= f^{\pm}(k') - f^{\pm}(k) \\ &= f_o(E_{k'}) - k'_x \mathcal{E} \phi^{\pm}(E_{k'})[\partial f_o(E_{k'})/\partial E_{k'}] \\ &\quad - f_o(E_k) + k_x \mathcal{E} \phi^{\pm}(E_k)[\partial f_o(E_k)/\partial E_k] \end{aligned}$$

From energy conservation arguments, $E_{k'} = E_k$, one can replace $[\partial f_o(E_{k'})/\partial E_{k'}]$ by $[\partial f_o(E_k)/\partial E_k]$.

$$f^{\pm}(k')[1-f^{\pm}(k)]-f^{\pm}(k)[1-f^{\pm}(k')]$$
$$= \mathcal{E}\phi^{\pm}(E_k)[\partial f_o(E_k)/\partial E_k][k_x-k'_x]$$

Substituting this result, along with VI, into V gives

$$[\partial f^{\pm}/\partial t]_{EL} = \sum_{k'}(2\pi N_A/2\hbar N^2)\sum_m \overset{\pm}{w}_m^{\pm}|V(k-k')\mp mJ(k-k')|^2$$
$$*\delta(E_k-E_{k'})\mathcal{E}\phi^{\pm}(E_k)[\partial f_o(E_k)/\partial E_k][k_x-k'_x]$$

Replacing the summation over k' by an integration and assuming $V(k,k') = V[2k\sin(\theta/2)]$, $k_x-k'_x = k_x(1-\cos\theta)$ (since only electrons at the Fermi surface take part in conduction).

$$[\partial f^{\pm}/\partial t]_{EL} = (2\pi/\hbar N^2)(N_A/2)\mathcal{E}\phi^{\pm}(E_k)[\partial f_o(E_k)/\partial E_k]$$
$$*(V/8\pi^3)(1/2)(2M/\hbar^2)^{3/2}k_x\sum_m \overset{\pm}{w}_m^{\pm}$$
$$*\iiint E_{k'}^{1/2}|V[2k\sin(\theta/2)]\mp mJ[2k\sin(\theta/2)]|^2$$
$$*\delta(E_k-E_{k'})(1-\cos\theta)\sin\theta dE_{k'}d\theta d\phi$$
$$= (1/4\pi\hbar)(N_A/N)(V/N)(2M/\hbar^2)^{3/2}E_k^{1/2}k_x\mathcal{E}$$
$$*[\partial f_o(E_k)/\partial E_k]\phi^{\pm}(E_k)\sum_m \overset{\pm}{w}_m^{\pm}$$
$$*(1/2)\int|V[2k\sin(\theta/2)]\mp mJ[2k\sin(\theta/2)]|^2$$
$$*(1-\cos\theta)\sin\theta d\theta$$

The inelastic part of $[\partial f^{\pm}/\partial t]_{COLL}$ arises from the process which is accompanied by a change of the spin direction. When dealing with this inelastic contribution, $[\partial f^{+}/\partial t]_{IN}$ and $[\partial f^{-}/\partial t]_{IN}$ must be treated separately. In terms of transition probabilities,

$$[\partial f^{+}/\partial t]_{IN} = \sum_{k'} W(k'_{-}\rightarrow k_{+})f^{-}(k')[1-f^{+}(k)]$$
$$-W(k_{+}\rightarrow k'_{-})f^{+}(k)[1-f^{-}(k')]$$

where

$$W(k'_{-}\rightarrow k_{+}) = W(k_{+}\rightarrow k'_{-}) = (2\pi/\hbar)(N_A/2N^2)\,|J(k'-k)|^2 \\ *\sum_m^{\pm}\{S(S+1)-m(m+1)\}W_{m+1}^{\pm}\delta(E_k+E_g-E_{k'})$$

$E_g = g\mu H$, the energy by which the Mn spin system changes due to the change of the f component of spin in the magnetic field H . g is the g factor of the Mn ion while μ is the Bohr magneton. Upon substitution,

$$[\partial f^{+}/\partial t]_{IN} = \sum_{k'}\Big\{(2\pi/\hbar)(N_A/2N^2)\,|J(k'-k)|^2\sum_m^{\pm}\{S(S+1)-m(m+1)\} \\ *W_{m+1}\delta(E_k+E_g-E_{k'})f^{-}(k')[\,1-f^{+}(k)\,] \\ -(2\pi/\hbar)(N_A/2N^2)\,|J(k'-k)|^2\sum_m^{\pm}\{S(S+1)-m(m+1)\} \\ *W_m^{\pm}\delta(E_k+E_g-E_{k'})f^{+}(k)[\,1-f^{-}(k')\,]\Big\} \\ = (2\pi/\hbar)(N_A/2N^2)\,|J(k'-k)|^2\sum_m^{\pm}\{S(S+1)-m(m+1)\} \\ *\delta(E_k+E_g-E_{k'})\{\,W_{m+1}^{\pm}f^{-}(k')[1-f^{+}(k)] \\ -W_m^{\pm}f^{+}(k)[1-f^{-}(k')]\,\}$$

It can easily be shown, using I, that

$$W_{m+1}^{\pm}f^{-}(E_{k'})[1-f^{+}(E_k)] - W_m^{\pm}f^{+}(E_k)[1-f^{-}(E_{k'})] \\ = W_m^{\pm}[\partial f_o(E_k)/\partial E_k][\,1-f_o(E_{k'})/1-f_o(E_k)\,] \\ *\{\hbar k_x\phi^{+}(E_k)-k'_x\phi^{-}(E_{k'})\,\}$$

Substituting this result

$$[\partial f^{+}/\partial t]_{IN} = \sum_{k'}(2\pi/\hbar)(N_A/2N^2)\,|J(k'-k)|^2\sum_m^{\pm}\{S(S+1)-m(m+1)\} \\ *\delta(E_k+E_g-E_{k'})W_m^{\pm}[\partial f_o(E_k)/\partial E_k] \\ *[\,1-f_o(E_{k'})/1-f_o(E_k)\,] \\ *\{\hbar k_x\phi^{+}(E_k)-k'_x\phi^{-}(E_{k'})\,\}$$

Replacing the summation over k' by an integration (assuming $k-k' = k(1-\cos\theta)$ and $J(k'-k) = [2k\sin(\theta/2)]$ due to the fact that only electrons at the Fermi surface take part in conduction)

$$
\begin{aligned}
[\partial f^{+}/\partial t]_{IN} = {} & (V/8\pi)^3 \iiint (2\pi/\hbar)(N_A/2N^2)\,|J[2k\sin(\theta/2)]|^2 \\
& \sum_m^{\pm}\{S(S+1)-m(m+1)\}\delta(E_k+E_q-E_{k'})W_m^{\pm} \\
& *[\partial f_o(E_k)/\partial E_k][1-f_o(E_{k'})/1-f_o(E_k)]\; k_x\mathcal{E} \\
& *\{\phi^{+}(E_k)-\cos\theta\;\phi^{-}(E_{k'})\}k'^2\sin\theta\; dk'd\theta d\phi \\
= {} & (1/4\pi\hbar)(N_A/N)(V/N)(2M/\hbar^2)^{3/2}k_x\mathcal{E} \\
& *\sum_m^{\pm}\{S(S+1)-m(m+1)\}W_m^{\pm} \\
& *(1/2)\iint |J[2k\sin(\theta/2)]|^2 \\
& *[\partial f_o(E_k)/\partial E_k)][1-f_o(E_{k'})/1-f_o(E_k)] \\
& *\{\phi^{+}(E_k)-\cos\theta\;\phi^{-}(E_{k'})\}E_{k'}^{1/2}\sin\theta\; dE_{k'}\,d\theta \\
= {} & (1/4\pi\hbar)(N_A/N)(V/N)(2M/\hbar^2)^{3/2}k_x\mathcal{E} \\
& *[\partial f_o(E_k)/\partial E_k]E_k^{1/2}\sum_m^{\pm}\{S(S+1)-m(m+1)\} \\
& *W_m^{\pm}[1-f_o(E_k+E_q)/1-f_o(E_k)] \\
& *(1/2)\int |J[2k\sin(\theta/2)]|^2 \\
& *\{\phi^{+}(E_k)-\cos\theta\;\phi^{-}(E_k)\}\sin\theta d\theta \\
= {} & (1/4\pi\hbar)(N_A/N)(V/N)(2M/\hbar^2)^{3/2}k_x\mathcal{E} \\
& *[\partial f_o(E_k)/\partial E_k]E_k^{1/2}\sum_m^{\pm}\{S(S+1)-m(m+1)\} \\
& *W_m^{\pm}[1-f_o(E_k+E_q)/1-f_o(E_k)] \\
& *\{(1/2)\int |J[2k\sin(\theta/2)]|^2\sin\theta d\theta\;\phi^{+}(E_k) \\
& -(1/2)\int |J[2k\sin(\theta/2)]|^2\cos\theta\sin\theta d\theta\;\phi^{-}(E_k)\}
\end{aligned}
$$

If one assumes the electrons to possess an equilibrium Fermi-Dirac distribution then

$$
\begin{aligned}
&[1-f_o(E_k+E_q)/1-f_o(E_k)] \\
&\quad = \{\ 1-(\ \exp[E_k+E_q-E_F/Kt]+1\ )^{-1}\ \} \\
&\quad\ *\{\ 1-(\ \exp[E_k-E_F/Kt]+1\ )^{-1}\ \}^{-1} \\
&\quad = \{\ \exp[E_k+E_q-E_F/Kt]\ \} \\
&\quad\ *\{\ \exp[E_k+E_q-E_F/Kt]+1\ \}^{-1} \\
&\quad\ *\{\ \exp[E_k-E_F/Kt]\ \}^{-1} \\
&\quad\ *\{\ \exp[E_k-E_F/Kt]+1\ \} \\
&\quad = \exp[E_q/Kt]\{\ \exp[E_k-E_F/Kt]+1\ \} \\
&\quad\ *\{\ \exp[E_k+E_q-E_F/Kt]+1\ \}^{-1}
\end{aligned}
$$

Thus,

$$
\begin{aligned}
[\partial f^+/\partial t]_{IN} = {} & (1/4\pi\hbar)(N_A/N)(V/N)(2M/\hbar^2)^{3/2}k_x\mathcal{E} \\
& *[\partial f_o(E_k)/\partial E_k]E_k^{1/2}\sum_m^{\pm}\{S(S+1)-m(m+1)\} \\
& *W_m^{\pm}\exp[E_q/Kt]\{\ \exp[(E_k-E_F)/Kt]+1\ \} \\
& *\{\ \exp[(E_k+E_q-E_F)/Kt]+1\ \}^{-1} \\
& *\{\ (1/2)\int |J[2k\sin(\theta/2)]|^2 \sin\theta d\theta\ \phi^+(E_k) \\
& -(1/2)\int |J[2k\sin(\theta/2)]|^2 \cos\theta\sin\theta d\theta\ \phi^-(E_k)\ \}
\end{aligned}
$$

Similarly, it can be shown that

$$
\begin{aligned}
[\partial f^-/\partial t]_{IN} = {} & (1/4\pi\hbar)(N_A/N)(V/N)(2M/\hbar^2)^{3/2}k_x\mathcal{E} \\
& *[\partial f_o(E_k)/\partial E_k]E_k^{1/2}\sum_m^{\pm}\{S(S+1)-m(m+1)\} \\
& *W_m^{\pm}\{\ \exp[(E_k-E_F)/Kt]+1\ \} \\
& *\{\ \exp[(E_k-E_q-E_F)/Kt]+1\ \}^{-1} \\
& *\{\ (1/2)\int |J[2k\sin(\theta/2)]|^2 \sin\theta d\theta\ \phi^-(E_k) \\
& -(1/2)\int |J[2k\sin(\theta/2)]|^2 \cos\theta\sin\theta d\theta\ \phi^+(E_k)\ \}
\end{aligned}
$$

Substituting $[\partial f^{\pm}/\partial t]_{EL}$, $[\partial f^{+}/\partial t]_{IN}$ and $[\partial f^{-}/\partial t]_{IN}$ into the Boltzman equation (putting $E_k = E_F$) gives two simultaneous equations for $\phi^{\pm}(E_F)$. The first is

$$
\begin{aligned}
&[\partial f_o(E_F)/\partial E_F](\hbar k_X/M)e\mathcal{E} + (1/4\pi\hbar)(N_A/N)(V/N)(2M/\hbar^2)^{3/2} \\
&*E_F^{1/2}k_X\mathcal{E}[\partial f_o(E_F)/\partial E_F]\phi^{+}(E_F)\sum_m^{\pm}W_m^{\pm} \\
&*(1/2)\int |V[2k\sin(\theta/2)]-mJ[2k\sin(\theta/2)]|^2 \\
&*(1-\cos\theta)\sin\theta d\theta \\
&+ (1/4\pi\hbar)(N_A/N)(V/N)(2M/\hbar^2)^{3/2}k_X\mathcal{E} \\
&*[\partial f_o(E_F)/\partial E_F]E_F^{1/2}\sum_m^{\pm}\{S(S+1)-m(m+1)\} \\
&*W_m^{\pm}\{2\exp[E_q/Kt]\}\{\exp[E_q/Kt]+1\}^{-1} \\
&*\{(1/2)\int |J[2k\sin(\theta/2)]|^2\sin\theta d\theta\ \phi^{+}(E_F) \\
&-(1/2)\int |J[2k\sin(\theta/2)]|^2\cos\theta\sin\theta d\theta\ \phi^{-}(E_F)\} \\
&= 0
\end{aligned}
$$

Or,

$$
\begin{aligned}
&(\hbar e/M) + (1/4\pi\hbar)(N_A/N)(V/N)(2M/\hbar^2)^{3/2}E_F^{1/2} \\
&*\Big\{\sum_m^{\pm}\{S(S+1)-m(m+1)\}W_m^{\pm}\{2\exp[E_q/Kt]\} \\
&*\{\exp[E_q/Kt]+1\}^{-1}[A\phi^{+}(E_F)-B\phi^{-}(E_F)] \\
&*[\sum_m^{\pm}m^2W_m^{\pm}D-2\sum_m^{\pm}mW_m^{\pm}F+\sum_m^{\pm}W_m^{\pm}G]\phi^{+}(E_F)\Big\} = 0
\end{aligned}
$$

where

$$A = (1/2)\int |J[2k\sin(\theta/2)]|^2\sin\theta d\theta$$

$$B = (1/2)\int |J[2k\sin(\theta/2)]|^2\cos\theta\sin\theta d\theta$$

$$D = A-B$$

$$F = (1/2)\int J[2k\sin(\theta/2)]V[2k\sin(\theta/2)](1-\cos\theta)\sin\theta d\theta$$

$$G = (1/2)\int |V[2k\sin(\theta/2)]|^2 (1-\cos\theta)\sin\theta d\theta$$

Similarly, the second is given by

$$(\hbar e/M) + (1/4\pi\hbar)(N_A/N)(V/N)(2M/\hbar^2)^{3/2} E_F^{1/2}$$
$$*\Big\{ \sum_m^{\pm}\{S(S+1)-m(m+1)\}W_m^{\pm}\{\ 2\exp[E_q/Kt]\ \}$$
$$*\{\ 1+\exp[E_q/Kt]\ \}^{-1}[\ A\phi^-(E_F)-B\phi^+(E_F)\ ]$$
$$+\ [\sum_m^{\pm} m^2 W_m^{\pm} D+2\sum_m^{\pm} m W_m^{\pm} F+\sum_m^{\pm} W_m^{\pm} G\ ]\phi^-(E_F)\Big\} = 0$$

Solving these two equations for $[\phi^+(E_F)+\phi^-(E_F)]^{-1}$ gives

$$[\phi^+(E_F)+\phi^-(E_F)]^{-1} = -(M/8\pi e\hbar^2)(N_A/N)(V/N)(2M/\hbar^2)^{3/2} E_F^{1/2}$$
$$* \Big\{ 2G+D[\ \sum_m^{\pm} m^2 W_m^{\pm}+\sum_m^{\pm}\{S(S+1)-m(m+1)\}$$
$$*W_m^{\pm}\{\ 1+\tanh(E_q/Kt)\ \}\ ]$$
$$-\ [\ 4F^2(\sum_m^{\pm} m W_m^{\pm})^2\ ][\ 2G+D\sum_m^{\pm} m^2 W_m^{\pm}$$
$$+(A+B)\sum_m^{\pm}\{S(S+1)-m(m+1)\}$$
$$*W_m^{\pm}\{\ 1+\tanh(E_q/Kt)\ \}\ ]^{-1}\ \Big\}$$

1.9 THE WORKING FORM OF THE RESISTIVITY EQUATION

The equation for the anomalous resistivity in dilute manganese doped platinum samples was previously found to be given by the expression

$$\rho = -(6\pi^2/e)(\hbar/E_F^{3/2})(\hbar^2/2M)^{3/2}[\phi^+(E_F)+\phi^-(E_F)]^{-1}$$

Making the substitution for $[\phi^+(E_F)+\phi^-(E_F)]^{-1}$,

$$\rho = (3\pi/4)(M/e^2)(1/\hbar E_F)(V/N)(N_A/N)\left\{ 2G \right.$$
$$+D[\sum_m^{\pm} m^2 W_m^{\pm} + \sum_m^{\pm}\{S(S+1)-m(m+1)\}$$
$$*W_m^{\pm}\{\ 1+\tanh(E_q/Kt)\ \}\ ] - 4(\sum_m^{\pm} m W_m^{\pm})^2 F^2$$
$$*[\ 2G+D\sum_m^{\pm} m^2 W_m^{\pm} + (A+B)\sum_m^{\pm}\{S(S+1)-m(m+1)\}$$
$$\left. *W_m^{\pm}\{\ 1+\tanh(E_q/Kt)\ \}\ ]^{-1} \right\}$$

As can be seen from its definition, the coefficient G arises from the purely spin-independant interaction (due to its independance of J); D, A and B, on the other hand, come from the purely spin-dependant interaction. The coefficient F is a result of the cross term of the two interactions.

If J(k,k') and V(k,k') are assumed to be isotropic - independant of k and k' - the coefficients A, B, D, F and G can all be simplified. For instance,

$$A = (1/2)\int |J[2k\sin(\theta/2)]|^2 \sin\theta d\theta$$
$$= (1/2)J^2\int \sin\theta d\theta$$
$$= -(1/2)J^2\cos\theta \Big/_0^{\pi}$$
$$= J^2$$

Similarly, it can be shown that in the isotropic limit,

$$B = 0$$

$$D = J^2$$

$$F = VJ$$

$$G = V^2$$

Experimentally, it has been found that, in the presence of an external magnetic field, the total magnetization of the Mn spins vanish, these spins tending to order antiferromagnetically. Thus, $\sum_m^{\pm} mW_m^{\pm} = 0$. With these two simplifications,

$$\begin{aligned}
\rho(H,t) &= \rho(0,t) \\
&= (3\pi/4)(M/e^2)(1/\hbar E_F)(V/N)(N_A/N) \\
&\quad * \left\{ 2V^2+J^2[\sum_m^{\pm} m^2 W_m^{\pm} + \sum_m^{\pm} \{S(S+1)-m(m+1)\} W_m^{\pm}] \right\} \\
&= (3\pi/4)(M/e^2)(1/\hbar E_F)(V/N)(N_A/N) \\
&\quad *[\ 2V^2+J^2\{\sum_m^{\pm} m^2 W_m^{\pm} + \sum_m^{\pm} S(S+1) W_m^{\pm} \\
&\quad -\sum_m^{\pm} m^2 W_m^{\pm} - \sum_m mW_m^{\pm}\}\ ] \\
&= (3\pi/4)(M/e^2)(1/\hbar E_F)(V/N)(N_A/N) \\
&\quad *[\ 2V^2+J^2 S(S+1) \sum_m^{\pm} W_m^{\pm}\ ] \\
&= (3\pi/4)(M/e^2)(1/\hbar E_F)(V/N)(N_A/N) \\
&\quad *[\ 2V^2+2J^2 S(S+1)\ ]
\end{aligned}$$

In the presence of an external field H, all the Mn spins tend to align, the probability W_m that m takes on a value of S or -S being one. Thus,

$$\begin{aligned}
\rho(H,t) = (3\pi/4)(M/e^2)(1/\hbar E_F)(V/N)(N_A/N) \Big\{ & 2V^2 \\
& +J^2[\ 2S^2+2S\{1+\tanh(E_q/Kt)\}\ ] - 16S^2V^2J^2 \\
& *[\ 2V^2+2S^2J^2+2J^2S\{1+\tanh(E_q/Kt)\}\ ]^{-1} \Big\}
\end{aligned}$$

Measurements of $\Delta\rho(H,t) = \rho(0,t)-\rho(H,t)$ were made on the dilute Pt-Mn samples. Theoretically, this quantity is given by

$$\Delta\rho(H,t) = \rho(0,t)-\rho(H,t)$$

$$= (3\pi/4)(M/e^2)(1/\hbar E_F)(V/N)(N_A/N)$$
$$*[\ 2V^2+2J^2S^2+2J^2S\ ]$$
$$-\ (3\pi/4)(M/e^2)(1/\hbar E_F)(V/N)(N_A/N)$$
$$*[\ 2V^2+2J^2S^2+2J^2S+2J^2S\ \tanh(E_q/Kt)$$
$$-8S^2V^2J^2\{V^2+S^2J^2+J^2S+J^2S\ \tanh(E_q/Kt)\}^{-1}]$$

$$= (3\pi/2)(M/e^2)(1/\hbar E_F)(V/N)(N_A/N)$$
$$*[\ -J^2S\ \tanh(E_q/Kt)+4V^2J^2S^2 \qquad X$$
$$*\{V^2+J^2S^2+J^2S+J^2S\ \tanh(E_q/Kt)\}^{-1}]$$

This is the working form of the equation for the anomalous resistance of dilute manganese doped platinum.[8] It states that the difference between the alloy resistivity measured in zero field and that in an applied field H is a unique function of H/t (assuming lattice resistivity is not affected by the applied field and is therefore subtracted out of $\Delta\rho(H,t)$).

Chapter II

EXPERIMENTAL

2.1 INTRODUCTION

The resistivity, as a function of temperature, of dilute manganese doped platinum samples was determined using a multi-step method which involved both direct and alternating current measurements. Resistances were found by measuring the voltage drop across a sample carrying a known fixed current. The form factor (cross-sectional area to length ratio) of each specimen was measured and used along with these resistances to calculate the actual resistivity values.

$$\rho = R\ (A/L)$$

where ρ is the resistivity, R the resistance, A the cross-sectional area and L the length of the sample. The actual voltage drop at 4.2K of each sample was found using a standard four probe direct current technique.[9] Small changes in sample voltage, due to the variation of temperature, were monitored using an AC difference method; when used in

conjunction with the DC measurements, exact absolute voltage drops, at all temperatures of interest, could be calculated. Specimens were mounted in the core of a superconducting magnet so as to enable one to study the effect of a magnetic field on resistivity.

2.2 SAMPLE PREPARATION

Measurements were made on four samples of platinum, one pure, the other three containing manganese impurities of concentration .05, .10 and .15 atomic percent. These samples were prepared by melting together appropriate amounts of pure platinum (99.9999 % pure spectroscopy grade wire supplied by Leico Industries N.Y. and manufactured by Samuel Cohen and Co.) and manganese (99.99 % pure flake produced by Johnson-Matthey U.K.) in an argon arc furnace; this furnace was equipped with a water cooled copper hearth. To ensure homogeneity, the samples were inverted and remelted several times. Melting loses were negligibly small. The ensuing button-shaped alloys (approx. weight being 5 grams) were then cold rolled between Melinex sheets (so as to prevent contamination of samples by the rollers) and cut into long, thin specimens (sample lengths were approximately 10 cms.; typical values for width and thickness were .2 cms. and .02

cms. respectively). Because of their dilute nature, the Pt-Mn samples were assumed to possess a lattice spacing and crystal structure (f.c.c.) identical to that of pure Pt. Justification of this is provided in the phase diagram of figure 9.[10] Small form factors (cross-sectional area to length ratios) were used so as to yield convenient resistance values (of the order of .001 Ω). The final steps in the preparation process involved etching the samples in an acid mixture (1 part nitric acid, 3 parts hydrochloric acid and 1 part water) to remove any surface contamination and their exposure to a strain relieving anneal at 2×10^{-6} mm. of Hg and 577°C for 25.5 hours.

2.3 RESISTANCE MEASUREMENTS

As mentioned above, both AC and DC measurements were utilized in determining the voltage drop across a particular sample at a number of different temperatures. The former technique proves to be more accurate in determining small voltage differences. A single frequency alternating current (37 hz.) from a General Radio 1311-A audio oscillator is sent through both the sample under observation and a series connected variable adjusted resistance (Kelvin Varley type DP1211). The voltage difference between the two is then fed

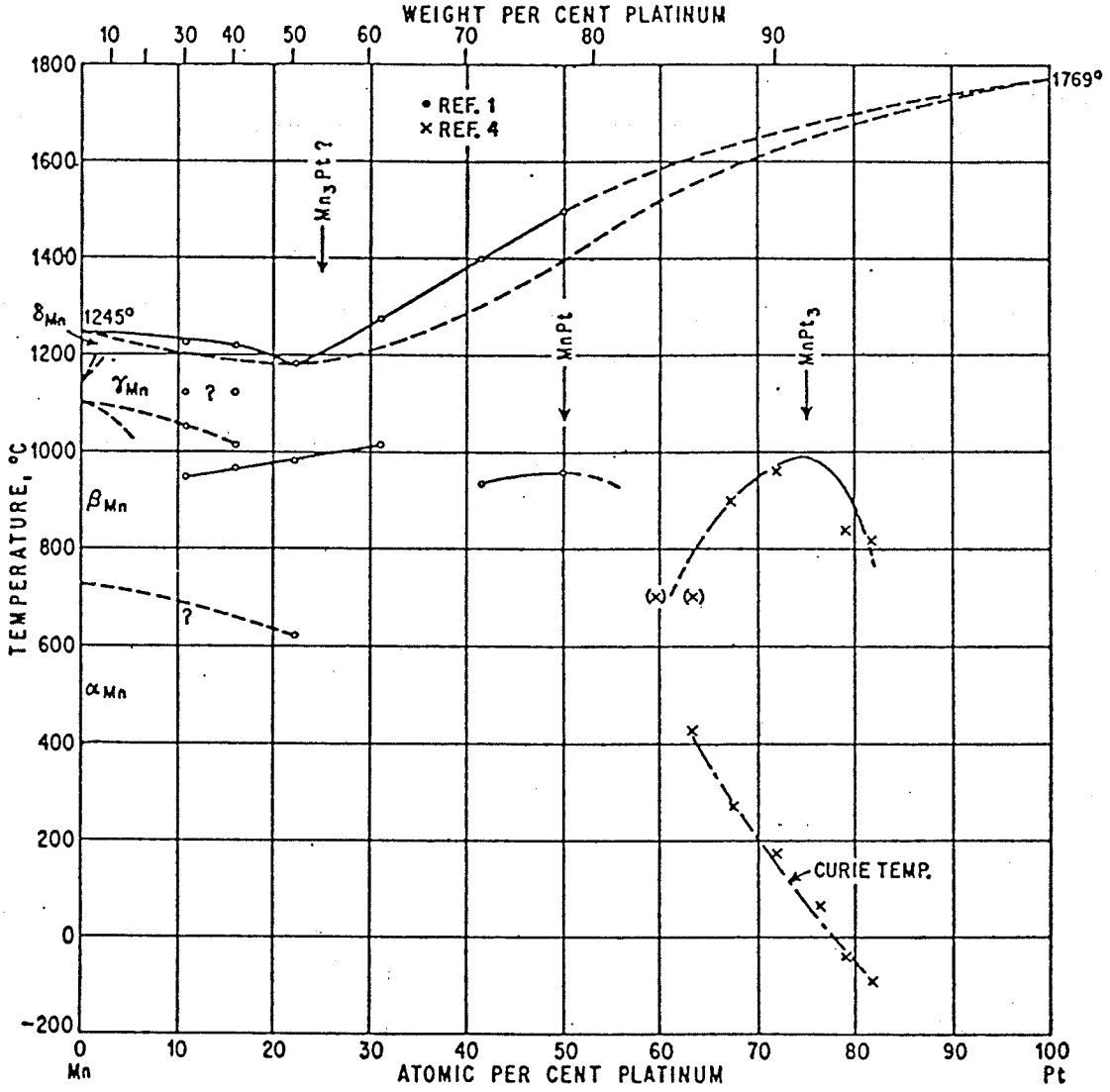

Figure 9: Platinum-Manganese phase diagram.

into a lock-in amplifier (Princeton Applied Research model HR-8) tuned to the driving frequency of the oscillator and monitored (via a ±10 V. output from the lock-in amplifier); because of the variable nature of the series resistance used, this difference can be kept small. The variation of this signal with small changes in sample temperature can then be observed. Any small current fluctuations have a negligible effect on the system. The basic circuit used in these measurements is shown in figure 10.

The presence of thermal emfs make the observation of small voltage changes very difficult when using the traditional four-terminal DC method. However, because it is found to be far more accurate than its counterpart when dealing with absolute voltage measurements, such a technique was employed for finding the absolute voltage drop across a sample at liquid helium's boiling temperature, 4.2K (once this voltage was known, it could be used in conjunction with the AC measurements to calculate absolute voltage drops at all temperatures of interest). The four probe technique is illustrated in figure 11. A Guideline constant current source (model 9770 B), stable to 1 part in 10^6, provides the highly stable direct current necessary. Sample selection (samples were simultaneously mounted in the apparatus and series connected) was carried out using a Guideline low thermal selector switch (model 9145 A10); it applied the voltage drop across the sample under consideration to a

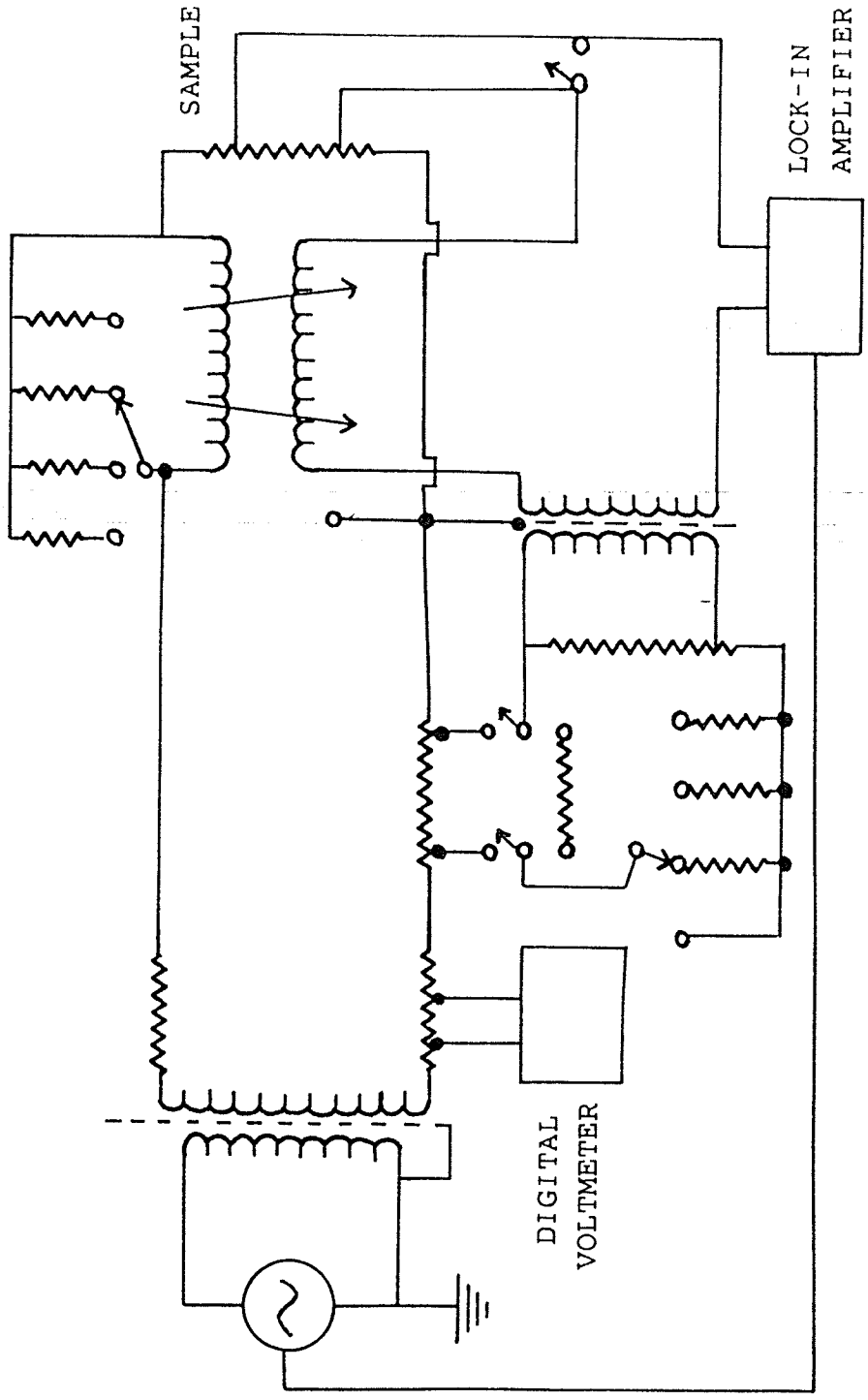

Figure 10: Circuit utilized in making AC measurements.

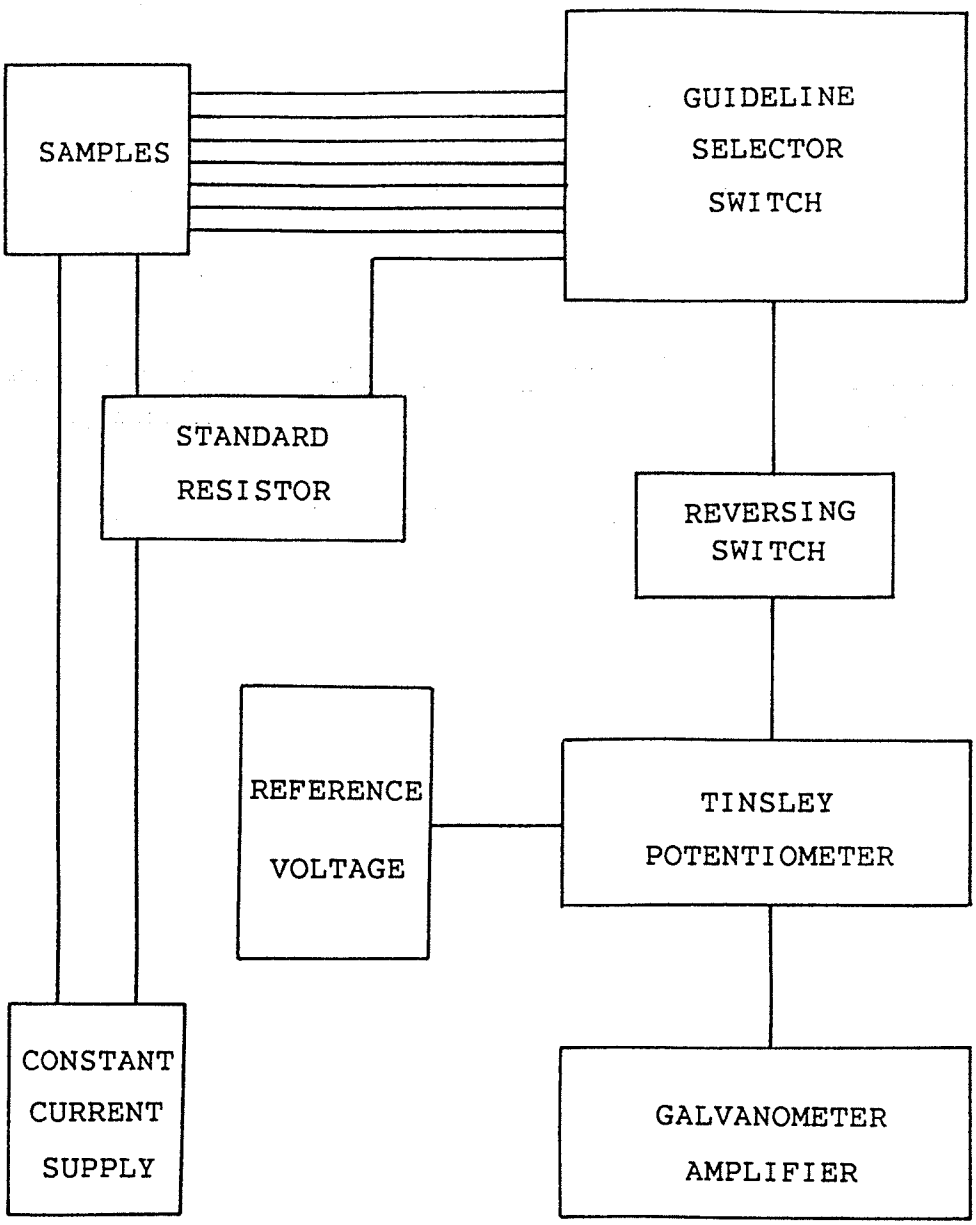

Figure 11: Schematic of the circuit used in the four-terminal DC method of measuring voltages.

Tinsley Diesselhorst thermoelectric free potentiometer (type 3589 R) in combination with a Tinsley photocell galvanometer amplifier (type M.S.2 45E). This potentiometer-galvanometer unit was capable of reproducible measurement to 10^{-8} volts. Voltages were determined for both direct and reverse sample current and average values were used; such a procedure, if carried out quickly, resulted in the cancellation of any thermally induced voltages which might have been present due to small temperature inhomogeneities in the samples. The current through the doped platinum strips was determined by measuring the voltage drop it produced across a .10 Ω Guideline standard resistor (model 9200) connected in series with the specimans.

2.4 CRYOGENIC EQUIPMENT

The four samples studied were mounted on a high thermal conductivity copper block so as to ensure temperature homogeneity. Each platinum strip actually rested on two knife edge supports (one at each end of the sample) which were insulated electrically but not thermally from the copper block (see figure 12). The copper block was lowered into a canister known as the sample space.

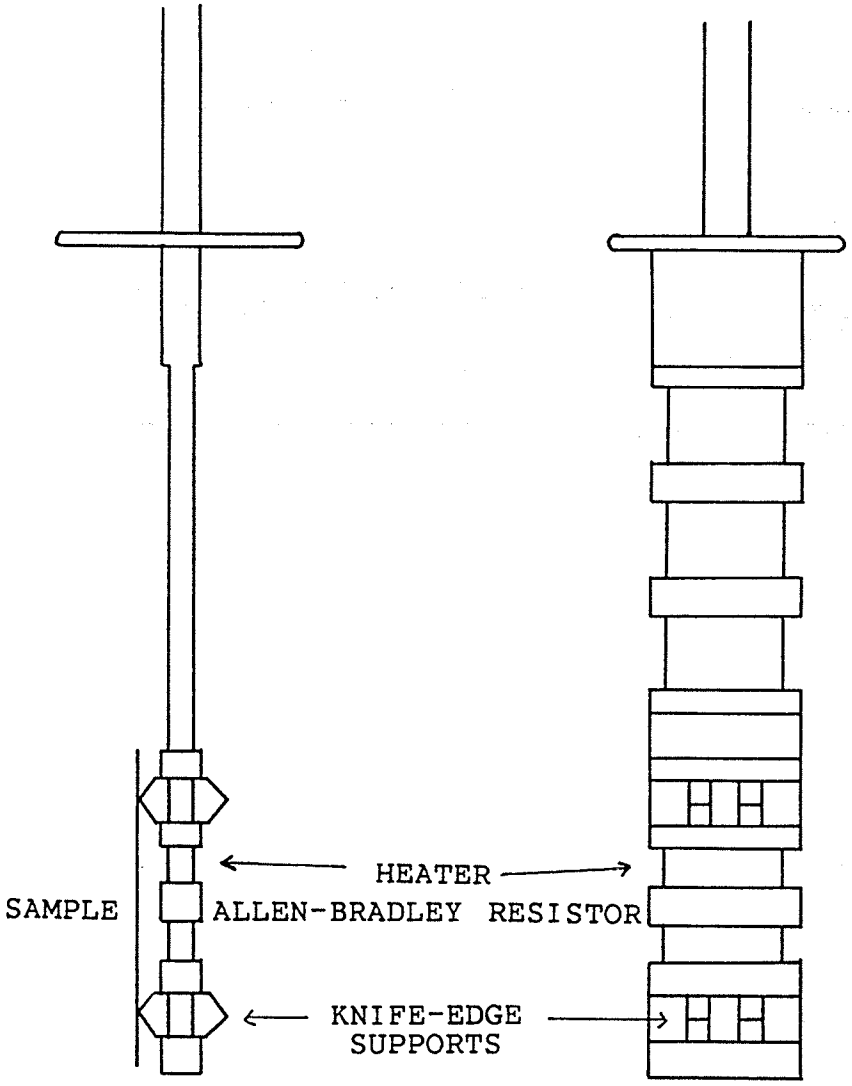

Figure 12: Copper block sample mount.

Directly surrounding the sample space was a gas thermometer bulb. This in turn was encased by the main vacuum space of the system and a liquid He^4 bath (see figure 13). When the main vacuum space is filled with He^4 gas at a pressure below atmospheric, the bath is in good thermal contact with the sample space, lowering the temperature of the copper block to 4.2K. Helium is then pumped into the sample space to a pressure above atmospheric so that it condenses to form a liquid in direct contact with the specimens. Once condensation is complete and the system has stabilized, temperature could be regulated using the vacuum system shown in figure 13. By evacuating the main vacuum space and pumping on the liquid helium directly surrounding the samples, temperatures below 4.2K (down to approx. 1K) could be achieved; manual regulation of the pumping speed enabled pressure and therefore temperature stabilization. Manometers were used to obtain an accurate He^4 vapor pressure reading when making measurements on all but the Pt+.15 at.% Mn sample. Vapor pressures for the above mentioned specimen were determined using a Datametrics electronic pressure sensor (type 590 Barocel). This device gave voltage readings which were directly proportional to the sample space pressure. These pressure values were then converted to temperatures using standard tables.

Sample temperatures were raised above 4.2K with a small heater coil wound around the copper mounting block. When working above 4.2K, He^4 is not condensed into the sample

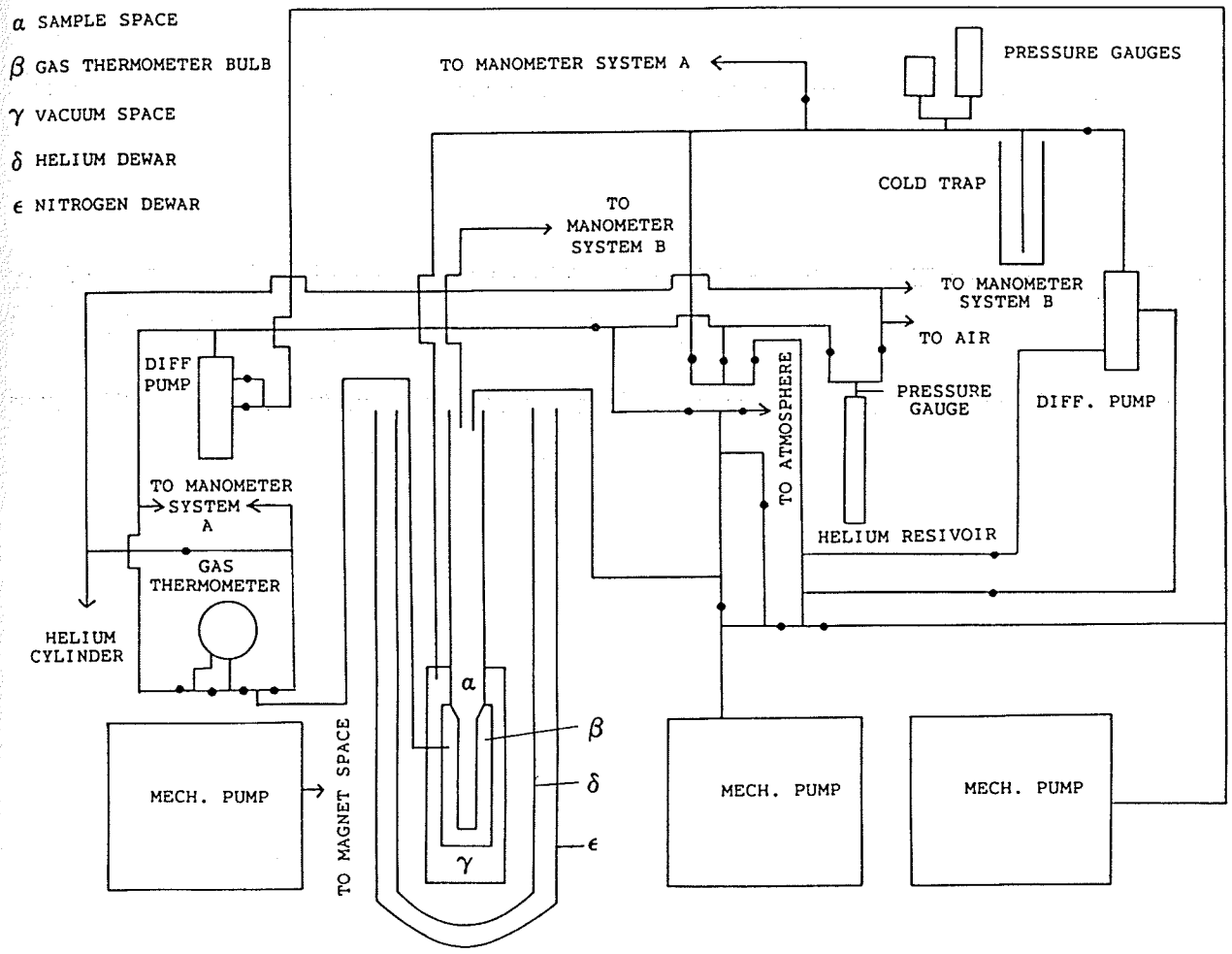

Figure 13: Vacuum system flow diagram.

space. Instead, it is filled with gaseous He^4 to a pressure of about 200 microms of mercury. The main vacuum space (the region between the liquid helium bath and the gas thermometer bulb) serves to couple thermally the helium bath and the gas thermometer-sample combination. The pressure in this space is lowered, as one moves up in temperature (at first a rotary pump is used intermitently; at higher temperatures, a rotary pump-diffusion pump system in continual operation is utilized) so as to lessen the coupling between samples and bath and thereby assist in warming. The contact between samples and bath is variable, depending upon the closeness to complete evacuation of the main vacuum space; the less gas this space contains, the lesser the coupling. This variable contact could allow one to decrease the sample temperature by small amounts. Small increases in sample temperature were achieved using an AC phase sensitive Wheatstone bridge, one of its arms being a 100 Ω Allen Bradly carbon resistor in thermal contact with the mounting block (its resistance varied approximately logarithmically with temperature - see figure 14). The bridge was balanced for a certain desired temperature (ie. for the carbon resistor resistance corresponding to the temperature under consideration). Any variation of temperature, and hence resistance, from this setting led to a rectified output current from the bridge. This output was then fed into the heater coil so as to bring the temperature

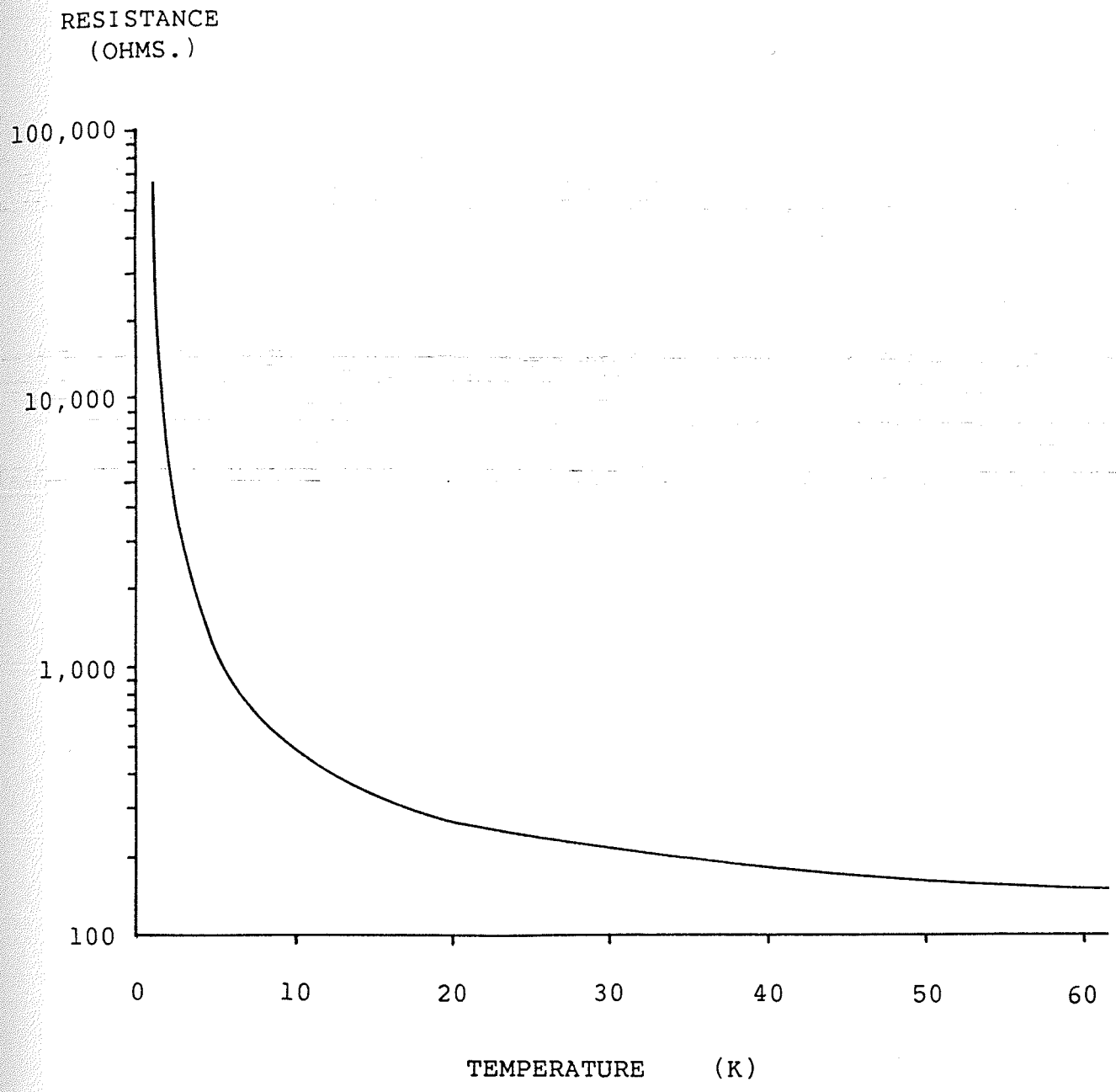

Figure 14: Resistance versus temperature curve of the Allen Bradly carbon resistor.

back up to the desired level. A schematic of the system is shown in figure 15. Temperatures above 4.2K were measured using a nonlinear gas thermometer, its bulb surrounding the sample space. A stainless steel capillary tube connected this bulb to the vacuum system and Wallace and Tierman pressure gauge. Before the samples are lowered to liquid helium temperature, the gas thermometer system is pumped out and then backfilled with He gas at 77K to a pressure of about 75 inches of water. The pressure of the sample space, the main vacuum space and the helium bath can be individually monitored and controlled. A liquid nitrogen dewar placed outside the helium dewar increases the cooling efficiency of the system. Rather than being responsible for lowering the temperature of the system from room temperature to 4.2K, the helium bath in such a set up is only required to lower the temperature below 77K.

2.5 FORM FACTOR

The form factors of the platinum samples were needed so as to enable the conversion of resistance to resistivity. These cross-sectional area to length ratios were determined using a technique described by Loram. The form factor F is given by

$$F = A/L$$

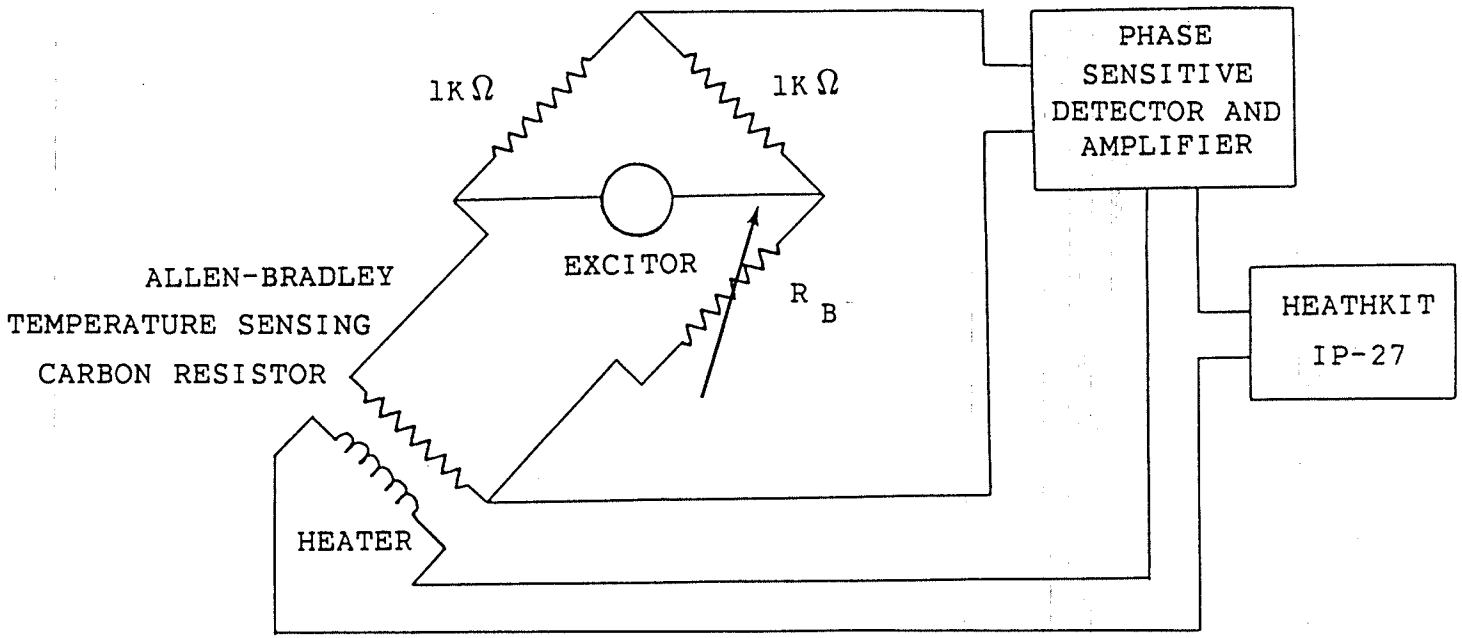

Figure 15: Above 4.2K Wheatstone bridge temperature stabilization system.

where A is the cross-sectional area and L is the length of the sample over which the voltage drop was taken (the knife-edge supports were used for voltage tap-off points; hence, L is the distance between the knife-edge supports used to mount each sample). Multiplying the right side of the above equation by l/l where l is the total length of the sample, one finds

$$F = Al/Ll = V/Ll = M/DLl$$

M being the mass of the sample, V its volume and D its density. This is the working form of the equation. Both L and l were measured using a travelling microscope; in each instance, a number of readings were made and averages taken. The density of all samples were taken to be that of pure platinum, 21.47 g/ml.[3] Hence, measurements of L, l and M enabled one to find F.

Chapter III

DISCUSSION

As mentioned previously, the resistivity vs. temperature curves of Pt+.05 at.% Mn, Pt+.10 at.% Mn and Pt+.15 at.% Mn samples were determined in an indirect fashion in each of five different magnetic field strengths (0, 12.5, 25, 50 and 75 Oe.). A pure platinum specimen was studied in zero field. Using AC techniques, relative sample voltages (relative to a value assigned to that sample, on the basis of convenience and not reflecting its true magnitude, at 4.2K) at a large number of closely spaced temperature points could be measured. The technique used enabled the accurate detection and determination of very small voltage changes, 10^{-9} volts being the reasonable limit. Measurements were taken between 1K and 10K, the step size ranging from .35 to .01K depending on the region of the voltage-temperature curve. A plot of a typical set of relative sample voltage vs. temperature data is shown in figure 16.

An accurate determination of the voltage drop across each sample, at 4.2K and in zero field, was made using a DC four probe technique. Ohm's Law was then utilized to convert these 4.2K voltages to resistances. After measuring sample

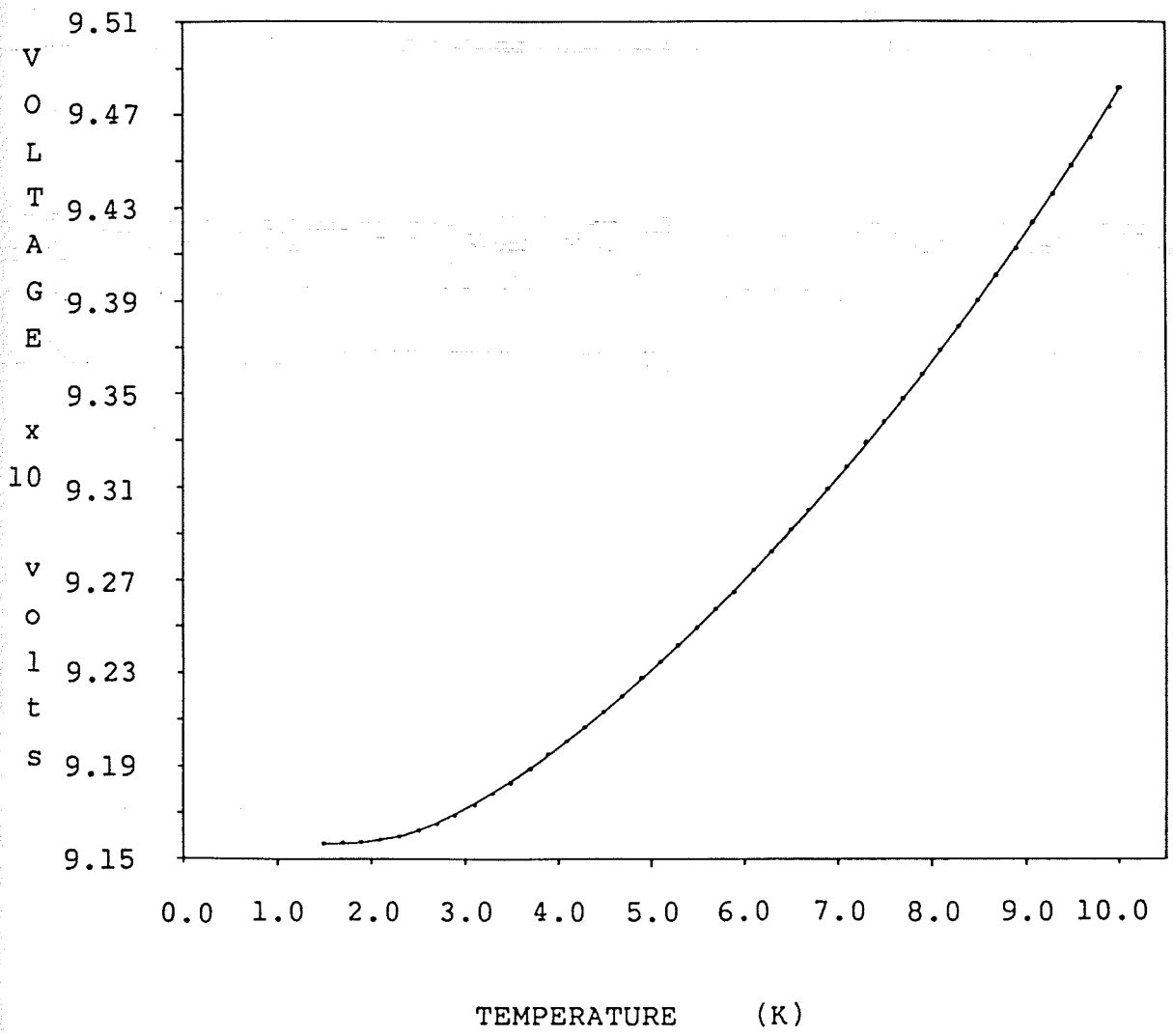

Figure 16: Relative sample voltage vs. temperature plot for Pt+.10 at.% Mn in a 75 Oe. field.

form factors, the resistivity at 4.2K of each specimen could be calculated. Table 1 lists the sample current, the voltage drops, resistances and resistivities at 4.2K, as well as the form factors, of each platinum specimen. Figures 17, 18 and 19 are relative sample voltage vs. magnetic field curves, taken at 4.2K, for the three platinum-manganese alloys. If a specimen's 4.2K voltage is known in zero field, then, by using these graphs, it can be determined for any magnetic field strength. Table 2 gives the 4.2K nonzero field data utilized in the analysis.

From the AC and DC measurements, accurate resistivity values for each temperature sampling point were calculated; five sets of temperature vs. resistivity data $\rho(H,t)$, one for each field strength, were obtained for all three alloys. Figure 20 shows plots of these data sets. As mentioned previously, resistivity measurements were carried out on the pure platinum sample in zero field only. The resistivity vs. temperature curve for this specimen is shown in figure 21. Figure 22 shows the same resistivity data plotted against temperature squared. The result, at low temperature, is a linear curve with a 0K resistivity of .04515 $\mu\Omega$cms and a t^2 coefficient of 20.6 $p\Omega cms K^{-2}$. Similar measurements carried out by Uher, Lee and Bass[11] led to a 0K resistivity of .00177 $\mu\Omega$cms and a t^2 coefficient of 15.4 $p\Omega cms K^{-2}$.

Figures 23, 24 and 25 show plots of $\Delta\rho(0,t) = \rho_{ALLOY}(0,t) - \rho_{Pt}(0,t)$ vs. temperature for the three different alloy

SAMPLE	CURRENT	VOLTAGE	FORM FACTOR	4.2K RESISTANCE	4.2K RESISTIVITY
PURE Pt	61.8347 mA.	10.60 μV.	2.656 cms.	.1714 $\mu\Omega$.	.04551 $\mu\Omega$ cms.
Pt+.05 at.% Mn	61.8460 mA.	58.12 μV.	2.1572 cms.	.9398 $\mu\Omega$.	.20273 $\mu\Omega$ cms.
Pt+.10 at.% Mn	61.8400 mA.	90.81 μV.	2.6055 cms.	1.4685 $\mu\Omega$.	.38262 $\mu\Omega$ cms.
Pt+.15 at.% Mn	61.8370 mA.	106.51 μV.	3.0483 cms.	1.7224 $\mu\Omega$.	.52504 $\mu\Omega$ cms.

TABLE 1

D.C. four probe measurements at 4.2K.

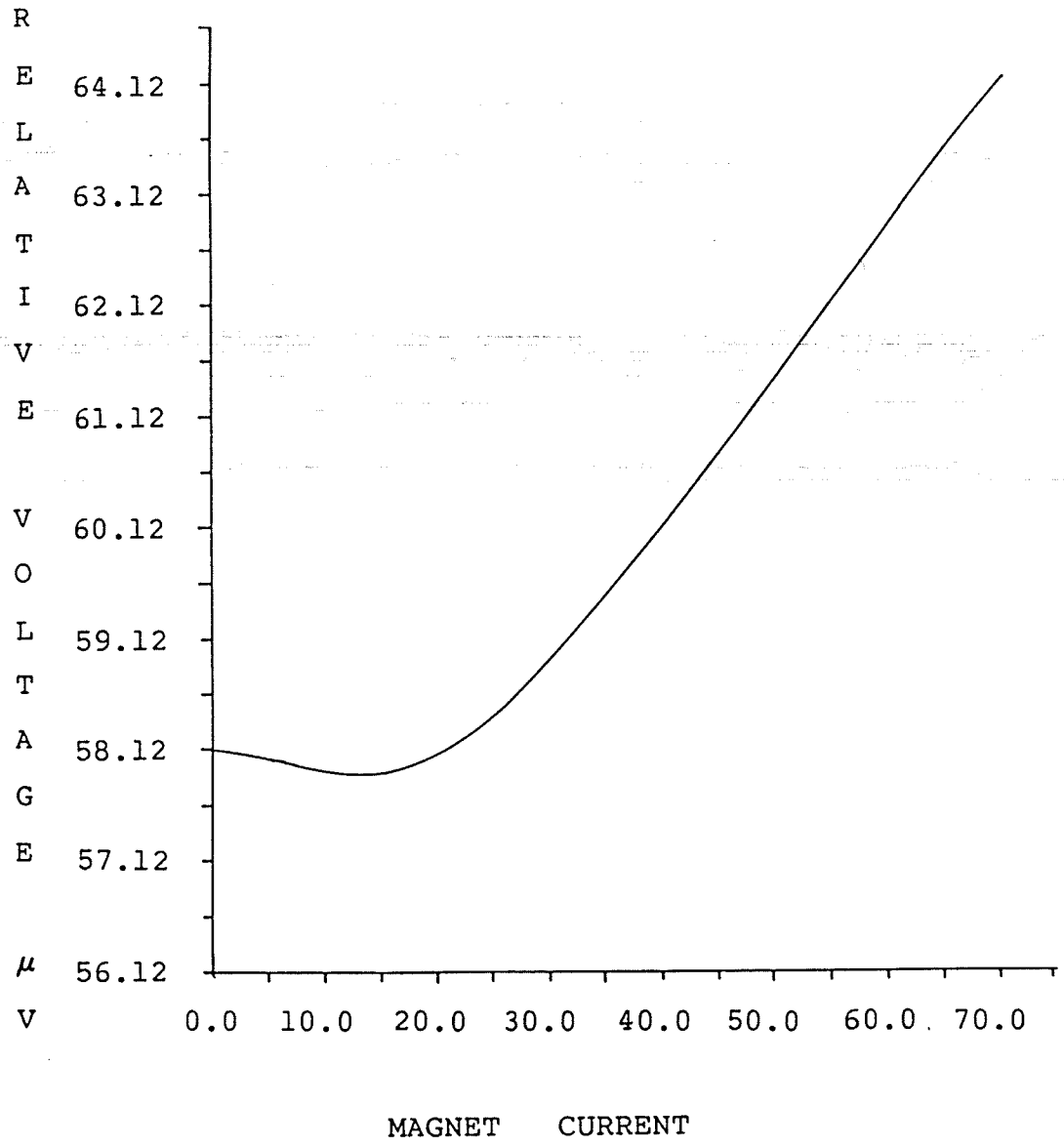

Figure 17: Relative sample voltage vs. magnetic field curve at 4.2K for Pt+.05 at.% Mn.

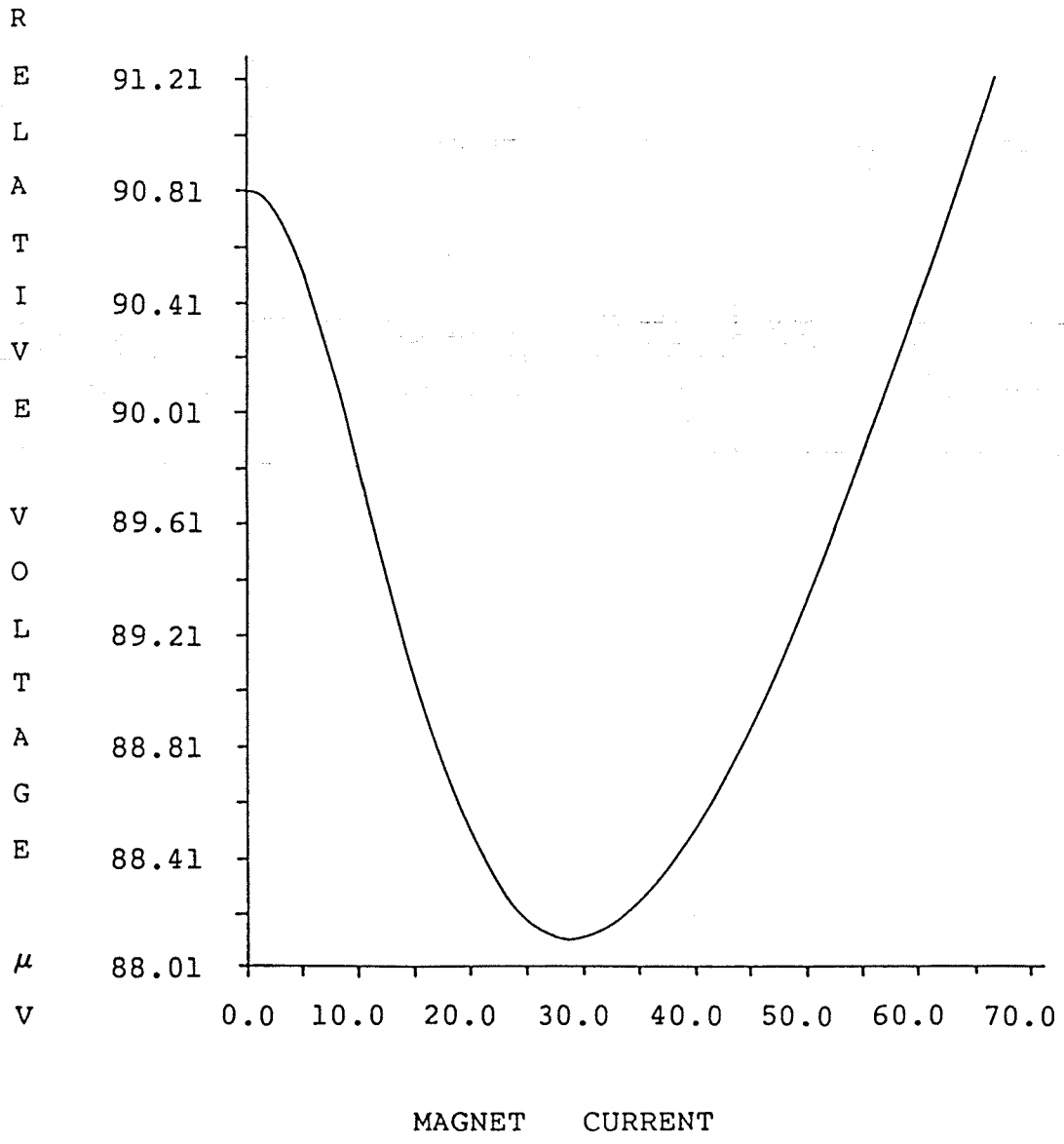

Figure 18: Relative sample voltage vs. magnetic field curve at 4.2K for Pt+.10 at.% Mn.

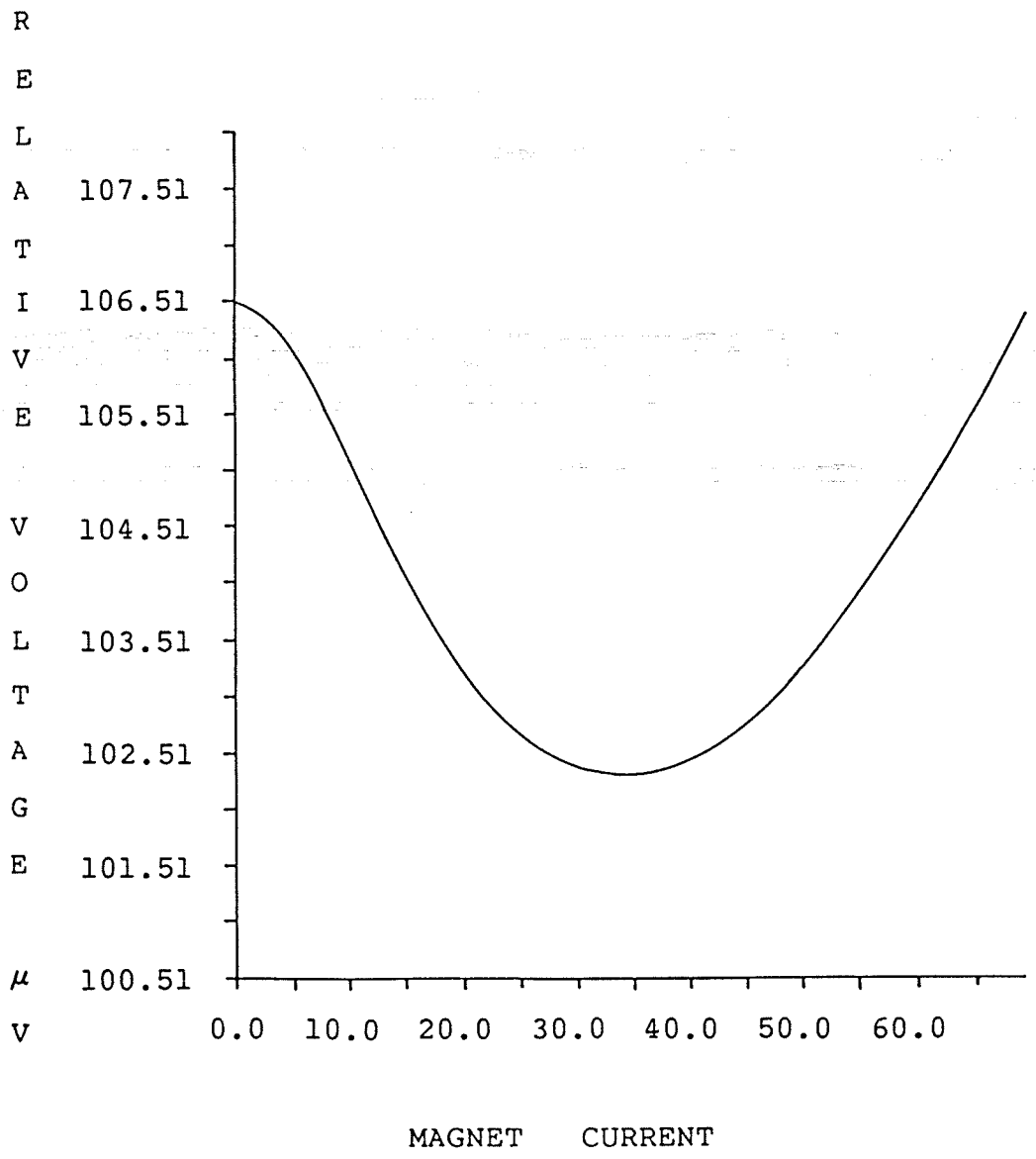

Figure 19: Relative sample voltage vs. magnetic field curve at 4.2K for Pt+.15 at.% Mn.

SAMPLE	4.2K VOLTAGE (0 Oe.)	4.2K VOLTAGE (12.5 Oe.)	4.2K VOLTAGE (25 Oe.)	4.2K VOLTAGE (50 Oe.)	4.2K VOLTAGE (75 Oe.)
Pt+.05 at.% Mn	58.12 μV.	57.92 μV.	58.12 μV.	60.31 μV.	63.09 μV.
Pt+.10 at.% Mn	90.81 μV.	89.73 μV.	88.42 μV.	88.63 μV.	90.69 μV.
Pt+.15 at.% Mn	106.51 μV.	104.98 μV.	103.11 μV.	102.54 μV.	105.09 μV.

TABLE 2

4.2K nonzero field resistivity data.

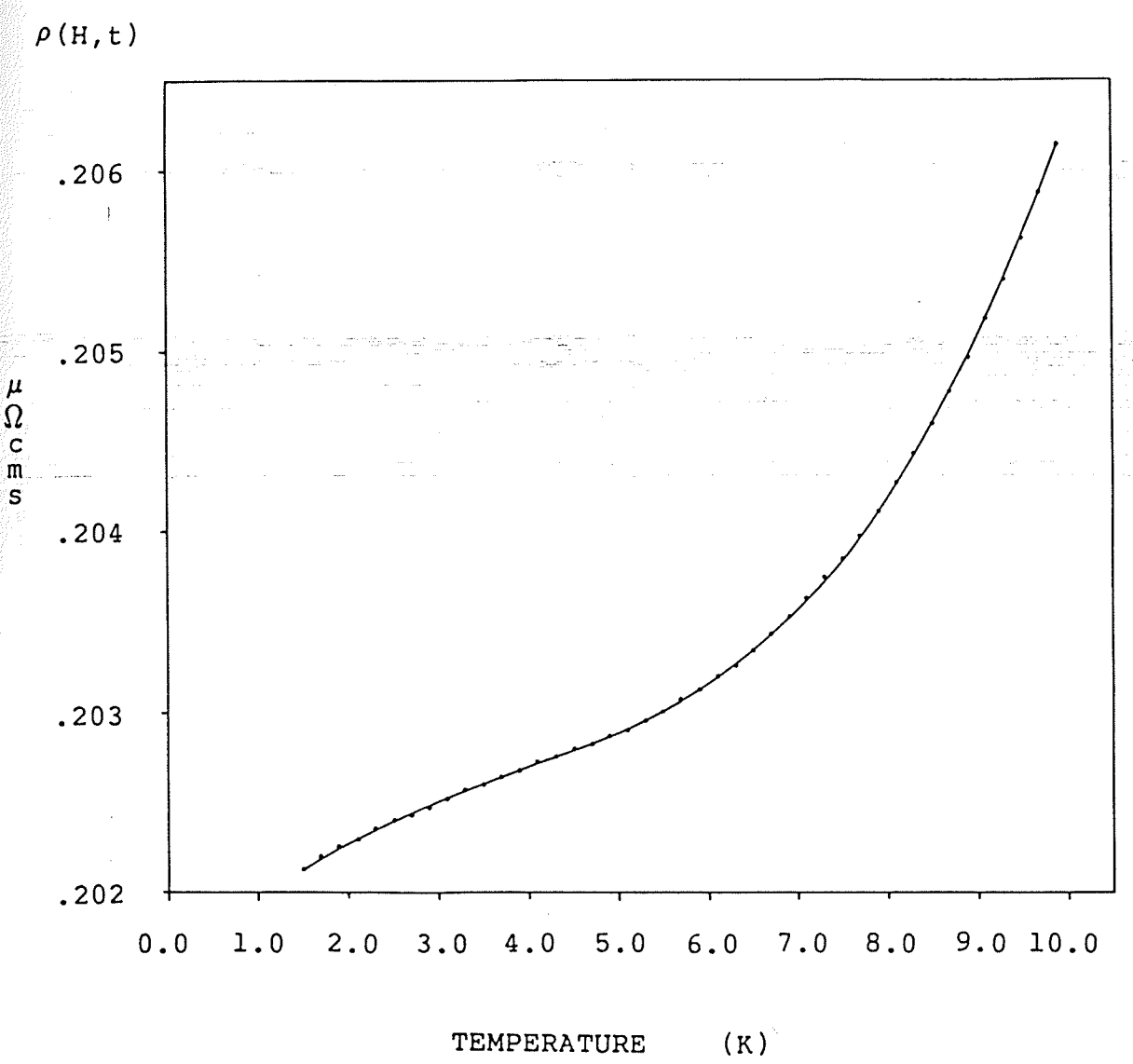

Figure 20: A) Resistivity vs. temperature curve for Pt+.05 at.% Mn in zero field.

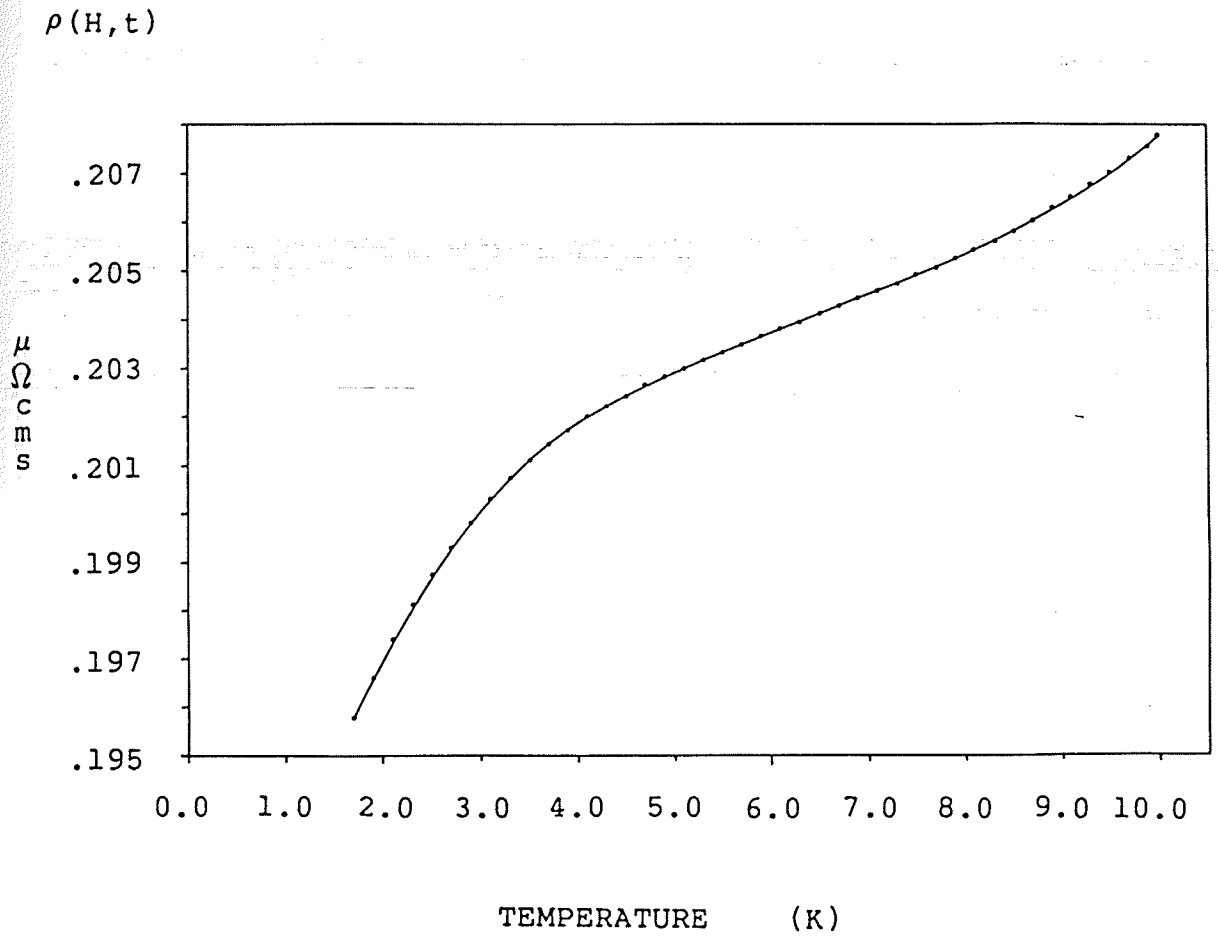

Figure 20: B) Resistivity vs. temperature curve for Pt+.05 at.% Mn in a 12.5 Oe. field.

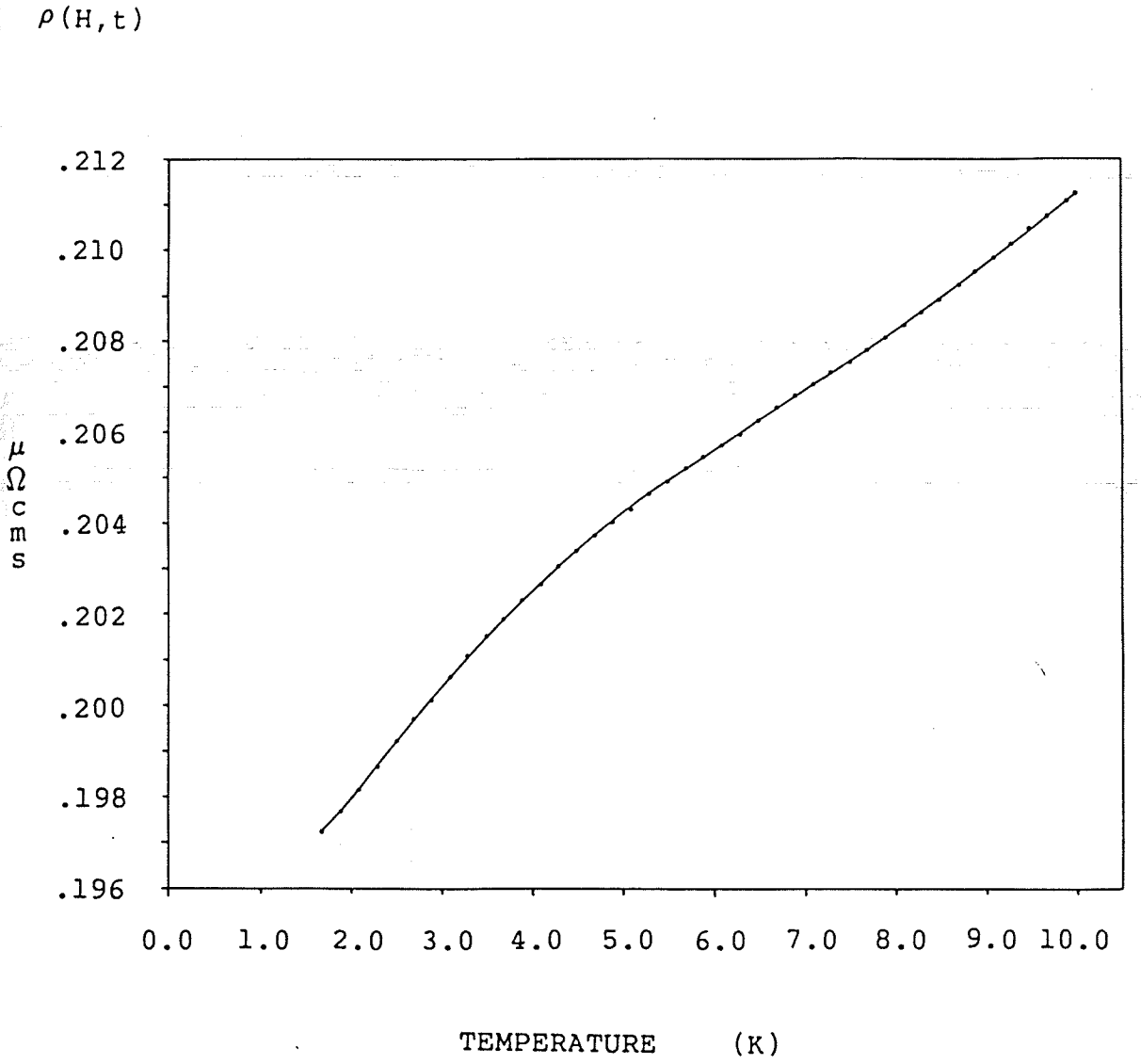

Figure 20: C) Resistivity vs. temperature curve for Pt+.05 at.% Mn in a 25 Oe. field.

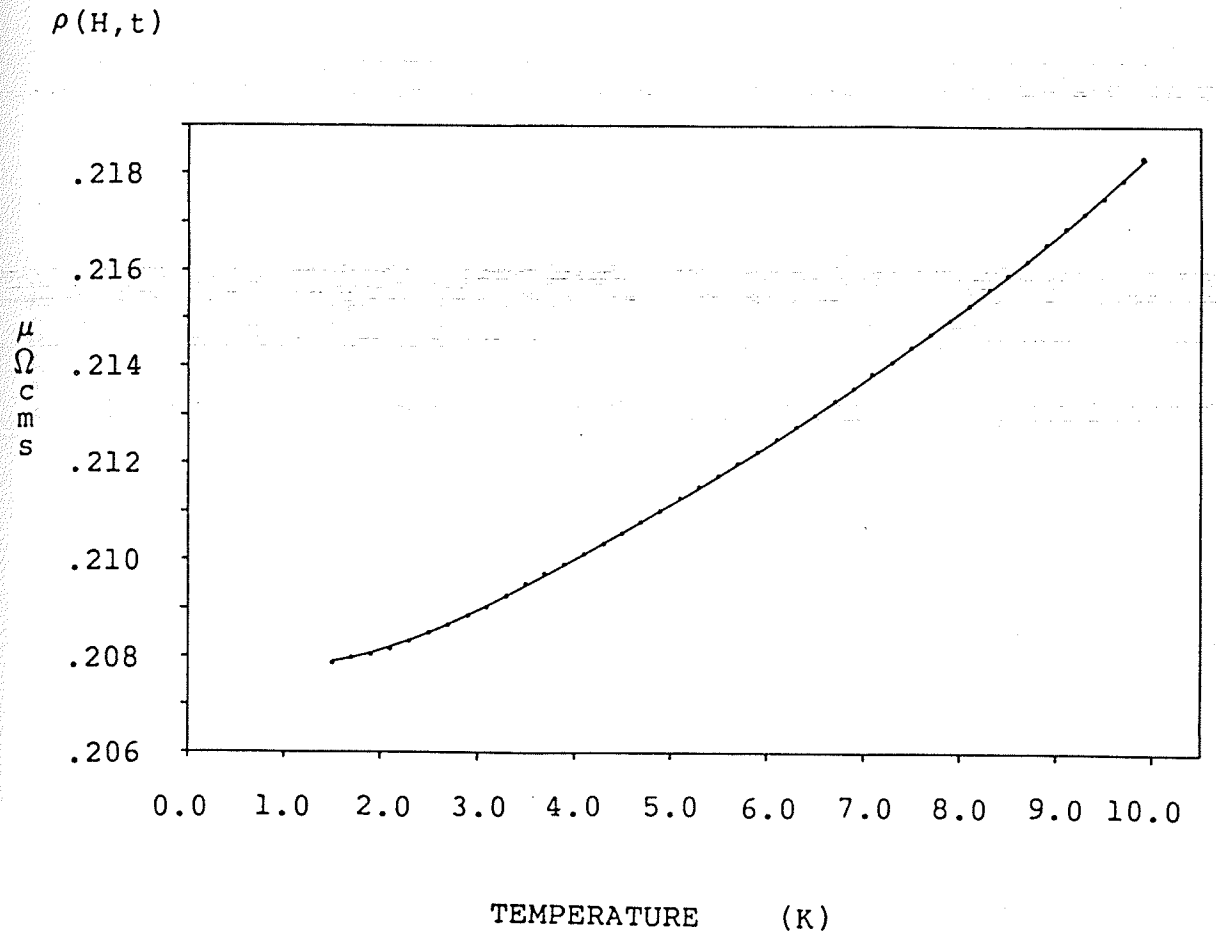

Figure 20: D) Resistivity vs. temperature curve for Pt+.05 at.% Mn in a 50 Oe. field.

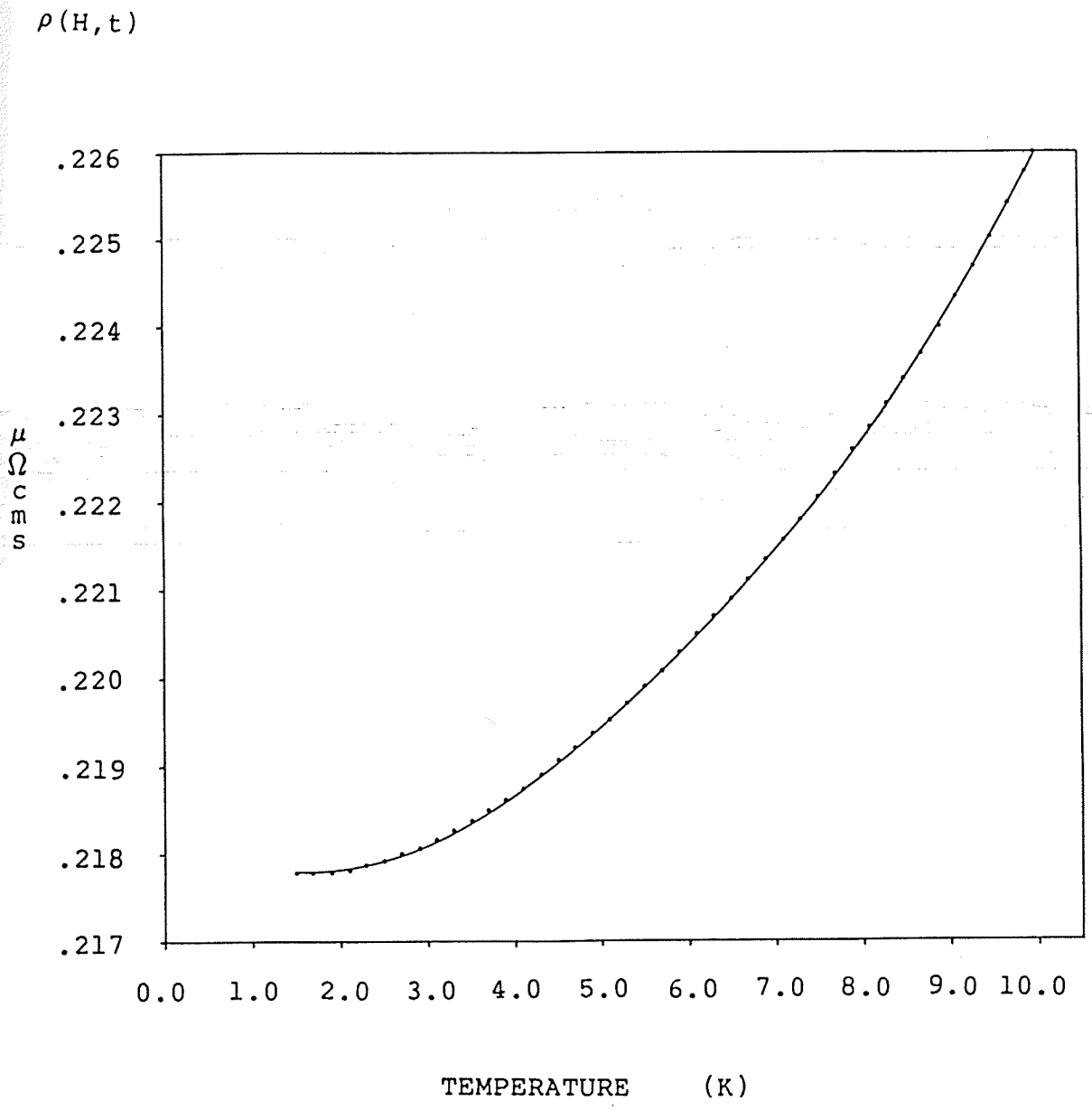

Figure 20: E) Resistivity vs. temperature curve for Pt+.05 at.% Mn in a 75 Oe. field.

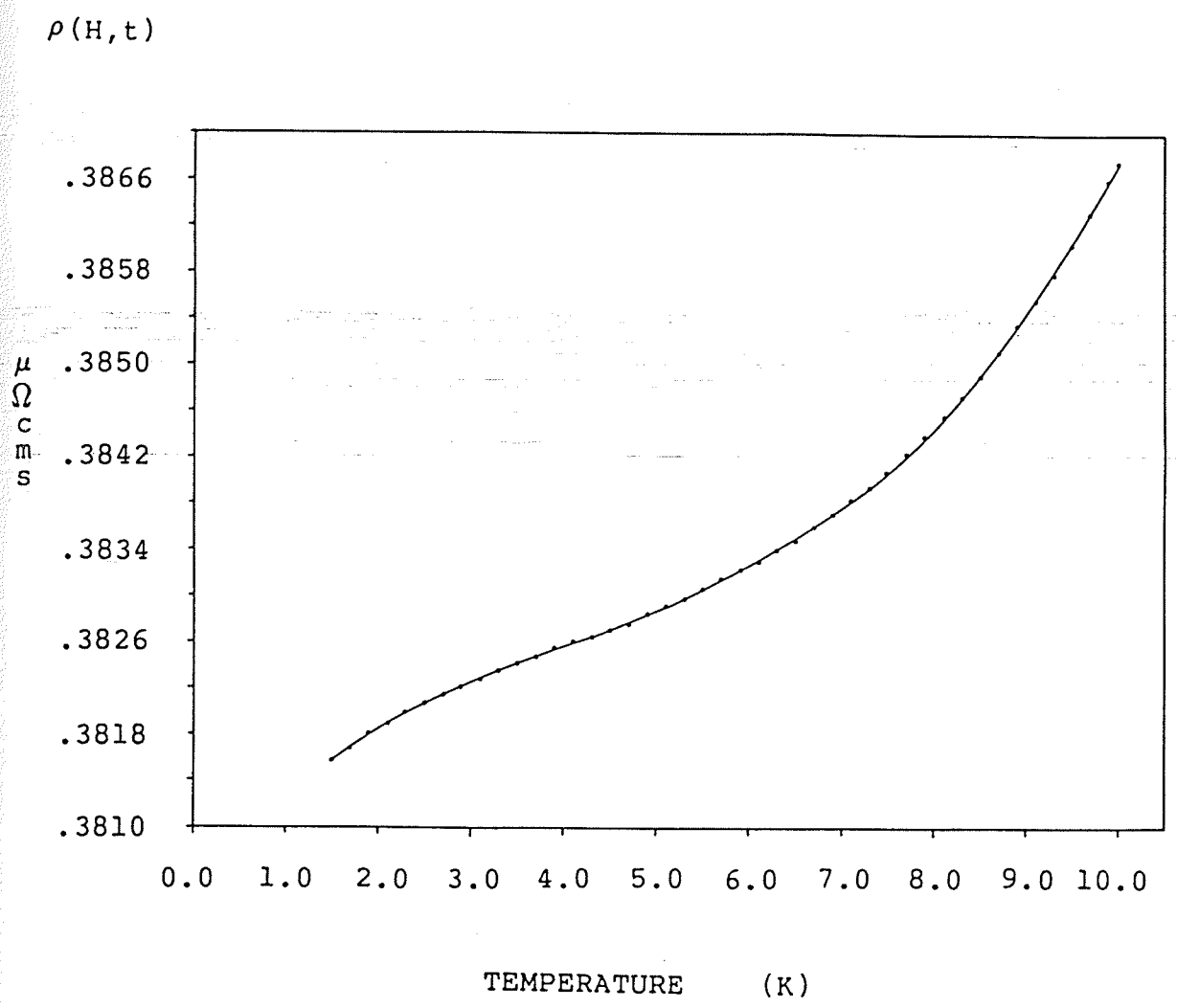

Figure 20: F) Resistivity vs. temperature curve for Pt+.10 at.% Mn in zero field.

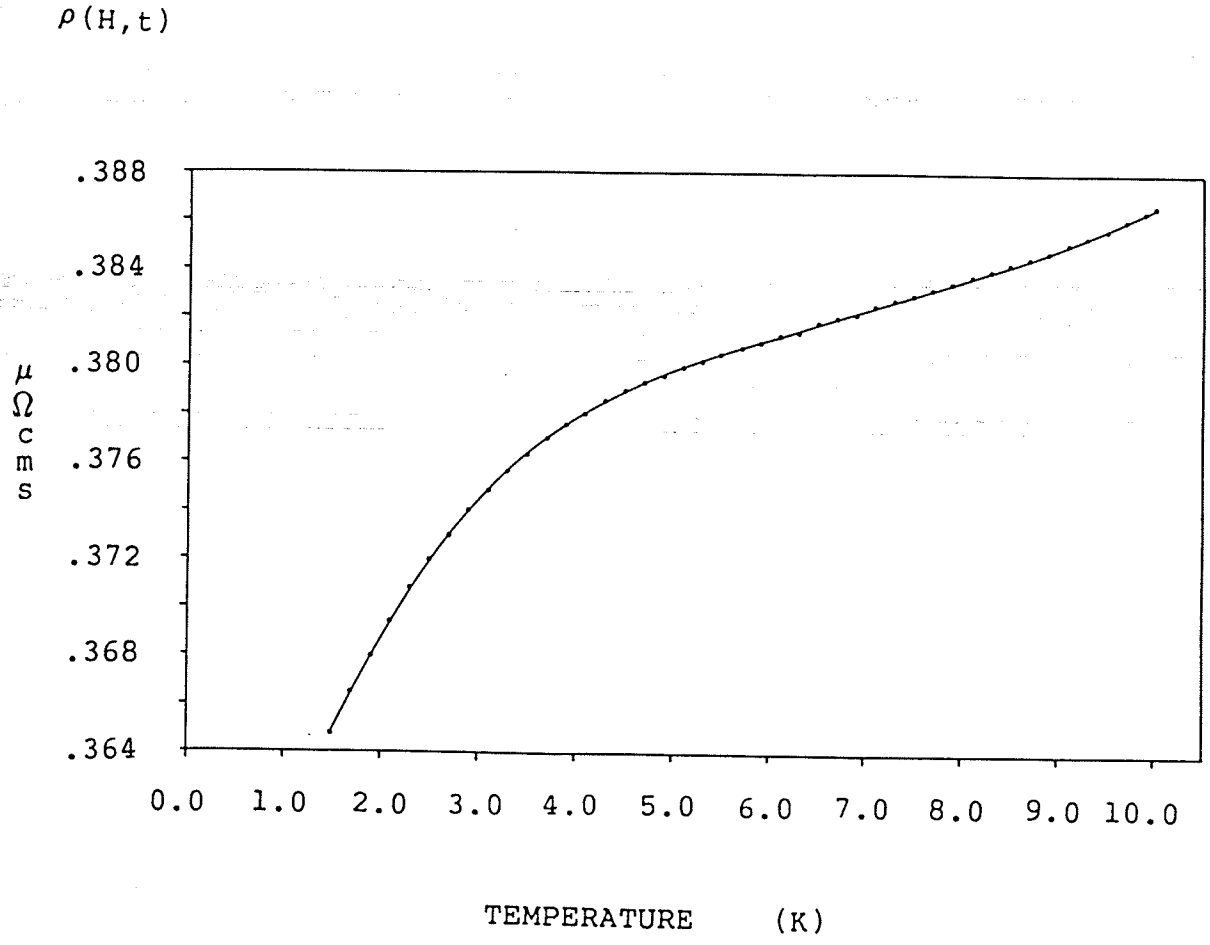

Figure 20: G) Resistivity vs. temperature curve for Pt+.10 at.% Mn in a 12.5 Oe. field.

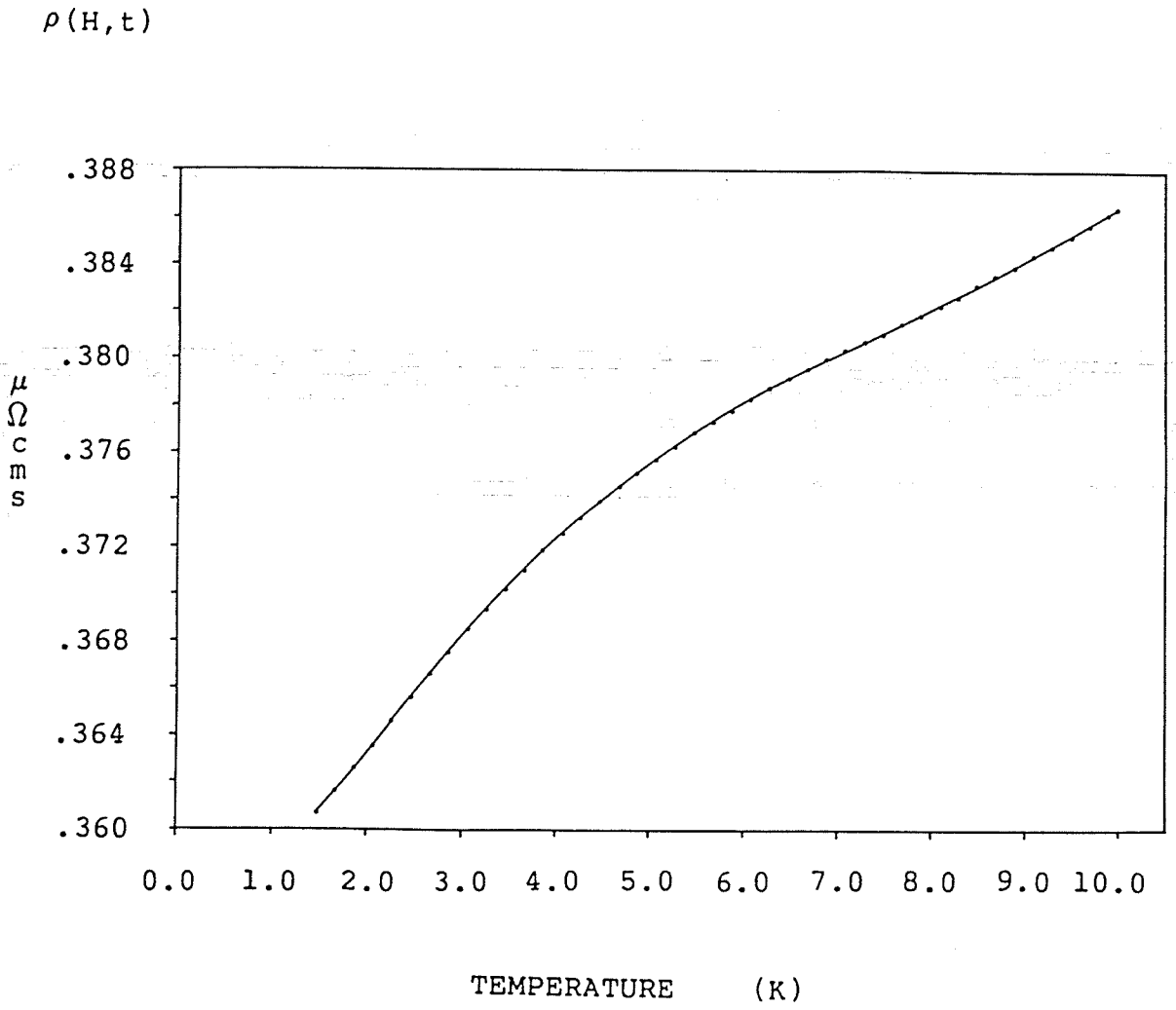

Figure 20: H) Resistivity vs. temperature curve for Pt+.10 at.% Mn in a 25 Oe. field.

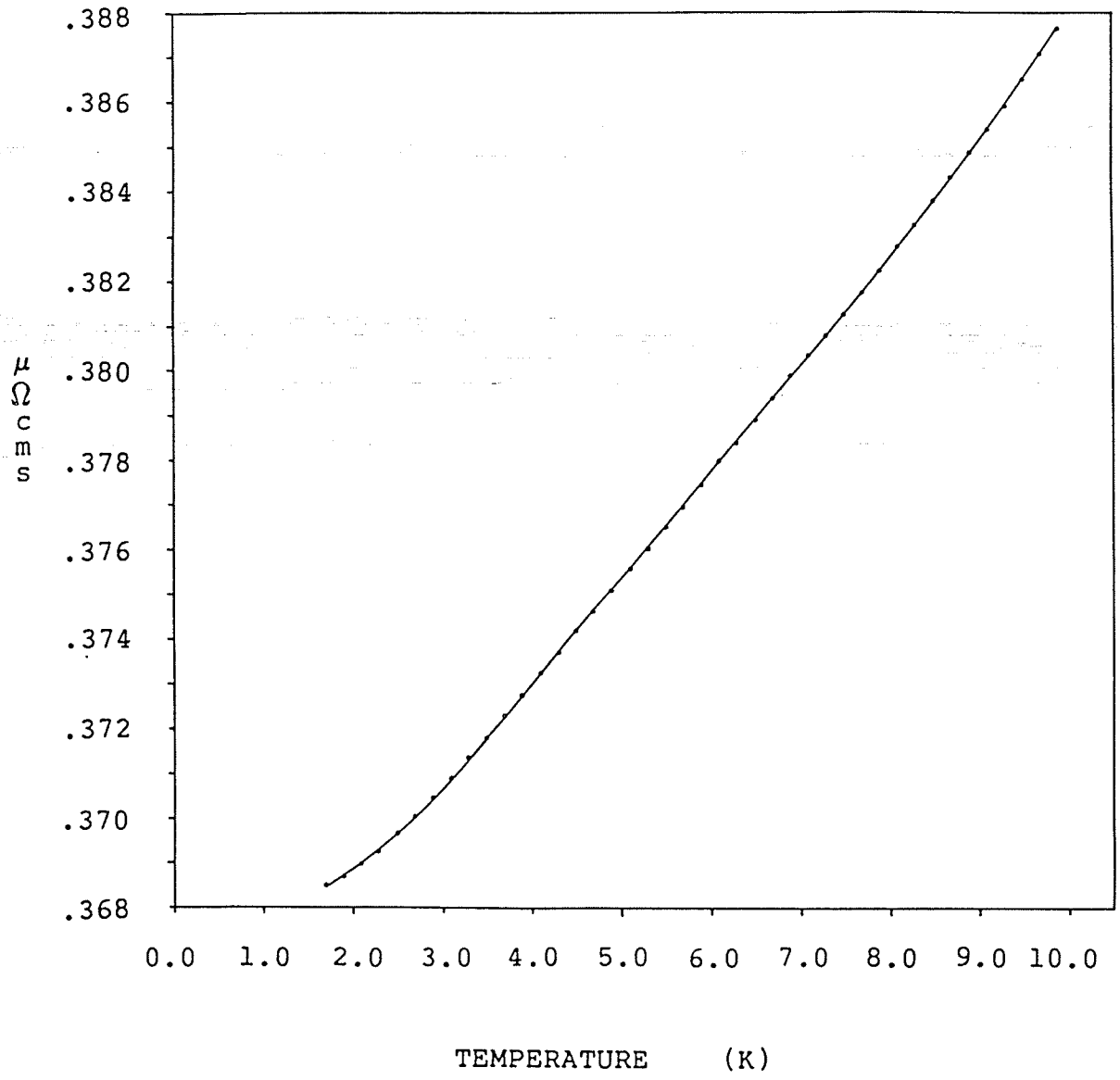

Figure 20: I) Resistivity vs. temperature curve for Pt+.10 at.% Mn in a 50 Oe.field.

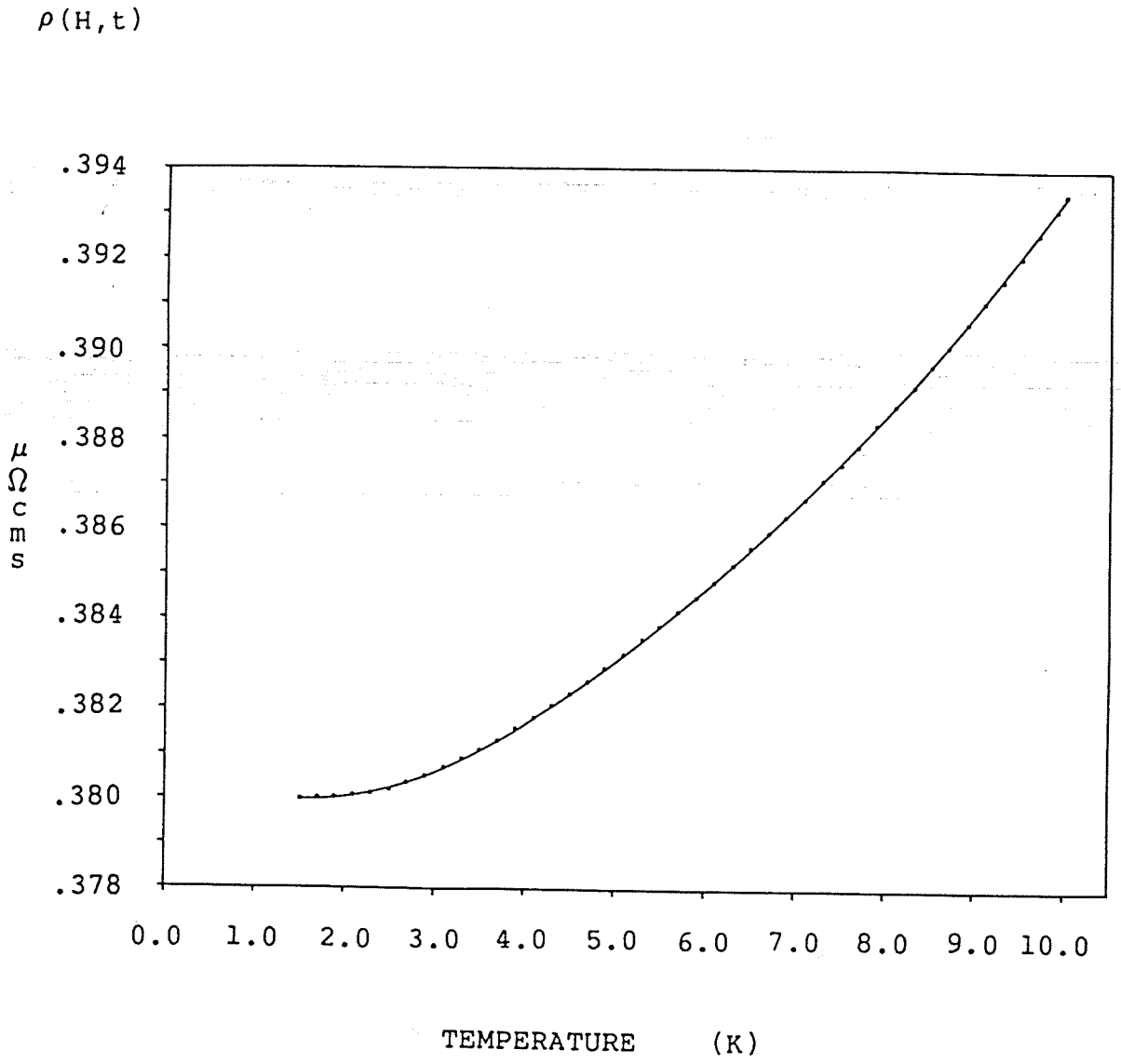

Figure 20: J) Resistivity vs. temperature curve for Pt+.10 at.% Mn in a 75 Oe. field.

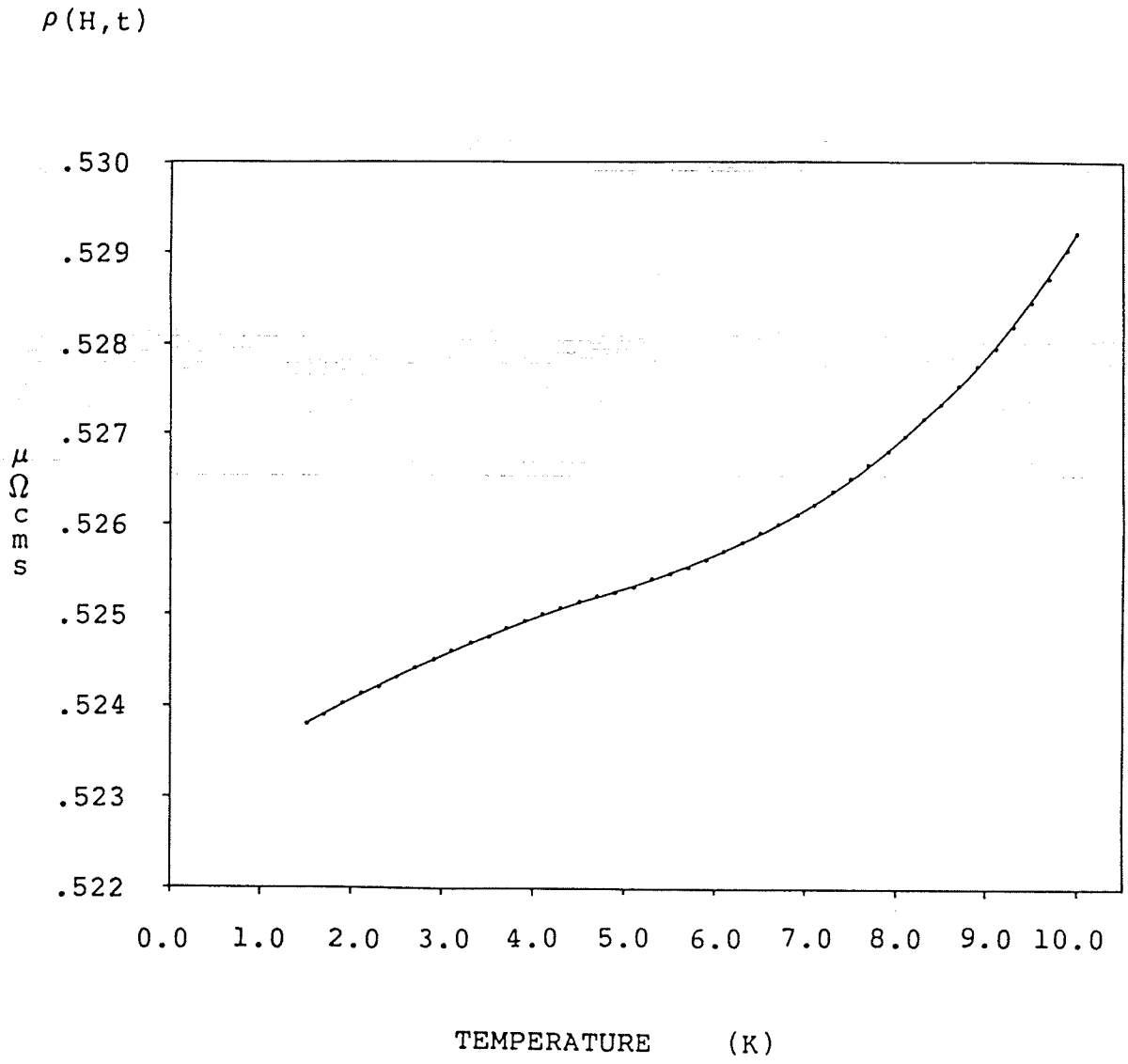

Figure 20: K) Resistivity vs. temperature curve for Pt+.15 at.% Mn in zero field.

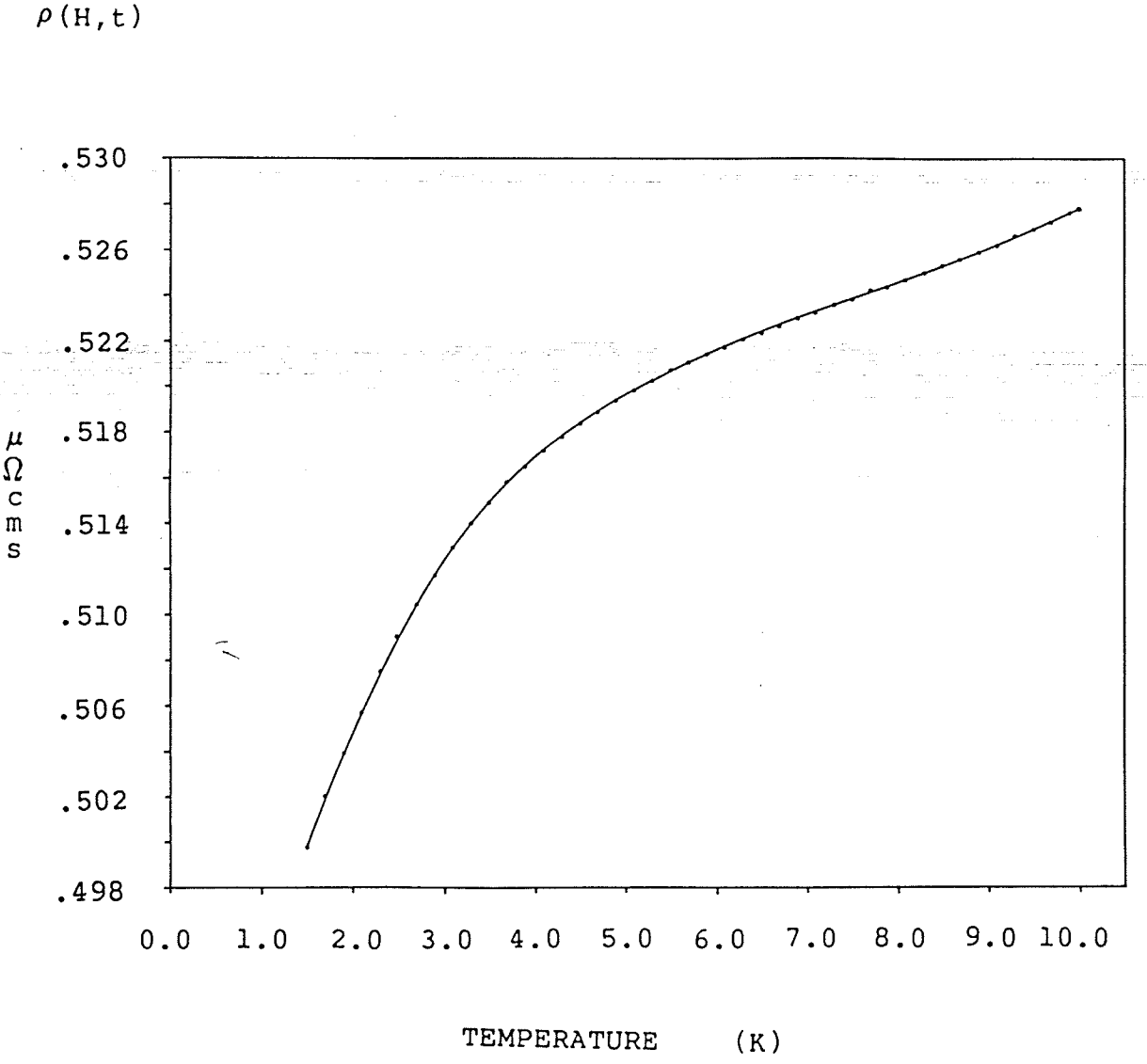

Figure 20: L) Resistivity vs. temperature curve for Pt+.15 at.% Mn in a 12.5 Oe. field.

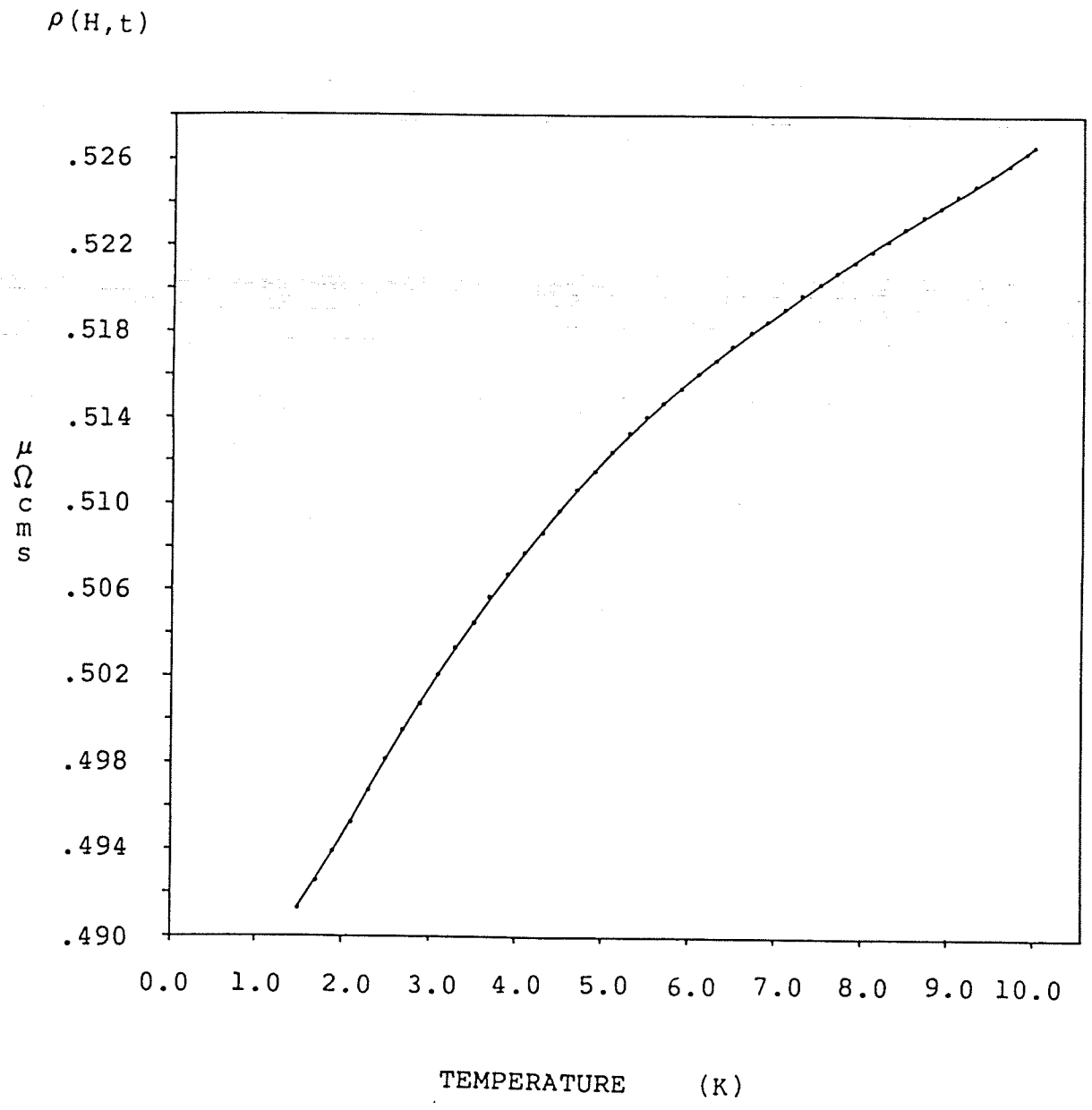

Figure 20: M) Resistivity vs. temperature curve for Pt+.15 at.% Mn in a 25 Oe. field.

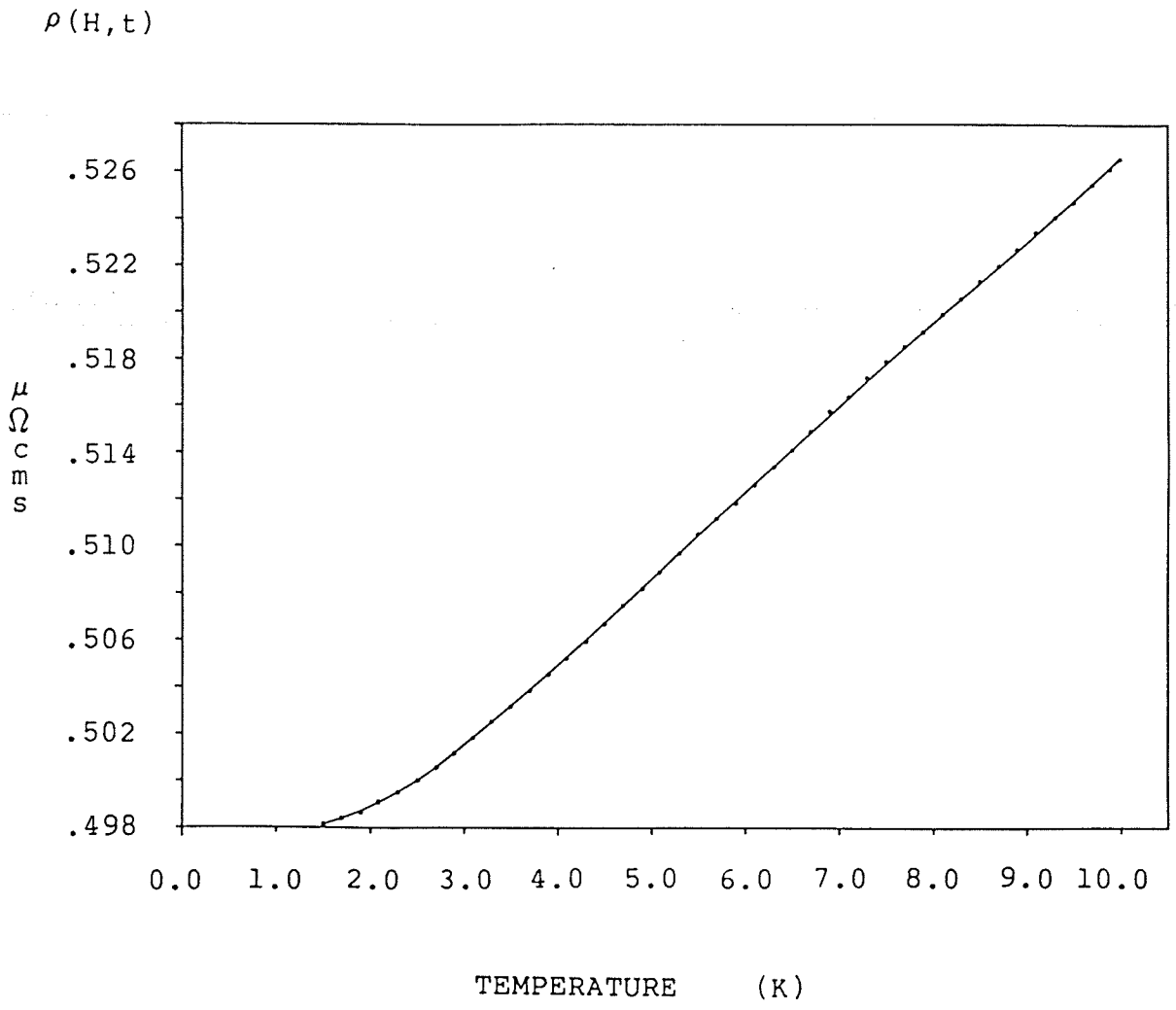

Figure 20: N) Resistivity vs. temperature curve for Pt+.15 at.% Mn in a 50 Oe. field.

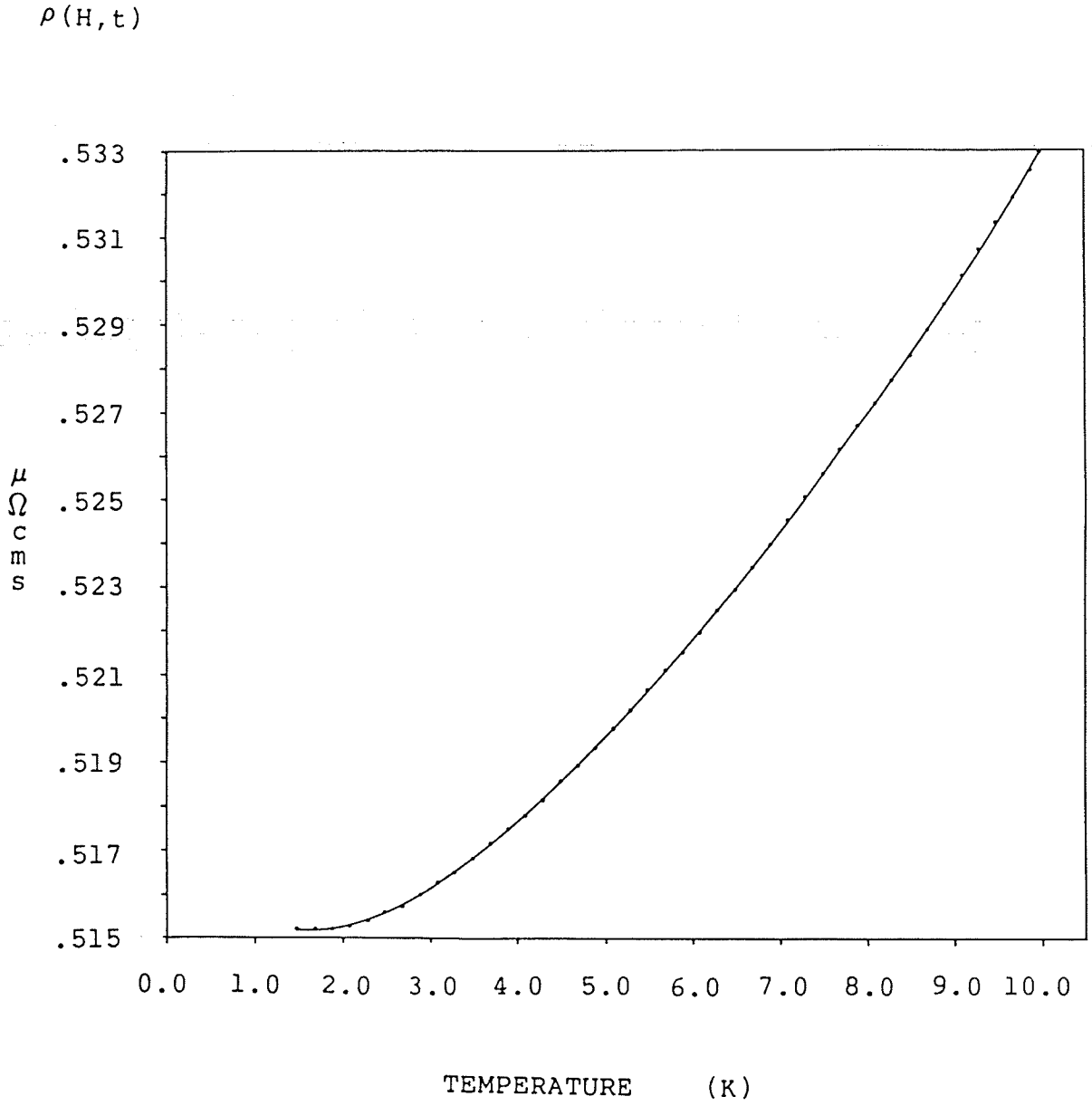

Figure 20: O) Resistivity vs. temperature curve for Pt+.15 at.% Mn in a 75 Oe. field.

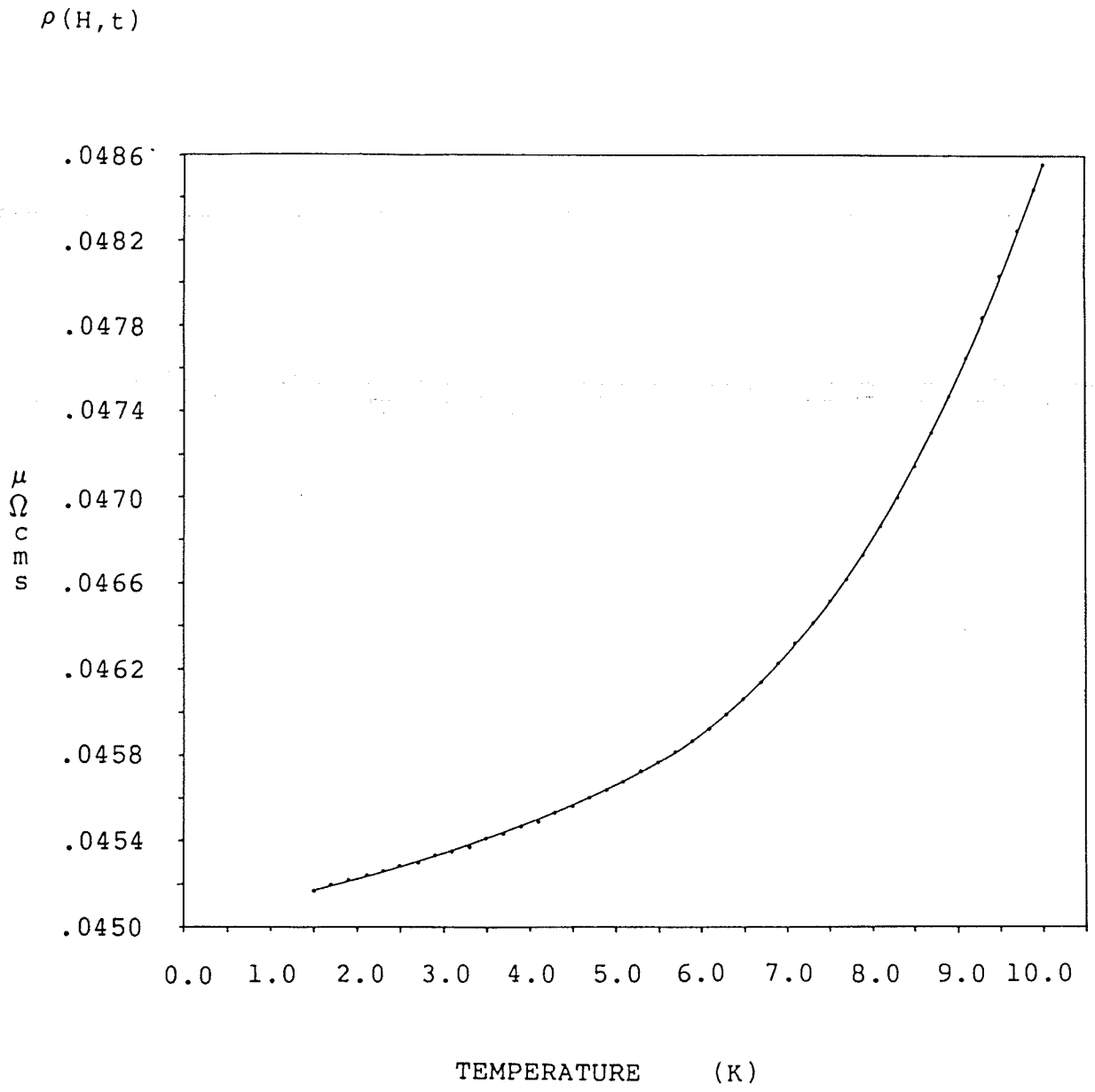

Figure 21: Resistivity vs. temperature curve for pure platinum in zero field.

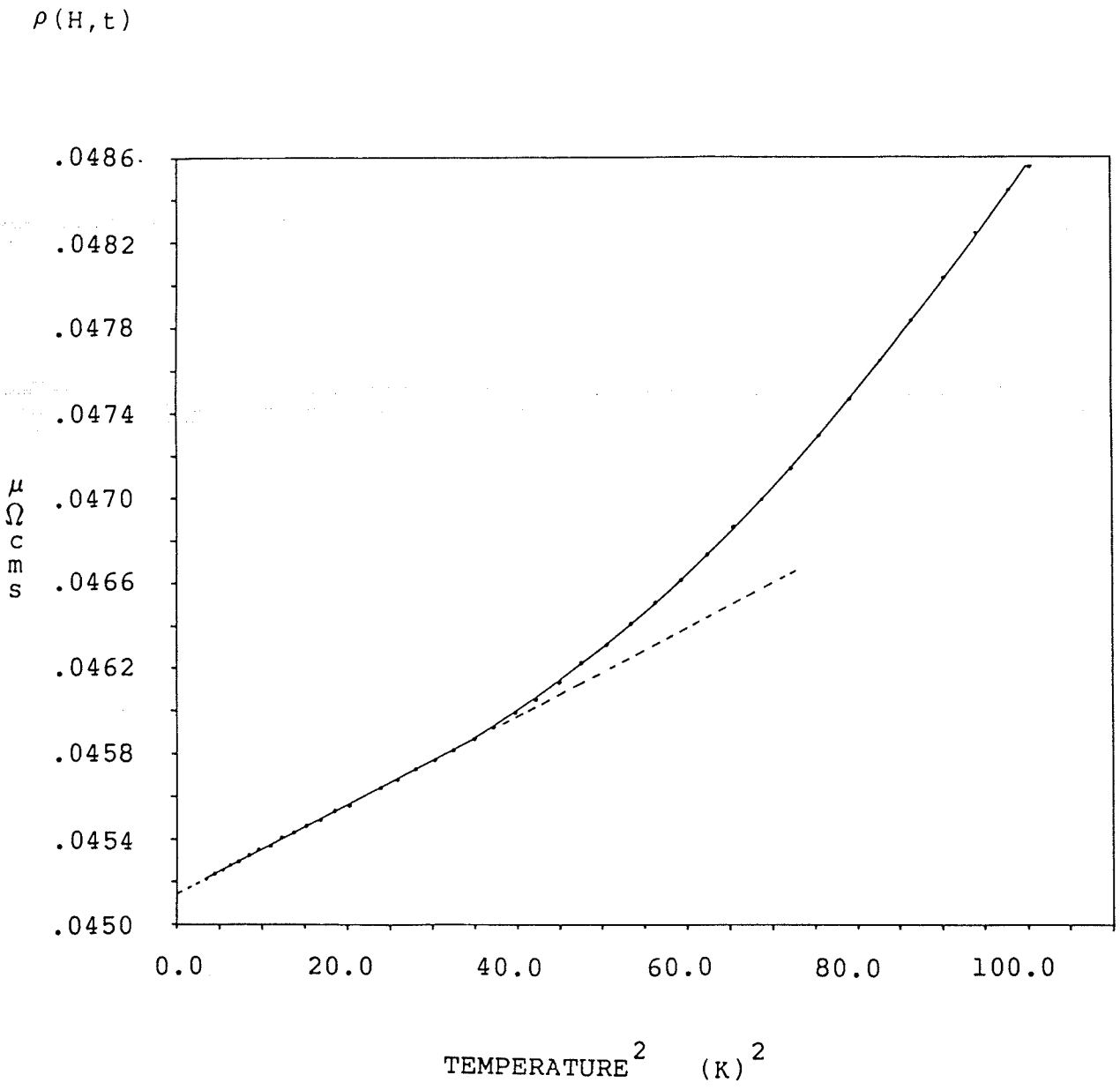

Figure 22: Resistivity vs. temperature squared curve for pure platinum in zero field.

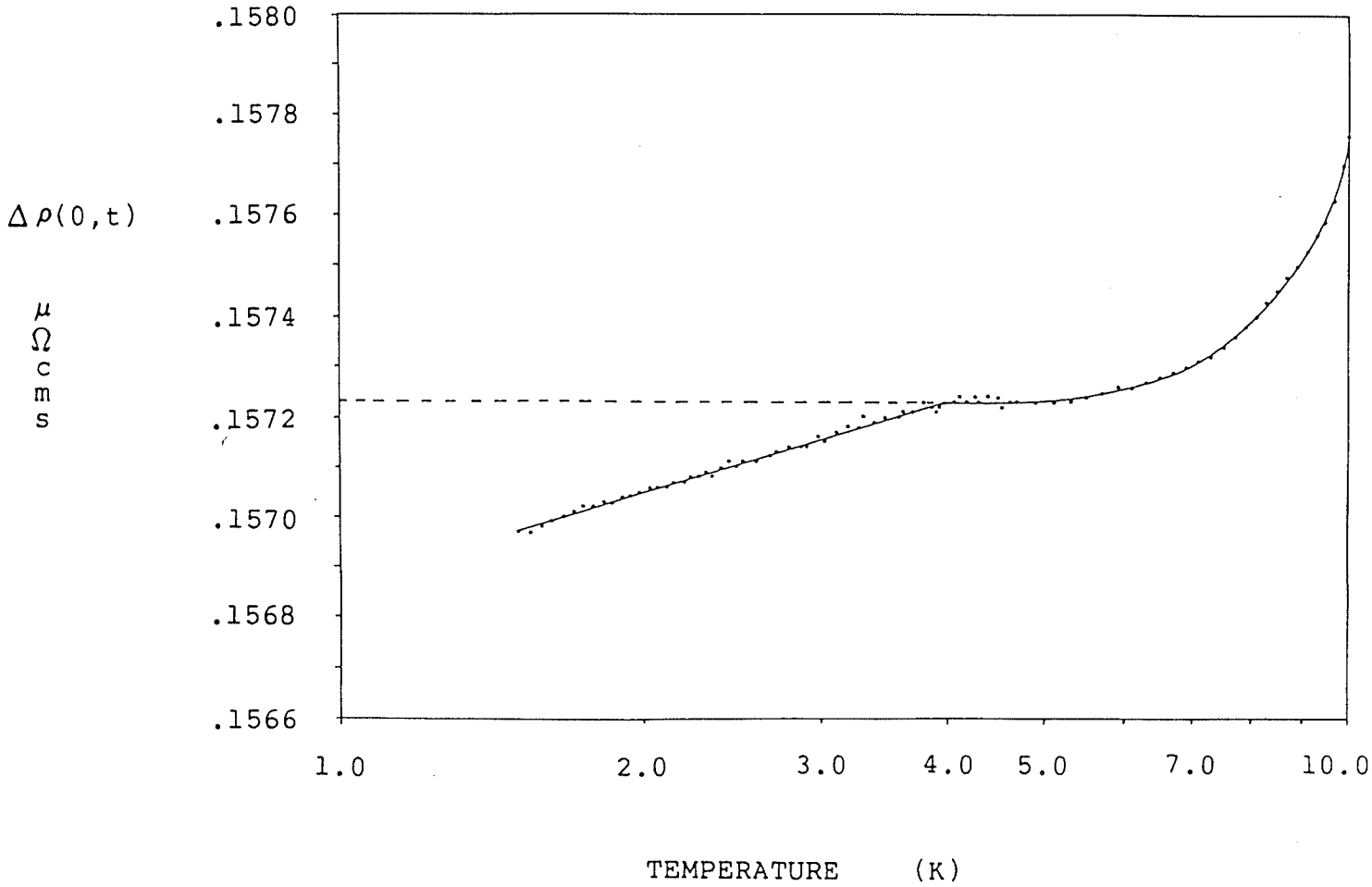

Figure 23: $\Delta\rho(0,t) = \rho_{ALLOY}(0,t) - \rho_{Pt}(0,t)$ vs. temperature plot for Pt+.05 at.% Mn.

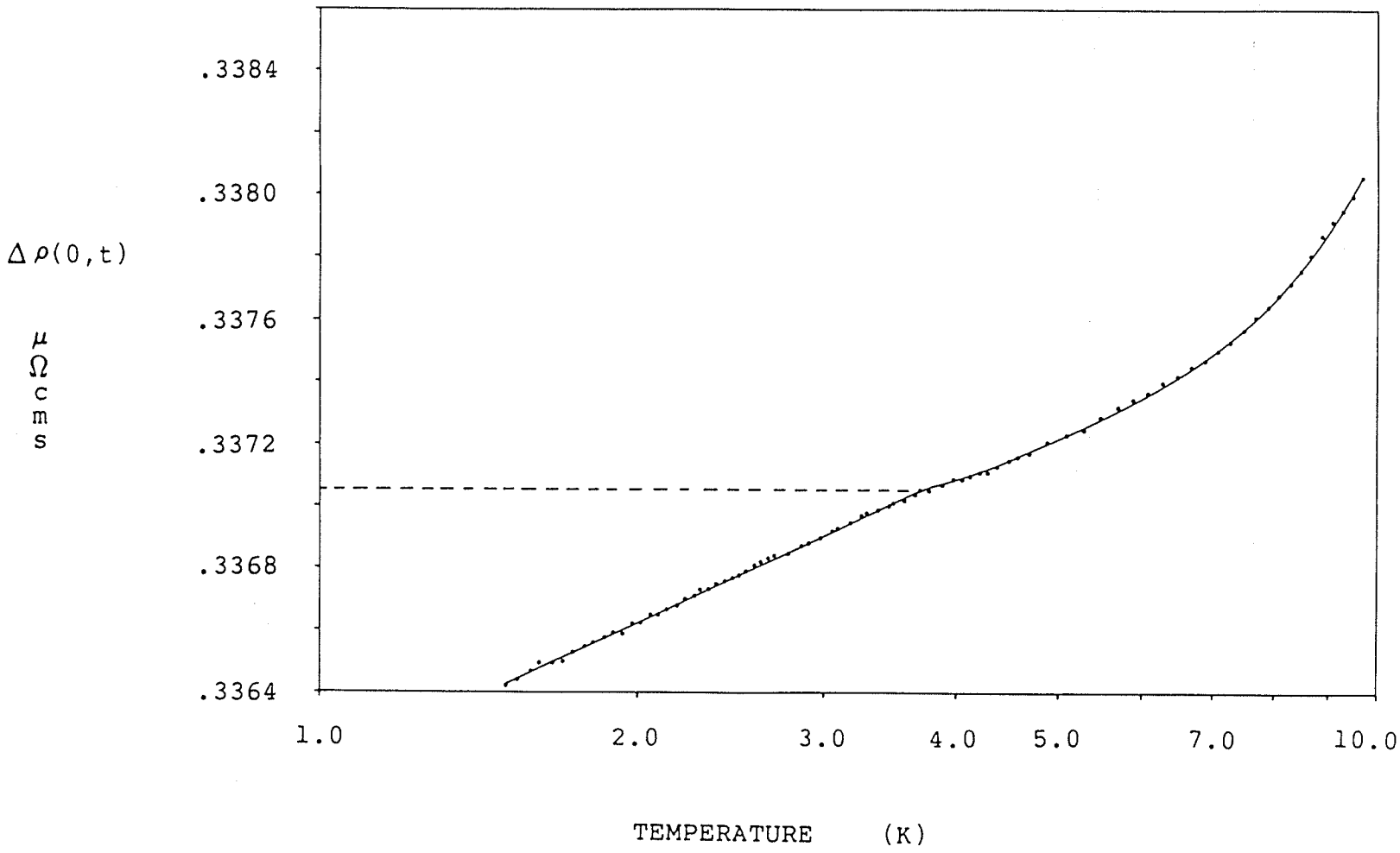

Figure 24: $\Delta\rho(0,t) = \rho_{ALLOY}(0,t) - \rho_{Pt}(0,t)$ vs. temperature plot for Pt+.10 at.% Mn.

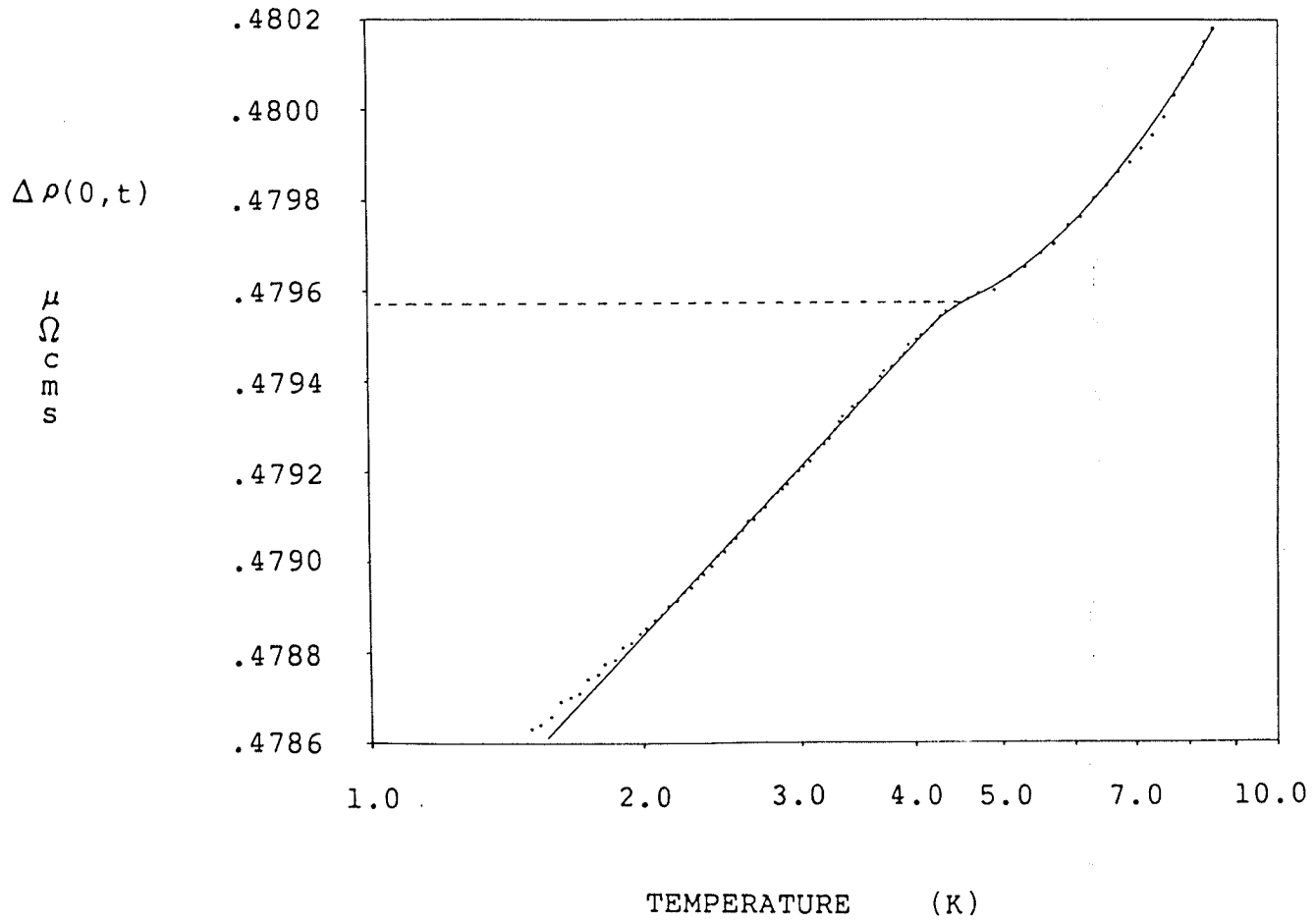

Figure 25: $\Delta\rho(0,t) = \rho_{ALLOY}(0,t) - \rho_{Pt}(0,t)$ vs. temperature plot for Pt+.15 at.% Mn.

concentrations. At low temperatures, all three curves exhibit a logarithmic dependance. However, such a behavior does not follow from the theoretical resistivity expression derived by Yosida. This is due to the fact that Yosida's calculation uses only the first Born approximation, transition probabilities being carried out to first order. Unfortunately, such first order approximations prove to be insufficient at low temperatures in zero field. Third order terms in the transition probabilities become significant, leading to a logarithmic term in the resistivity expression. This is responsible for the log dependance exhibited in the data shown. The dotted lines represent the assumed form of the curves after the logarithmic term has been eliminated. From these graphs, the magnitude of the log terms can be determined. Once this is done, it can be subtracted from the zero field resistivity data. This correction must be made so as to be consistent with theoretical calculations. The logarithmic term is assumed quenched at higher temperatures and in a field, both inhibiting this logrithmic variation. Table 3 gives the logarithmic slope as well as the 0K magnitude of this so called Kondo effect for all three impurity concentrations.

The quantity $\Delta\rho_{MAG}$, defined by

$$\Delta\rho_{MAG} = \rho_{ALLOY}(0,t) - \rho_{ALLOY}(H,t)$$

was then calculated. Here, H represents the magnetic field strength, it being a constant of magnitude 12.5, 25, 50 or

TABLE 3

The "Kondo effect" parameters.

SAMPLE	LOGRITHMIC SLOPE	0K MAGNITUDE
Pt+.05 at.% Mn	.00061 $\mu\Omega$ cms.	.00036 $\mu\Omega$ cms.
Pt+.10 at.% Mn	.00161 $\mu\Omega$ cms.	.00096 $\mu\Omega$ cms.
Pt+.15 at.% Mn	.00212 $\mu\Omega$ cms.	.00135 $\mu\Omega$ cms.

75 Oe. The resulting three sets of $\Delta\rho_{MAG}$ data, one set for each impurity concentration, are graphed as functions of H/t in figures 26, 27 and 28. Each data set is composed of four curves, corresponding to the four different values of H. These plots show quite clearly that the resistivity data is not a unique function of H/t. This is due to the fact that the normal Kohler magnetoresistance $\Delta\rho_K(H,t)$ has not been accounted for.[8] This contribution to resistivity arises from the bending of the conduction electrons from a straight line path (parallel to the electric field within the sample) by the applied magnetic field which tends to push the electrons in a direction perpendicular to their motion. It is assumed that the Kohler term[8] can be expressed as

$$\Delta\rho_K(H,t) = f[\ \rho_{ALLOY}(t),H\ ]$$

$\rho_{ALLOY}(t)$ being the total alloy resistivity at a temperature t. Since all $\Delta\rho_{MAG}$ curves represent data collected in a fixed field and since the fractional change in sample resistivity over the range measurements were taken was small, the Kohler resistance can be assumed to be a constant for the data taken in one field (ie. the Kohler term is a constant for each $\Delta\rho_{MAG}$ curve). Thus, subtracting the Kohler term from each resistivity curve shifts the entire curve by a fixed amount. It is assumed that correcting for the Kohler magnetoresistance shifts the $\Delta\rho_{MAG}$ data taken in all different fields so as to form one continuous curve.[8] Hence,

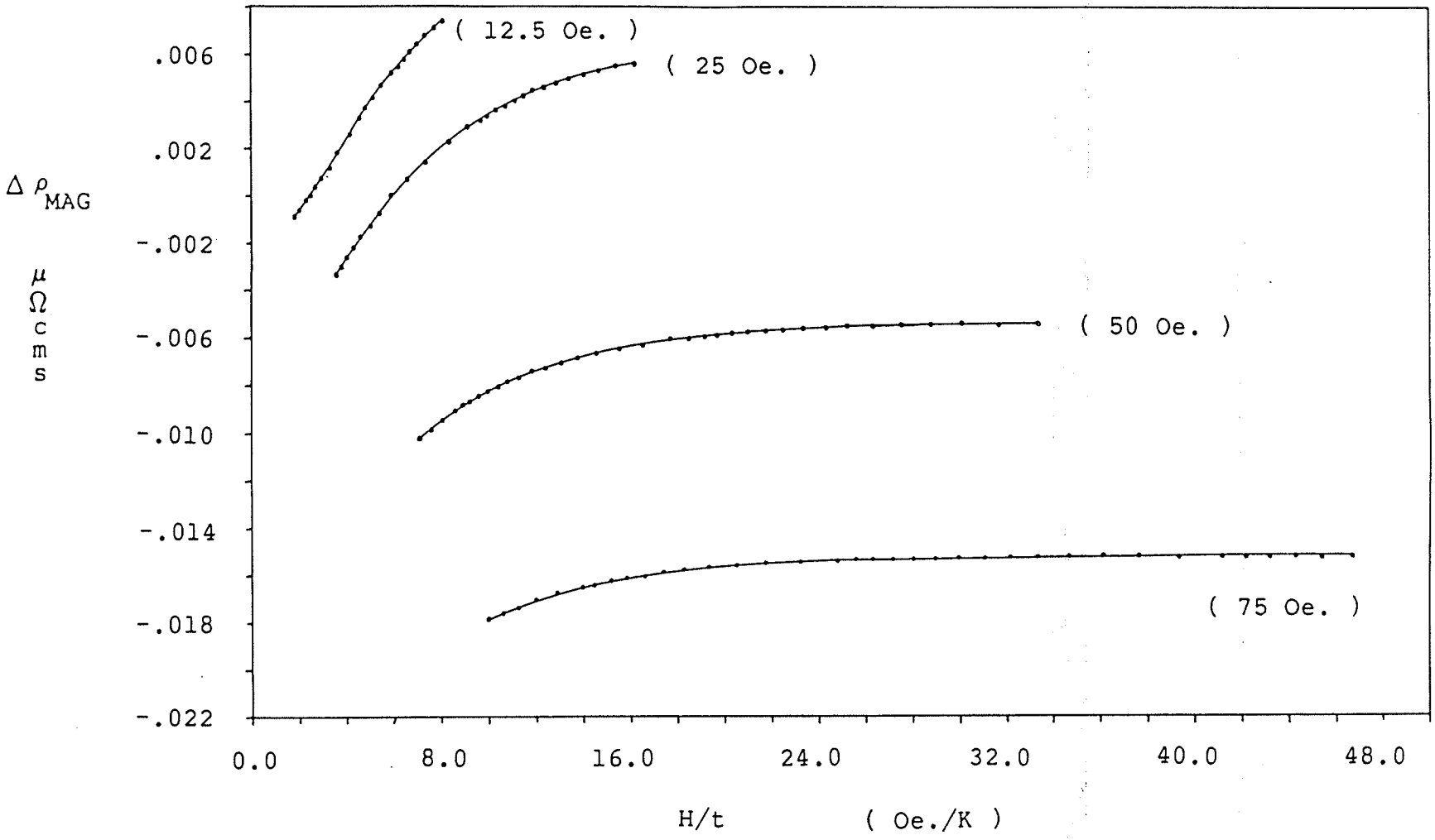

Figure 26: $\Delta \rho_{MAG}$ data for Pt+.05 at.% Mn plotted against H/t.

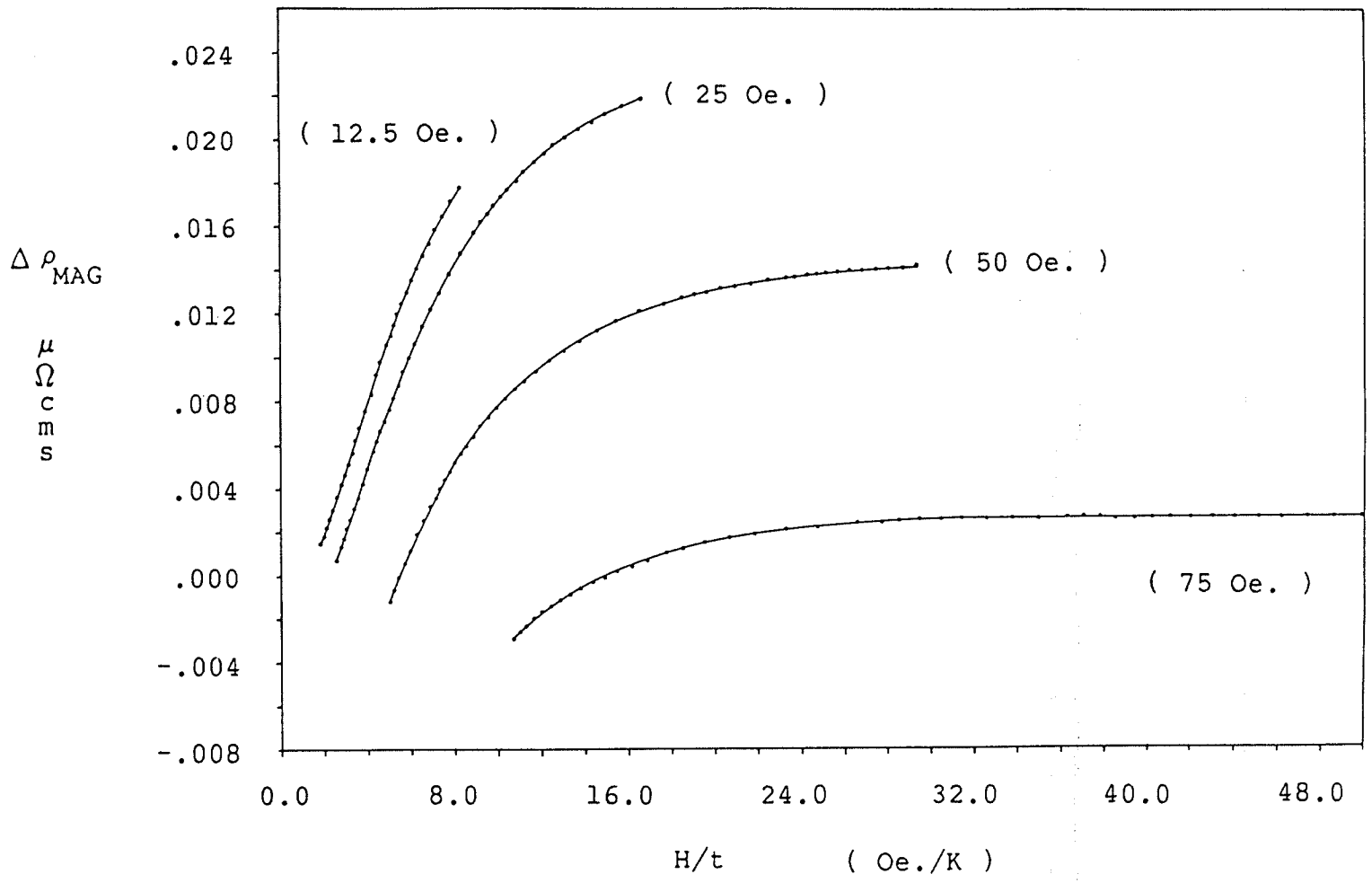

Figure 27: $\Delta \rho_{MAG}$ data for Pt+.10 at.% Mn plotted against H/t.

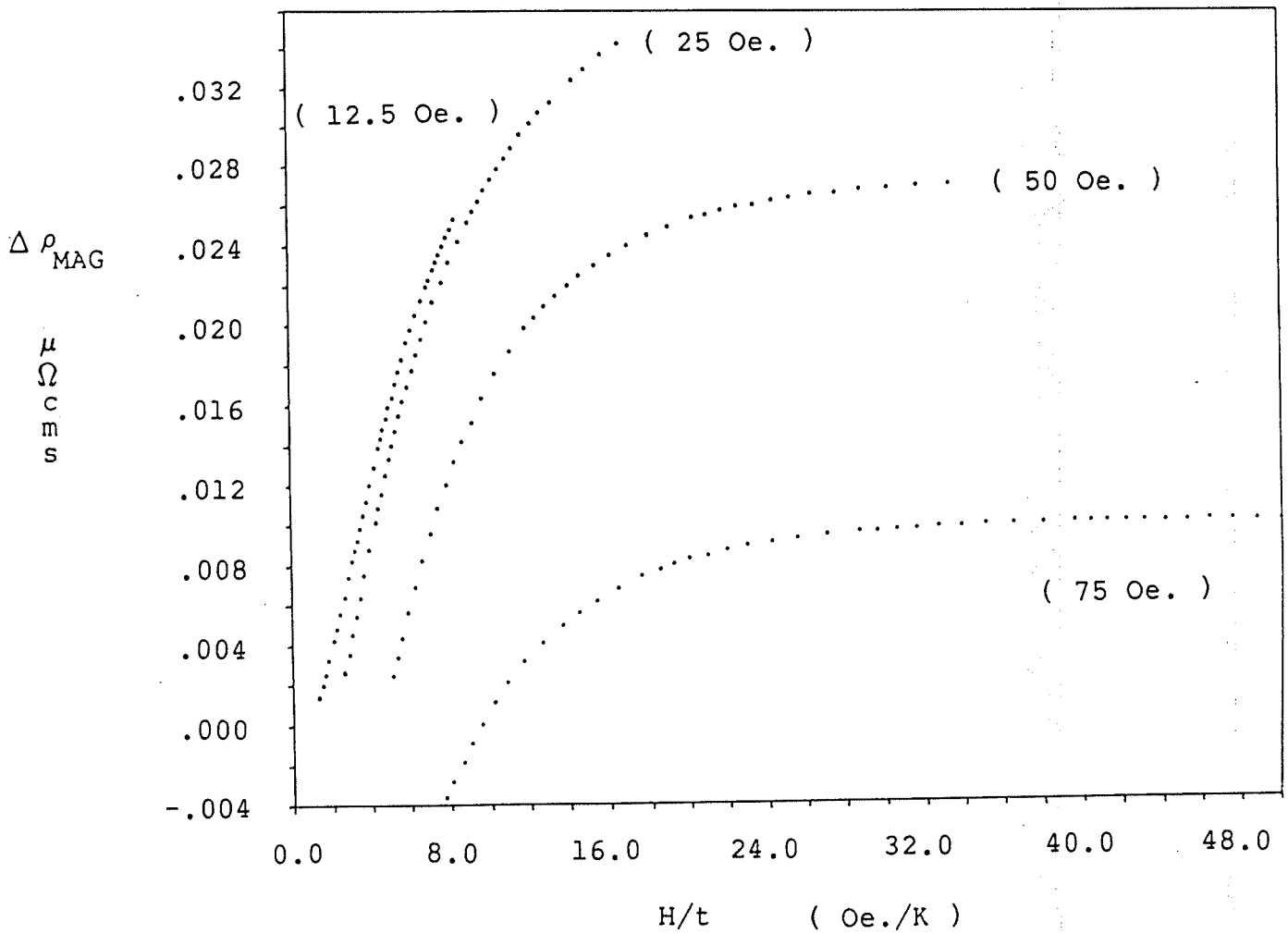

Figure 28: $\Delta \rho_{MAG}$ data for Pt+.15 at.% Mn plotted against H/t.

a fixed resistivity increment is subtracted from all the data measured in the 25, 50 and 75 Oe. fields so as to shift all three curves into forming a continuous curve containing the 12.5 oe. data. The Kohler correction factors for the 12.5 Oe. data cannot be estimated and the true zero of the data determined using this approach. Instead, an initial estimate is obtained by examining the low-field, high temperature data. In such a limit, the theoretical expression for $\Delta\rho_{MAG}$ reduces to[8]

$$\Delta\rho_{MAG}(H << t) \approx (1/18)(3\pi/2)(M/e^2)(1/\hbar E_F)(V/N)(N_A/N)$$
$$J^2S(S+1)\{\ 8S(S+1)[1-J^2S(S+1)/V^2]+3\ \}\alpha^2$$

where $\alpha = g\mu H/Kt$. A plot of $\Delta\rho_{MAG}(H << t)$ vs. $(H/t)^2$ will yield a straight line; when $(H/t)^2$ is set to zero, $\Delta\rho_{MAG}(H << t)$ will also take on a value of zero. Thus, by graphing the resistivity corresponding to the high temperature points of the 12.5 Oe. data vs. $(H/t)^2$ and extrapolating the straight line curve to $(H/t)^2 = 0$, an estimate of the true zero and therefore the Kohler correction term for this $\Delta\rho_{MAG}$ curve can be determined. Figure 29 illustrates this procedure. Table 4 shows the Kohler magnetoresistances for all three samples in each field. Figure 30, 31 and 32 show the resistivity, $\Delta\rho_{MAG}$, vs. H/t curves of each platinum-manganese specimen after the Kohler corrections have been made.

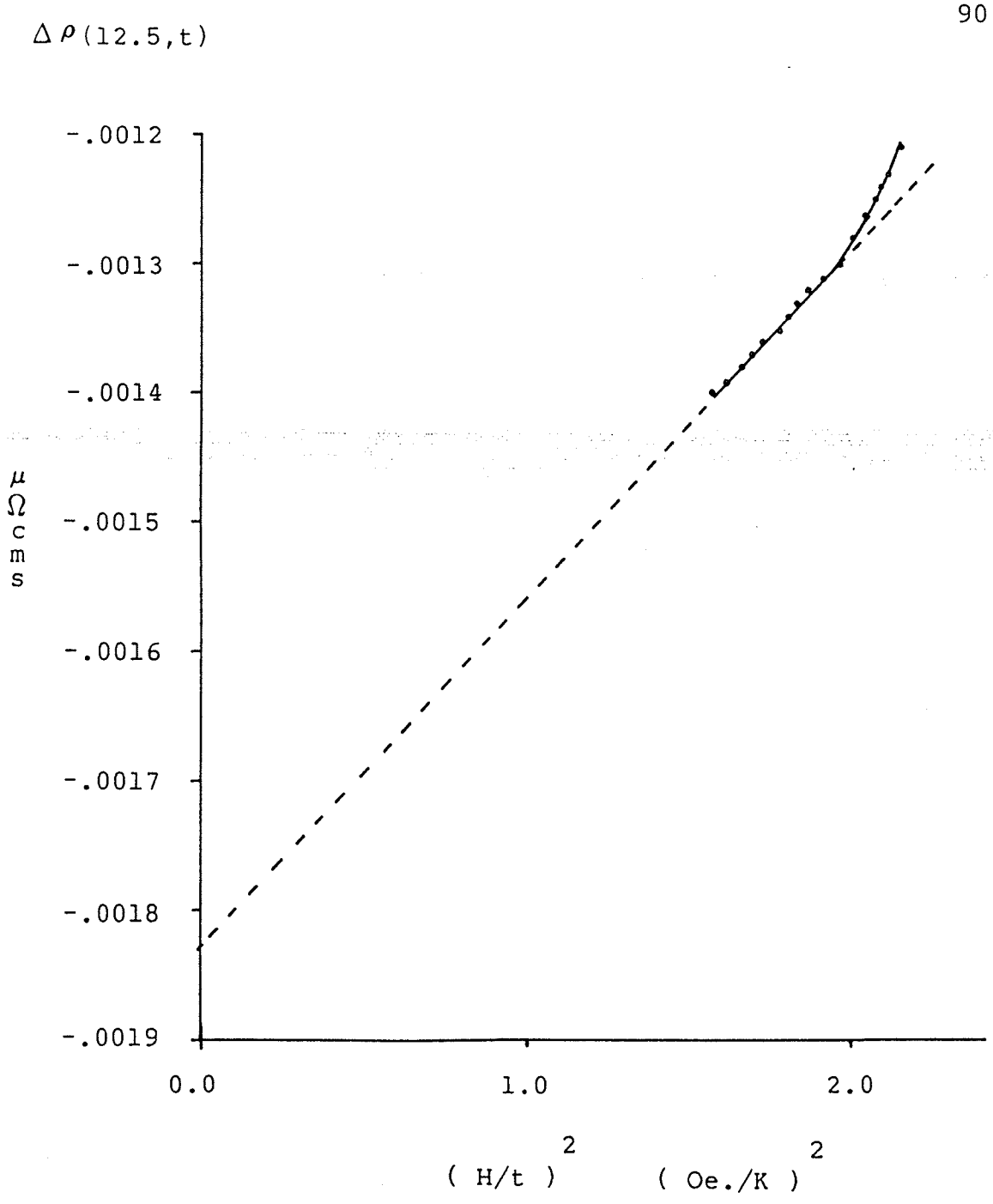

Figure 29: Estimating the Kohler magnetoresistance correction term for the 12.5 Oe. data of Pt+.05 at.% Mn.

TABLE 4

Kohler magnetoresistances.

SAMPLE	KOHLER CORR. (12.5 Oe.)	KOHLER CORR. (25 Oe.)	KOHLER CORR. (50 Oe.)	KOHLER CORR. (75 Oe.)
Pt+.05 at.% Mn	.00183 $\mu\Omega$ cms.	.00703 $\mu\Omega$ cms.	.01883 $\mu\Omega$ cms.	.02873 $\mu\Omega$ cms.
Pt+.10 at.% Mn	.00051 $\mu\Omega$ cms.	.00351 $\mu\Omega$ cms.	.01326 $\mu\Omega$ cms.	.02481 $\mu\Omega$ cms.
Pt+.15 at.% Mn	.00096 $\mu\Omega$ cms.	.00346 $\mu\Omega$ cms.	.01363 $\mu\Omega$ cms.	.03096 $\mu\Omega$ cms.

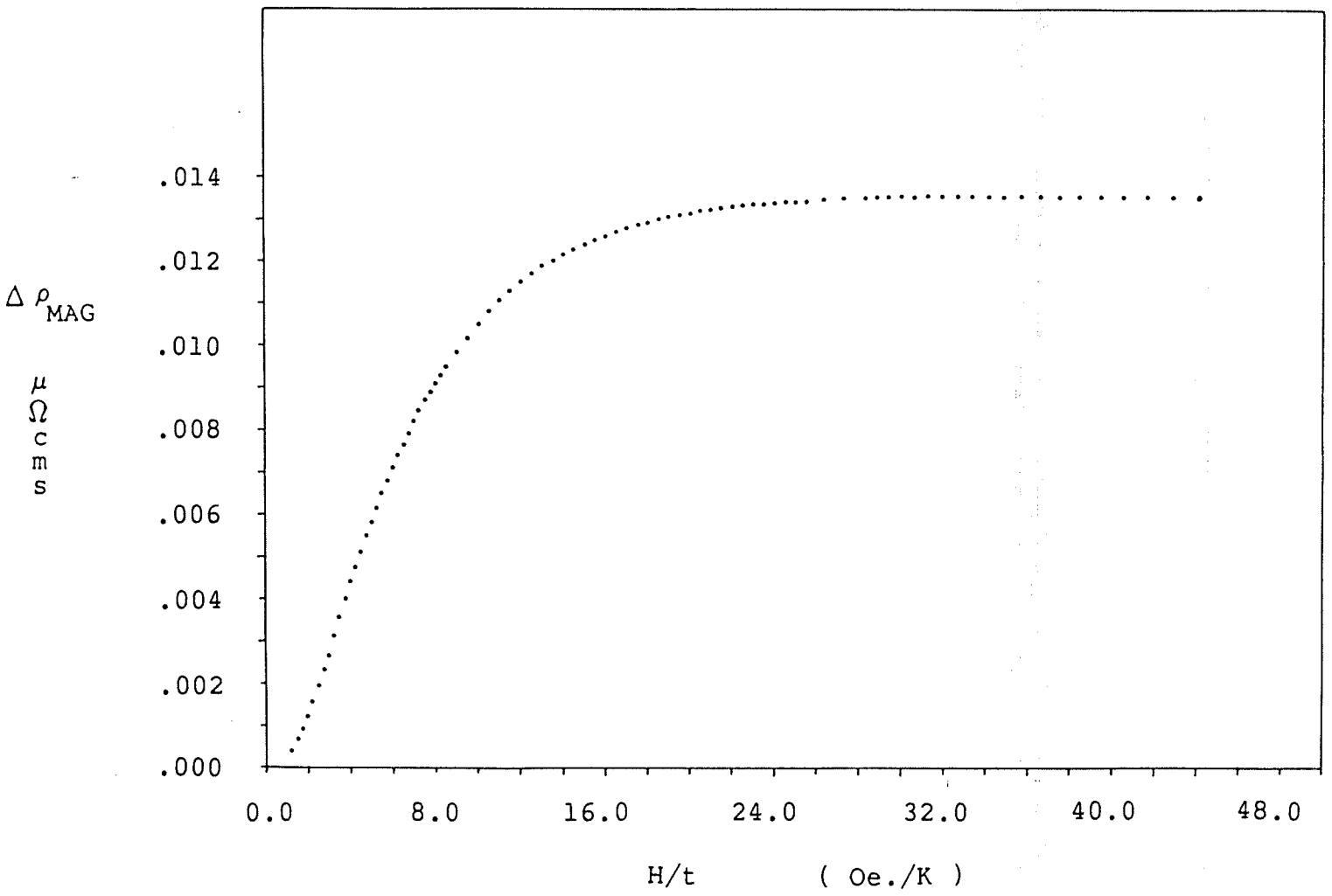

Figure 30: Pt+.05 at.% Mn incremental resistivity curves, after Kohler corrections have been made.

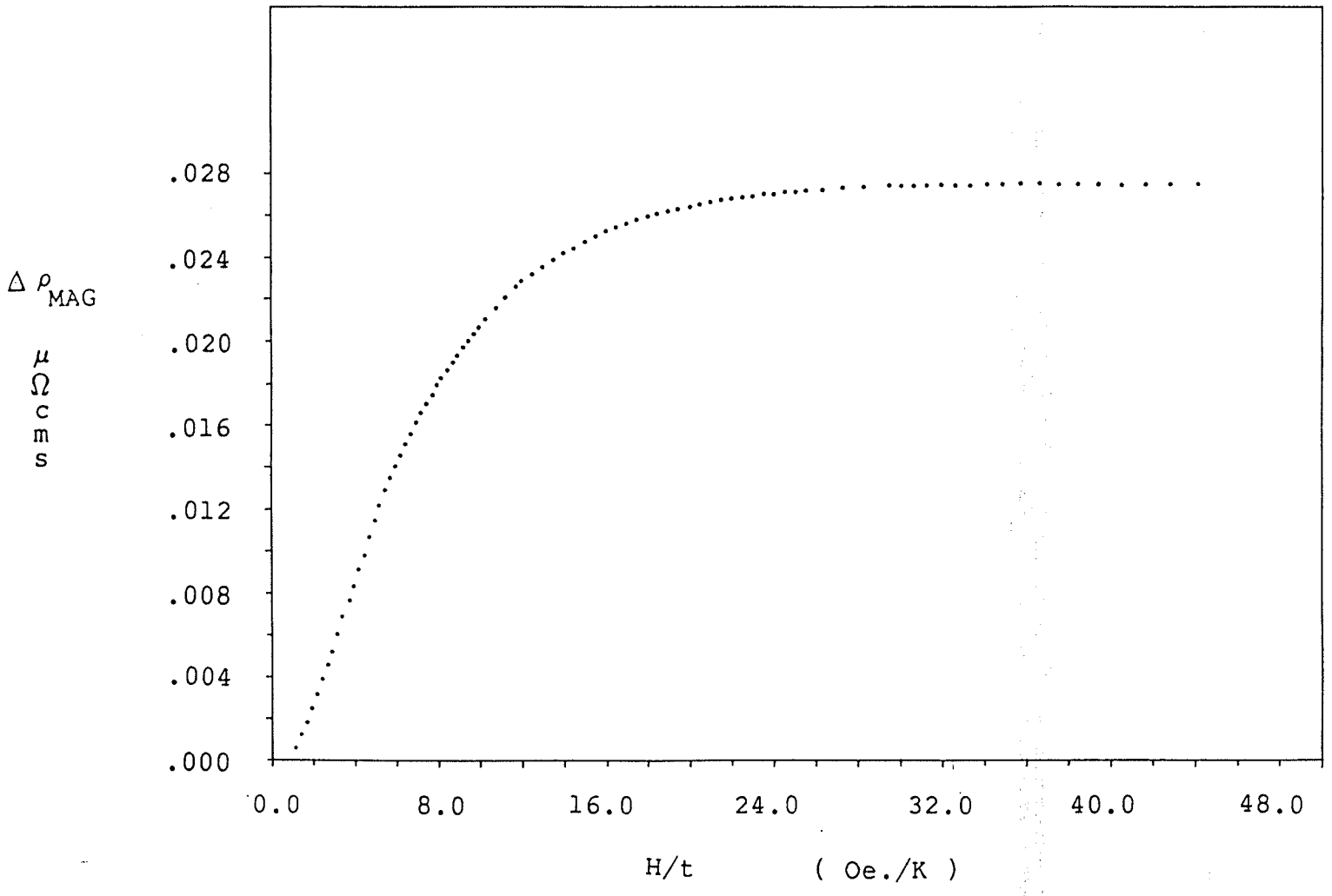

Figure 31: Pt+.10 at.% Mn incremental resistivity curves, after Kohler corrections have been made.

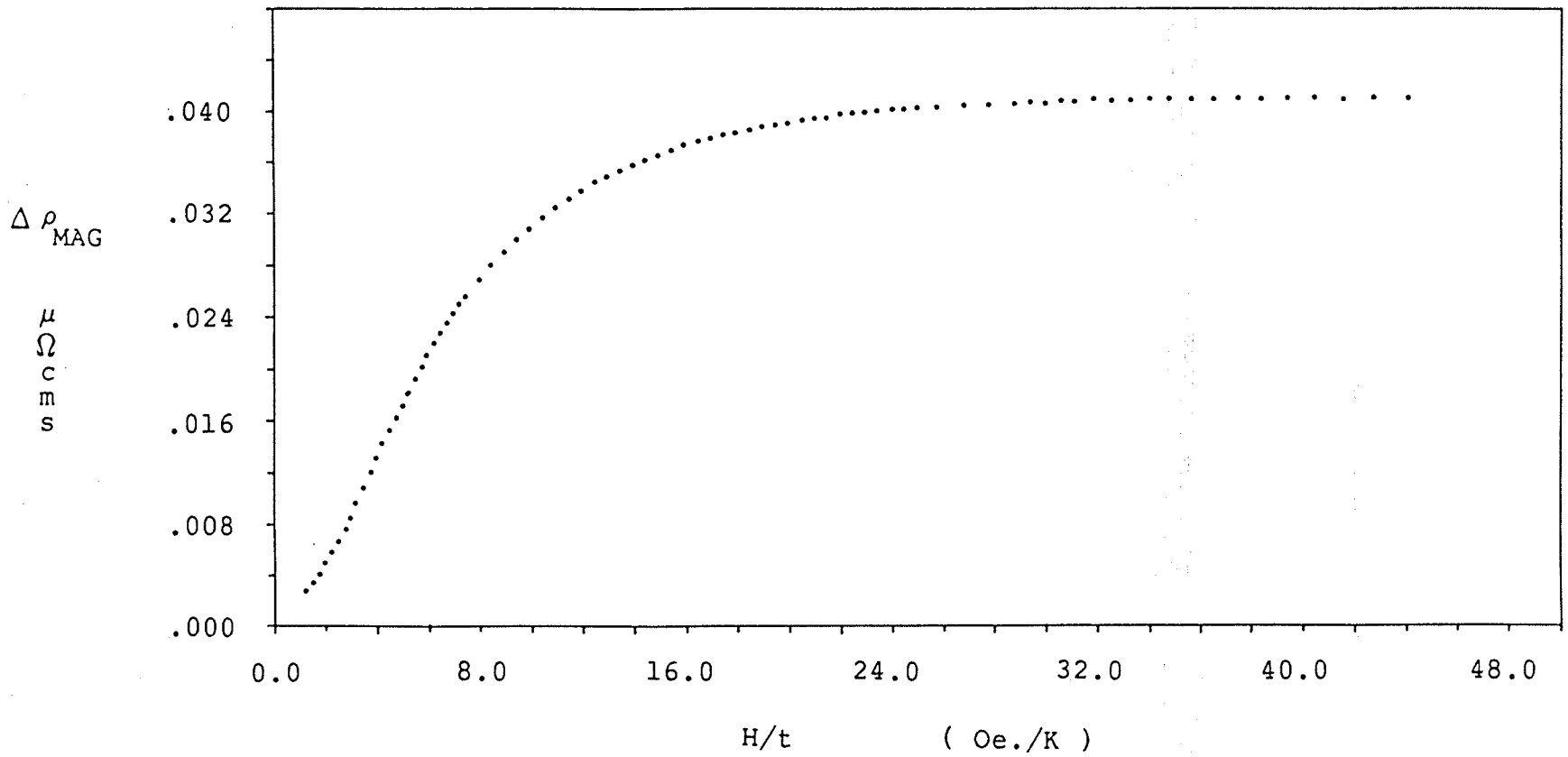

Figure 32: Pt+.15 at.% Mn incremental resistivity curves, after Kohler corrections have been made.

The theoretical s-d model expression for resistivity, developed by Yosida (equation X), was fit to each of the three $\Delta \rho_{MAG}$ curves. The fitting procedure followed a modified least squares approach discussed by Bevington[12]. This fitting program allowed the parameters g, S, J and V to vary freely until the best fit resulted. Small shifts in the zero position of the curve were also carried out to achieve a better fit. The fitting program is listed in Append. A. Table 5 lists the parameters of the " Best Fit" curves. Figures 33, 34 and 35 compare theoretical and experimental curves.

As shown by the results listed in table 5, the behavior of Mn ions in platinum can be associated with a spin of 5/2, that of an "isolated" Mn atom in a 3d (Mn^{++}) configuration. The g factor associated with these impurity ions, on the other hand, is slightly enhanced from its isolated atom value of 2.00. The Mn doped platinum, in the three concentrations studied, therefore constitute simple systems, the g factor of the impurity being slightly enhanced, the spin retaining its isolated ion value.

Measurements made on a Pt+.05 at.% Fe system by Swallow, Williams, Grassie and Loram[13] yielded a V of .586 ev. This value is comparable to those obtained for the platinum-manganese samples, the .05, .10 and .15 at.% specimens possessing V's of .576, .597 and .580 eV. respectively. The J values for the two systems, however, do

TABLE 5

Parameters of the "Best Fit" curves.

SAMPLE	g	S	J	V
Pt+.05 at.% Mn	2.26	2.50	.0336 eV.	.576 eV.
Pt+.10 at.% Mn	2.17	2.51	.0335 eV.	.597 eV.
Pt+.15 at.% Mn	2.14	2.50	.0328 eV.	.580 eV.

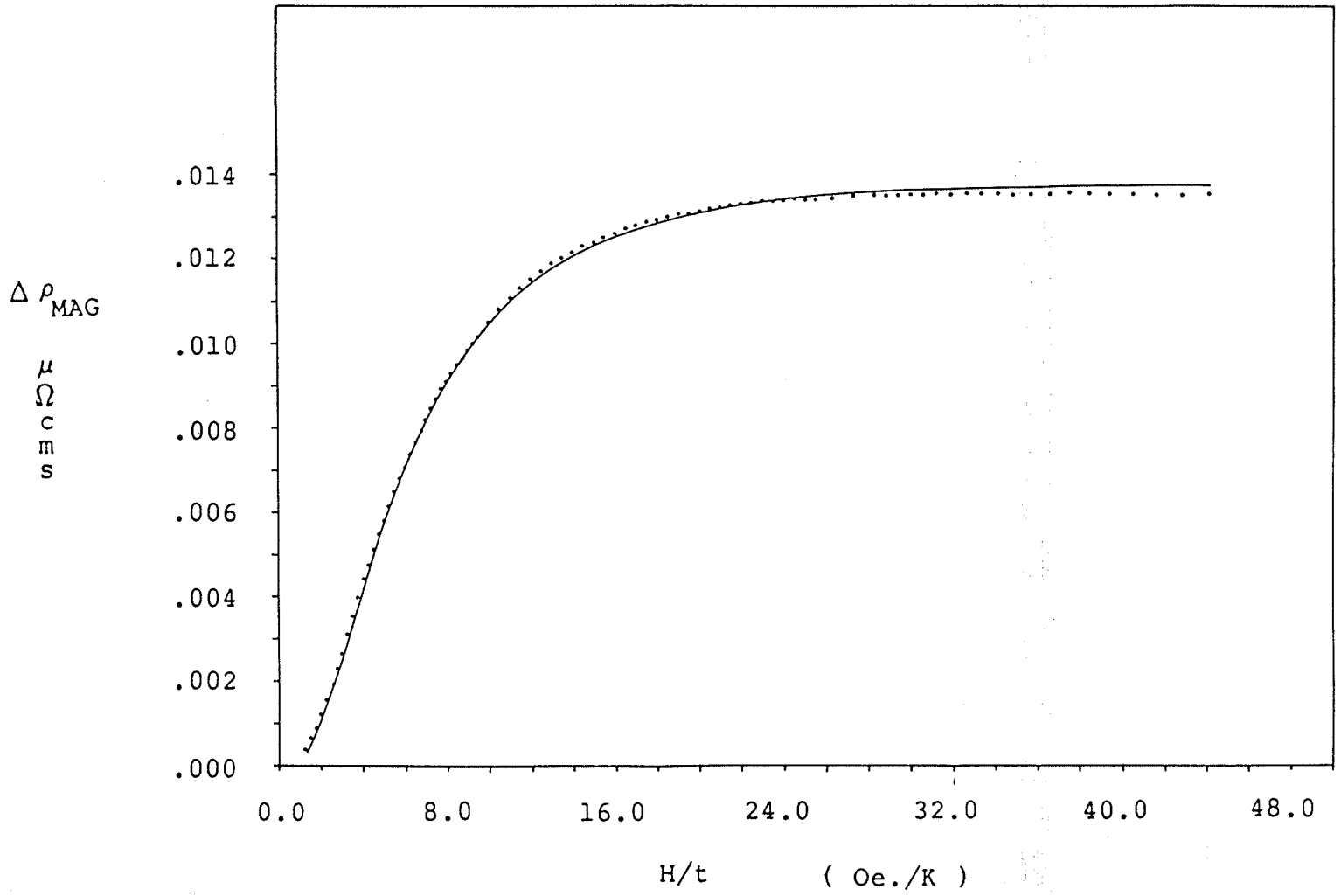

Figure 33: Theoretical and experimental resistivity curves for Pt+.05 at.% Mn.

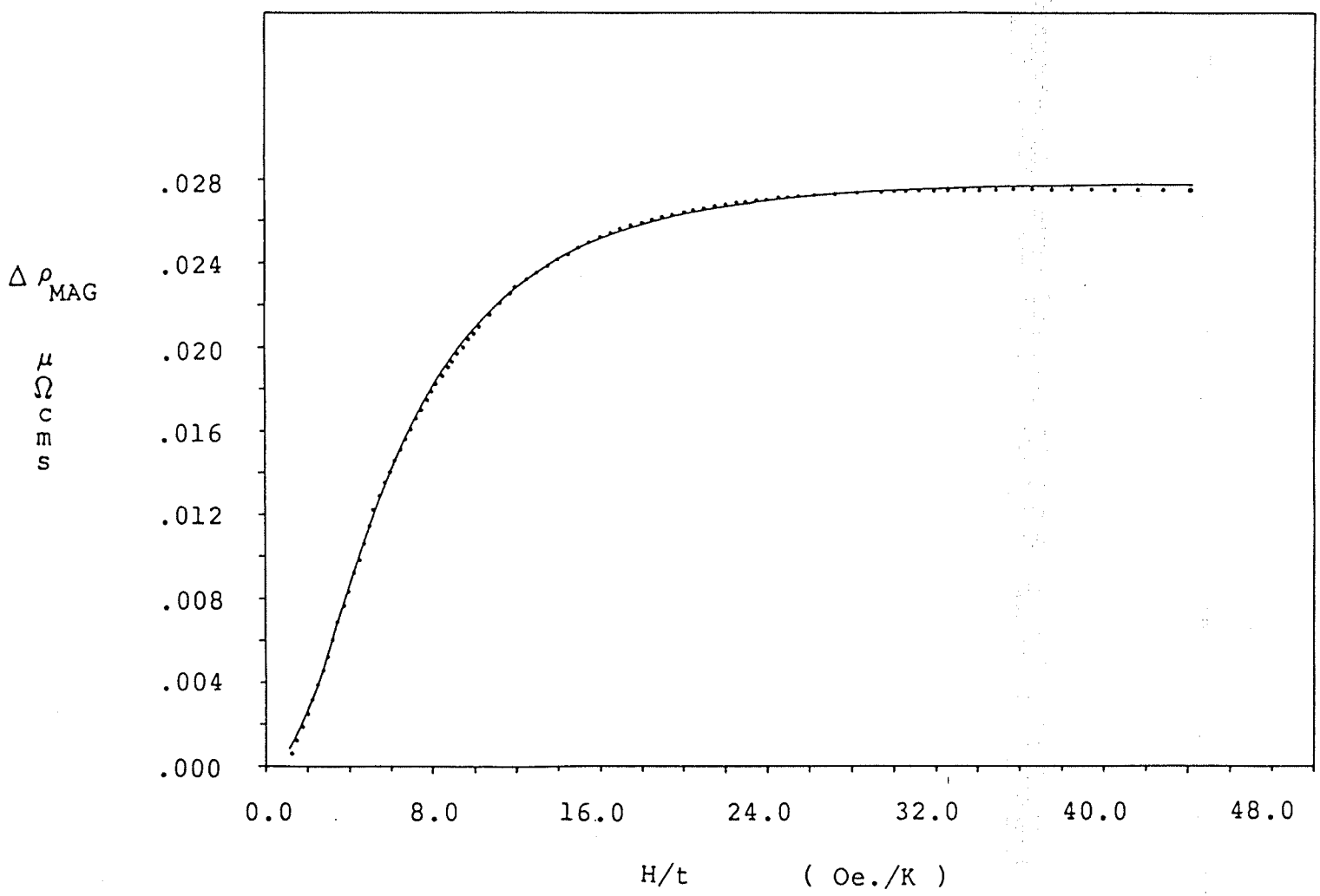

Figure 34: Theoretical and experimental resistivity curves for Pt+.10 at.% Mn.

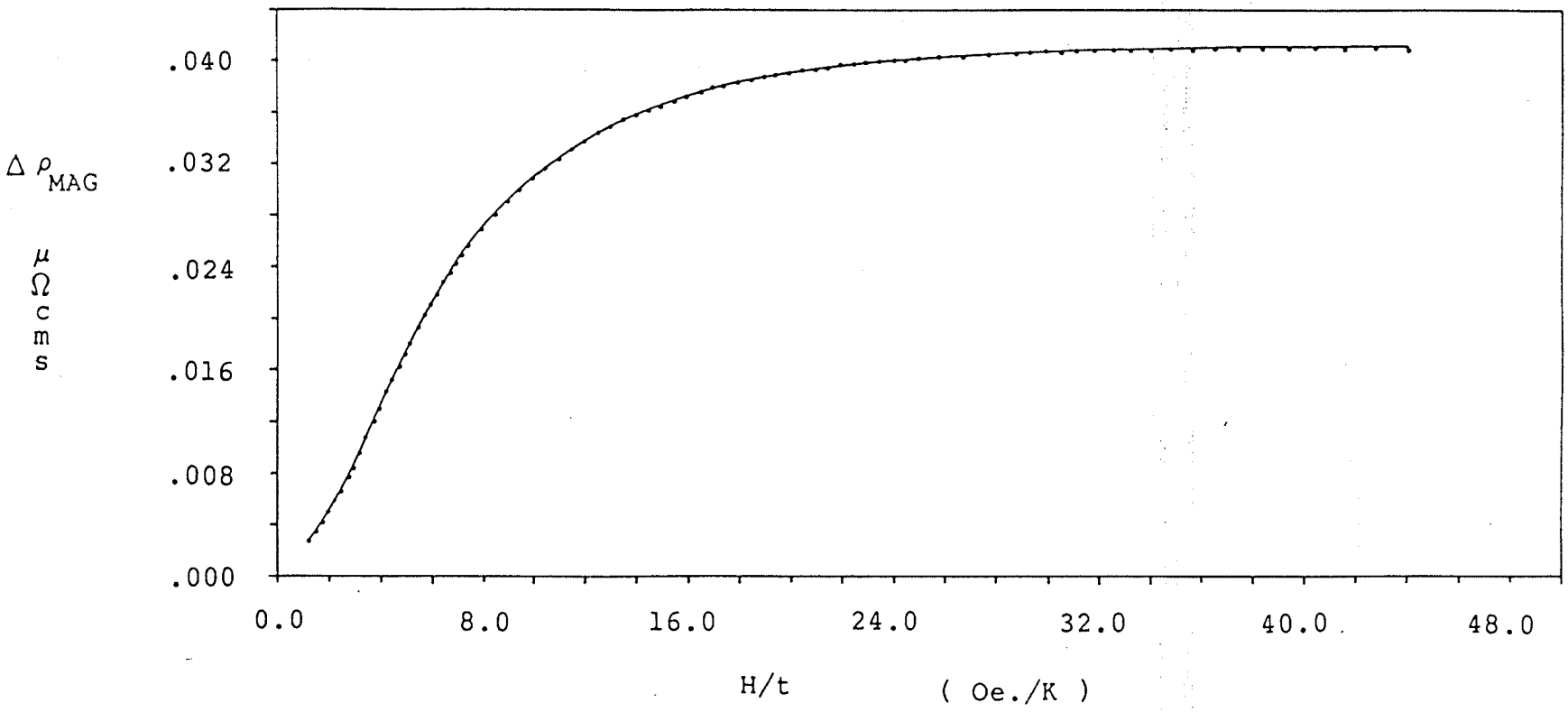

Figure 35: Theoretical and experimental resistivity curves for Pt+.15 at.% Mn.

not correspond. That for Pt+.05 at.% Fe is much larger, it being .041 eV. as compared to .0336, .0335 and .0328 eV. for the .05, .10 and .15 at.% Mn samples.

Resistivity measurements carried out by Kleiman and Williams[8] on Pd+.15 at.% Mn led to J and V values of .019 eV. and .50 eV. respectively. Both turn out to be considerably smaller than that for platinum-manganese. In this palladium-manganese system, both the g factor and spin S associated with the manganese impurity ions are enhanced. According to Kleiman and Williams, the $\bar{g}$ factor was determined to be 2.44 while the spin S was found to be 3.0.

Both Pd and Pt are complicated metals, with both s-like and d-like conduction bands overlapping at the Fermi energy. The s electrons have a low effective mass (Vuillemin 1966) and hence control the conductivity while the d-electrons are heavy and relatively well localized and hence dominate the magnetic properties (Anderson 1970). The assumed exchange coupling between local Mn spins (S) and the Pt conduction elecrons (of spin σ) of the form $-2JS\cdot\sigma$ leads to an enhancement of the g factor of (Shaltiel et al. 1964)

$$g_{EFF} = g_l + 2J_{dl}\psi_d/g_e\mu_B^2$$

where g_l and g_e are the g factors of the Mn spin and the conduction electrons respectively, and the assumption has been made that the dominant contribution to the g-shift comes from coupling to the d-band electrons (hence J_{dl} and

ψ_d) since they make the largest contribution to the Pauli susceptibility (ψ_d) of the host. Using the measured value of $\psi_d = 1.05 \times 10^{-6}$ emu/gm. (Foner et al. 1970), one obtains

1. PtFe: $g_{EFF} = 3.1$ so $J_{dl} = +0.144$ eV.
2. PtMn: $g_{EFF} = 2.26$ so $J_{dl} = +0.039$ eV.

Both the low value for J_{dl} and the normal bare value for S in PtMn compared with PtFe are quite consistent with the known properties of these systems. The latter exhibits giant moment ferromagnetism at low temperatures (as expected for an exchange enhanced spin and a large J_{dl}) while PtMn exhibits spin-glass behavior (ie. unenhanced spin and a small J_{dl}). Indeed the predicted effective moment of

$$P_{EFF} = g_{EFF}[\, S(S+1)\,]^{1/2} = 6.69$$

compare well with the experimentally determined value of

$$P_{EFF} = 6.5$$

at low concentration (Wasserman 1981).

In summary, these magnetoresistance data suggest that the PtMn system is one which is well described by a normal spin value of S = 5/2 and a small, positive g-shift. The latter are consistent with other, well established properties of this system.

Appendix A

CURVE FITTING PROGRAM

```
C  THE PURPOSE OF THIS PROGRAM IS TO MAKE A LEAST-SQUARES FIT TO A
   NONLINEAR FUNCTION WITH A LINEARIZATION OF THE FITTING FUNCTION.
C
C  DESCRIPTION OF THE PARAMETERS:
C  X         -ARRAY OF DATA POINTS FOR INDEPENDENT VARIABLE
C  Y         -ARRAY OF DATA POINTS FOR DEPENDENT VARIABLE
C  NPTS      -NUMBER OF PAIRS OF DATA POINTS
C  NTERMS    -NUMBER OF PARAMETERS
C  CHANGE    -NUMBER OF INCREMENTS REQUIRED FOR PARAMETERS A
C  PRECISION-
C  FLAMDA    -PROPORTION OF GRADIENT SEARCH INCLUDED
C  YFIT      -ARRAY OF CALCULATED VALUES OF Y
C  CHISQR    -REDUCED CHI SQUARE FOR FIT
C
C  THE SUBROUTINES USED IN THIS PROGRAM ARE FOUND IN 'DATA
C  REDUCTION AND ERROR ANALYSIS' BY P.R.BEVINGTON
C
C  SUBROUTINES AND FUNCTION PROGRAMS USED:
C  CURFIT     -BEVINGTON PG.237-239
C  FUNCTN     -BEVINGTON PG.214
C  FCHISQ     -BEVINGTON PG.194
C  FDERIV     -BEVINGTON PG.242
```

```
C  MATINV    -BEVINGTON PG.302-303
C
C
      REAL X(150), Y(150), A(10), YFIT(150), FLAMDA, OLDCHISQR,
     +CHISQR, CHANGE, TEST, SIGMAA(10), ARRAY(10,10), BB(10,10)
      CHARACTER*1 ARRAYE(132),ARRAYT(132)
      READ(4,*) NPTS
      READ(4,*) NTERMS
      READ(4,*) CHANGE
      READ(4,*) PRECISION
      READ(4,*) (A(J),J=1,NTERMS)
      DO 2 I=1,NPTS
         READ(4,*) X(I),Y(I)
         Y(I)=Y(I)-.00040
    2 CONTINUE
      OLDCHISQR=0.
    6 FLAMDA=.001
      CALL CURFIT(ARRAY,BB,X,Y,NPTS,NTERMS,A,CHANGE,SIGMAA,FLAMDA,
     +YFIT,CHISQR)
      WRITE(9,*) (A(K),K=1,NTERMS)
      WRITE(9,200) CHISQR
  200 FORMAT(' ','CHISQR=',E14.8)
      TEST = ABS((OLDCHISQR/CHISQR)-1)
      IF (TEST.GT.PRECISION) THEN DO
         OLDCHISQR=CHISQR
         GO TO 6
      END IF
```

```
      S=A(2)
      EX=A(3)
      R1=.43877+.04080-EX
      R2=2.*S+1.
      RJ=SQRT((2.*R1*R2-.43877-SQRT(3.51*R1*S*R2+.1925))/
     +(2.769*S*R2**2.))
      V=SQRT(R1/1.385-RJ*RJ*S*(S+1.))
      WRITE(9,*) A(1),A(2),RJ,V,A(3)
      DO 7 K=1,NPTS
         YAK=(YFIT(K)-Y(K))*25000.
         WRITE(9,5) X(K),Y(K),YFIT(K),YAK
    7 CONTINUE
    5 FORMAT (' ',5X,F5.2,5X,F8.6,5X,F8.6,5X,F4.1)
      STOP
      END
C
C
C  SUBROUTINE CURFIT MAKES A LEAST-SQUARES FIT TO A NONLINEAR
C  FUNCTION WITH A LINEARIZATION OF THE FITTING FUNCTION
C
C
      SUBROUTINE CURFIT(ARRAY,BB,X,Y,NPTS,NTERMS,A,CHANGE,SIGMAA,
     +FLAMDA,YFIT,CHISQR)
      DOUBLE PRECISION ARRAY(NTERMS,NTERMS),WKAREA(20),
     +BB(NTERMS,NTERMS)
      DIMENSION X(1), Y(1), A(1), SIGMAA(1), YFIT(1)
      DIMENSION ALPHA(10,10), BETA(10), DERIV(10), B(10)
```

```
      II=0
   11 NFREE=NPTS-NTERMS
      IF (NFREE) 13,13,31
   13 CHISQR=0
      GO TO 110
C
C  EVALUATE ALPHA AND BETA MATRICES
C
   31 DO 34 J=1,NTERMS
      BETA(J)=0
      DO 34 K=1,J
   34 ALPHA(J,K)=0
   41 DO 50 I=1,NPTS
      CALL FDERIV(X,I,A,CHANGE,NTERMS,DERIV)
      DO 46 J=1,NTERMS
      BETA(J)=BETA(J)+(Y(I)-FUNCTN(X,I,A))*DERIV(J)
      DO 46 K=1,J
   46 ALPHA(J,K)=ALPHA(J,K)+DERIV(J)*DERIV(K)
   50 CONTINUE
   51 DO 53 J=1,NTERMS
      DO 53 K=1,J
   53 ALPHA(K,J)=ALPHA(J,K)
C
C  EVALUATE CHI SQUARE AT STARTING POINT
C
   61 DO 62 I=1,NPTS
   62 YFIT(I)=FUNCTN(X,I,A)
```

```
   63 CHISQI=FCHISQ(Y,NPTS,NFREE,YFIT)
C
C  INVERT MODIFIED CURVATURE MATRIX TO FIND NEW PARAMETERS
C
   71 DO 74 J=1,NTERMS
      DO 73 K=1,NTERMS
   73 ARRAY(J,K)=ALPHA(J,K)/SQRT(ALPHA(J,J)*ALPHA(K,K))
   74 ARRAY(J,J)=1.+FLAMDA
      CALL MATINV(ARRAY,NTERMS,DET)
   81 DO 84 J=1,NTERMS
      B(J)=A(J)
      DO 84 K=1,NTERMS
   84 B(J)=B(J)+BETA(K)*ARRAY(J,K)/SQRT(ALPHA(J,J)*ALPHA(K,K))
C
C  IF CHI SQUARE INCREASED, INCREASE FLAMDA AND TRY AGAIN
C
   91 DO 92 I=1,NPTS
   92 YFIT(I)=FUNCTN(X,I,B)
   93 CHISQR=FCHISQ(Y,NPTS,NFREE,YFIT)
      IF(CHISQI-CHISQR) 95,101,101
   95 FLAMDA=10.*FLAMDA
      II=II+1
      GO TO 71
C
C  EVALUATE PARAMETERS AND UNCERTAINTIES
C
  101 DO 103 J=1,NTERMS
```

```
      A(J)=B(J)
  103 SIGMAA(J)=DSQRT(ARRAY(J,J)/ALPHA(J,J))
      FLAMDA=FLAMDA/10.
  110 RETURN
      END
C
C
C
      SUBROUTINE FDERIV(X,I,A,CHANGE,NTERMS,DERIV)
      DIMENSION X(1),A(1),DERIV(1)
   11 DO 18 J=1,NTERMS
      AJ=A(J)
      DELTA=A(J)/CHANGE
      A(J)=AJ+DELTA
      YFIT=FUNCTN(X,I,A)
      A(J)=AJ-DELTA
      DERIV(J)=(YFIT-FUNCTN(X,I,A))/(2.*DELTA)
   18 A(J)=AJ
      RETURN
      END
C
C
C
      FUNCTION FCHISQ(Y,NPTS,NFREE,YFIT)
      DIMENSION Y(1),YFIT(1)
   11 CHISQ=0
   12 IF (NFREE) 13,13,20
```

```
   13 FCHISQ=0.
      GO TO 40
   20 DO 30 I=1,NPTS
   30 CHISQ=CHISQ+(Y(I)-YFIT(I))**2
   31 FREE=NFREE
   32 FCHISQ=CHISQ/FREE
   40 RETURN
      END
C
C
C
      FUNCTION FUNCTN(X,I,PAR)
      REAL A,B,Z,V,J,S,ESZ,T,ALFA,G,UB,HOT,KB
      DIMENSION PAR(1),X(1)
      A=9.23
      C=.15
      KB=1.38062E-16
      UB=9.27410E-21
      G=PAR(1)
      S=PAR(2)
      EX=PAR(3)
      R1= .43877+.04080-EX
      R2=2.*S+1.
      J=SQRT((2.*R1*R2-.43877-SQRT(3.51*R1*S*R2+.1925))/
     +(2.769*S*R2**2.))
      V=SQRT(R1/1.385-J*J*S*(S+1.))
      HOT=X(I)*1000.
```

```
      ALFA=G*UB*HOT/KB
      T=TANH(ALFA/2.)
      ESZ=(2.*S+1.)/2./TANH((2.*S+1.)*ALFA/2.)-1./2./T
      XX=J*J*ESZ*T
      YY=(2*V*J*ESZ)**2
      Z=V*V+J*J*(S*(S+1)-ESZ*T)
      DPHT=A*C*(XX+YY/Z)
      FUNCTN=DPHT+EX
      RETURN
      END
C
C
C
      SUBROUTINE MATINV(ARRAY,NORDER,DET)
      DOUBLE PRECISION ARRAY(NORDER,NORDER),AMAX,SAVE
      DIMENSION IK(10),JK(10)
   10 DET=1.
   11 DO 100 K=1, NORDER
      AMAX=0.
   21 DO 30 I=K, NORDER
      DO 30 J=K, NORDER
   23 IF (DABS(AMAX) - DABS(ARRAY(I,J))) 24,24,30
   24 AMAX= ARRAY(I,J)
      IK(K)=I
      JK(K)=J
   30 CONTINUE
   31 IF (AMAX) 41,32,41
```

```
32 DET=0.
   GO TO 140
41 I=IK(K)
   IF (I-K) 21,51,43
43 DO 50 J=1, NORDER
   SAVE = ARRAY(K,J)
   ARRAY(K,J)=ARRAY(I,J)
50 ARRAY(I,J)= -SAVE
51 J=JK(K)
   IF (J-K) 21,61,53
53 DO 60 I=1, NORDER
   SAVE=ARRAY(I,K)
   ARRAY(I,K)=ARRAY(I,J)
60 ARRAY(I,J)= -SAVE
61 DO 70 I=1,NORDER
   IF (I-K) 63,70,63
63 ARRAY(I,K)= -ARRAY(I,K)/AMAX
70 CONTINUE
71 DO 80 I=1, NORDER
   DO 80 J=1, NORDER
   IF (I-K) 74,80,74
74 IF (J-K) 75,80,75
75 ARRAY(I,J)=ARRAY(I,J)+ARRAY(I,K)*ARRAY(K,J)
80 CONTINUE
81 DO 90 J=1, NORDER
   IF (J-K) 83,90,83
83 ARRAY(K,J)=ARRAY(K,J)/AMAX
```

```
 90 CONTINUE
    ARRAY(K,K)=1./AMAX
100 DET=DET*AMAX
101 DO 130 L=1,NORDER
    K=NORDER-L+1
    J=IK(K)
    IF (J-K) 111,111,105
105 DO 110 I=1, NORDER
    SAVE=ARRAY(I,K)
    ARRAY(I,K)= -ARRAY(I,J)
110 ARRAY(I,J)=SAVE
111 I=JK(K)
    IF (I-K) 130,130,113
113 DO 120 J=1,NORDER
    SAVE=ARRAY(K,J)
    ARRAY(K,J)= -ARRAY(I,J)
120 ARRAY(I,J)=SAVE
130 CONTINUE
140 RETURN
    END
$ENTRY
```

REFERENCES

1 J. Friedel, Can. J. Phys. 34, 1190 (1956); Nuovo Cimento Suppl. 7, 287 (1958); A. Blandin and J. Friedel, J. Phys. radium 20, 160 (1959)

2 E. Daniel and J. Friedel, Proceedings of the IXth International Conference on Low Temperature Physics, edited by J.G. Daunt, D.O. Edwards, F.J. Milford, and M. Yaqub (Plenum Press, New York, 1965), page 933.

3 P.W. Anderson, Phys. Rev. 124, 41 (1961).

4 L.L. Hirst, Phys. Kondens. Mat. 11, 255 (1970); in Magnetism and Magnetic Materials - 1974, edited by C.D. Graham, Jr., G.H. Lander and J.J. Rhyne, AIP Conference Proceedings No. 24 (American Institute of Physics, New York, 1975), page 11.

5 R.M. Roshko, "Some Electric and Magnetic Properties of Cr Impurities Dissolved in Exchange Enhanced Hosts", Thesis (U. of M.), 1979, Unpublished.

6 K. Yosida, Physical Review 107, 396 (1957).

7 N. Ashcroft and N. Mermin, "Solid State Physics", New York: Holt, Rinehart and Winston (1976).

8 R.N. Kleiman and G. Williams, J. Phys. F: Metal Physics 12, 169 (1982).

9 A.D.C. Grassie, G.A. Swallow, G. Williams and J.V. Loram, Phys. Rev. B3, 4154 (1971).

10 W.B. Pearson, "A Handbook of Lattice Spacings and Structures of Metals and Alloys", (Pergamon Press, New York, 1958).

11 Ctirad Uher, Chi-Wai Lee and J. Bass, Physics Letters 61A, 344 (1977).

12 P.R. Bevington, "Data Reduction and Error Analysis for the Physical Sciences", New York: McGraw Hill (1969).

13 G.A. Swallow, G. Williams, A.D.C. Grassie and J.W. Loram, J. Phys. F: Metal Physics 1, 511 (1971).